

PREPARATION OF SELENIUM NANOPARTICLES STABILIZED BY PULLULAN AND
DERIVATIVES



A Dissertation Submitted in Partial Fulfillment of the Requirements
for the Degree of Doctor of Philosophy in Chemistry

Department of Chemistry

FACULTY OF SCIENCE

Chulalongkorn University

Academic Year 2018

Copyright of Chulalongkorn University

การเตรียมอนุภาคขนาดนาโนเมตรของซีลีเนียมทำให้เสถียรด้วยพอลิแลนและอนุพันธ์



วิทยานิพนธ์นี้เป็นส่วนหนึ่งของการศึกษาตามหลักสูตรปริญญาวิทยาศาสตรดุษฎีบัณฑิต

สาขาวิชาเคมี ภาควิชาเคมี

คณะวิทยาศาสตร์ จุฬาลงกรณ์มหาวิทยาลัย

ปีการศึกษา 2561

ลิขสิทธิ์ของจุฬาลงกรณ์มหาวิทยาลัย

Dissertation Title PREPARATON OF SELENIUM NANOPARTICLES STABILIZED
BY PULLULAN AND DERIVATIVES
By Miss Punnida Nonsuwan
Field of Study Chemistry
Thesis Advisor Professor Nongnuj Muangsin, Ph.D.

Accepted by the FACULTY OF SCIENCE, Chulalongkorn University in Partial
Fulfillment of the Requirement for the Doctor of Philosophy

..... Dean of the FACULTY OF SCIENCE
(Professor Polkit Sangvanich, Ph.D.)

DISSERTATION COMMITTEE

..... Chairman
(Associate Professor Vudhichai Parasuk, Ph.D.)

..... Advisor
(Professor Nongnuj Muangsin, Ph.D.)

..... Examiner
(Professor Thawatchai Tuntulani, Ph.D.)

..... Examiner
(Associate Professor Nuanphun Chantarasiri, Ph.D.)

..... External Examiner
(Assistant Professor Thitiphon Chimsook, Ph.D.)

CHULALONGKORN UNIVERSITY

พรรณนิดา นนสุวรรณณ์ : การเตรียมอนุภาคขนาดนาโนเมตรของซีลีเนียมทำให้เสถียรด้วยพุลลูแลนและอนุพันธ์. (PREPARATION OF SELENIUM NANOPARTICLES STABILIZED BY PULLULAN AND DERIVATIVES) อ.ที่ปรึกษาวิทยานิพนธ์หลัก : ศ. ดร.นนุช เหมืองสิน

วัสดุผสมอนินทรีย์เคมีและอินทรีย์เคมีของอนุภาคซีลีเนียมระดับนาโนเมตร (SeNPs) ที่ถูกทำให้เสถียรด้วยอนุพันธ์ของพุลลูแลนถูกเตรียมขึ้นด้วยการสังเคราะห์สีเขียวและเป็นวิธีที่ง่าย อนุพันธ์ของพุลลูแลนที่ถูกดัดแปลงด้วยประจุบวกและกรดโฟลิก (FA-CP) ถูกนำมาผสมกับโซเดียมซีลีโนส (Na_2SeO_3) และอนุภาคซีลีเนียมระดับนาโนเมตร (SeNPs) ที่ถูกทำให้เสถียรด้วย FA-CP (SeNPs/FA-CP) ถูกเตรียมขึ้นหลังจากเติมซิสเตอีนซึ่งทำหน้าที่เป็นตัวรีดิวซ์ลงในสารละลายผสมดังกล่าว จากการทดลองพบว่าความเข้มข้นของซิสเตอีนและ FA-CP มีผลต่อรูปร่างและลักษณะทางสัญญาณวิทยาของ SeNPs/FA-CP โดยทรงกลมของ SeNPs/FA-CP ถูกเตรียมขึ้นเมื่อใช้อัตราส่วนของ Na_2SeO_3 :ซิสเตอีนเป็น 1:1 ซึ่งมีความเป็นพิษต่อเซลล์มะเร็งในขณะที่มีความเป็นพิษน้อยกว่าในเซลล์ปกติ นอกจากนี้อนุภาคซีลีเนียมระดับนาโนเมตรที่ถูกทำให้เสถียรด้วย FA-CP สามารถนำเข้าสู่เซลล์มะเร็งได้ดีเปรียบเทียบกับอนุภาคซีลีเนียมระดับนาโนเมตรที่ถูกทำให้เสถียรด้วยพุลลูแลน รูปทรงดอกไม้ของ SeNPs/FA-CP ถูกเตรียมขึ้นโดยไม่ได้คาดหวังเมื่อใช้อัตราส่วนของ Na_2SeO_3 :ซิสเตอีน เป็น 1:2 ซึ่งกลไกในการเกิดรูปทรงดอกไม้เกิดจากการเติบโตแบบไร้ทิศทางของแผ่น SeNPs/FA-CP จากการทดสอบความสามารถในการโหลดยา doxorubicin พบว่าสามารถโหลดได้มากกว่าทรงกลมของ SeNPs/FA-CP ถึง 3 เท่า แสดงให้เห็นว่ารูปทรงดอกไม้สามารถใช้เป็นแบบในการบรรจุยาได้ อีกทั้งยังมีความเป็นพิษมากต่อเซลล์มะเร็งขณะที่มีความเป็นพิษน้อยต่อเซลล์ปกติ เพื่อเพิ่มความสามารถในการโหลดยาที่มากขึ้นและสามารถใช้ได้กับยาที่หลากหลาย รูปทรงดอกไม้ของ SeNPs ที่ถูกทำให้เสถียรด้วยพุลลูแลนที่ดัดแปลงเพิ่มเติมด้วยไซโคลเด็คตริน (CD-FA-CP) ถูกพัฒนาขึ้น ซึ่งพบว่าการต่อไซโคลเด็คตรินเข้าไปช่วยเพิ่มความสามารถในการโหลดยาเพิ่มขึ้นถึง 4 เท่าเปรียบเทียบกับรูปทรงดอกไม้ของ SeNPs/FA-CP และยังสามารถโหลดยาที่หลากหลายนอกจาก doxorubicin ได้ เช่น curcumin และ methylene blue จากการศึกษาข้างต้นชี้ให้เห็นว่าวัสดุผสมอนินทรีย์เคมีและอินทรีย์เคมีของอนุภาคซีลีเนียมระดับนาโนเมตร (SeNPs) ที่ถูกทำให้เสถียรด้วยอนุพันธ์ของพุลลูแลนสามารถใช้เป็นวัสดุทางเลือกในระบบนำส่งยาสำหรับการรักษามะเร็งได้

จุฬาลงกรณ์มหาวิทยาลัย
CHULALONGKORN UNIVERSITY

ภาควิชา	ภาควิชาเคมี	ลายมือชื่อนิสิต
สาขาวิชา	เคมี	ลายมือชื่อ อ.ที่ปรึกษาวิทยานิพนธ์หลัก
ปีการศึกษา	2561	

5672893923 : DOCTOR OF PHILOSOPHY

Selenium nanoparticles pullulan hybrid microflower cancer treatment drug delivery

Punnida Nonsuwan : PREPARATON OF SELENIUM NANOPARTICLES STABILIZED BY PULLULAN AND DERIVATIVES. ADVISOR: Prof. Nongnuj Muangsin, Ph.D.

The inorganic/organic selenium nanoparticles (SeNPs)/pullulan derivative hybrid material was obtained using a simple and green strategy. The chemical structure of pullulan, folic acid decorated cationic pullulan (FA-CP) was designed for stabilizing SeNPs. The SeNPs stabilized by FA-CP were observed after the addition of a cysteine hydrochloride solution into the solution mixture of Na_2SeO_3 and FA-CP. The results suggested that the concentrations of cysteine and stabilizer were the key factors to control the shape and morphology of SeNPs. The spherical SeNP/FA-CP was found in ratio of Na_2SeO_3 to cysteine was 1:1. It exhibited low toxicity against normal cells while higher toxicity was showed in human cancer cell lines. Moreover, the enhancement of cellular uptake of spherical SeNPs/FA-CP was performed comparing with SeNPs stabilized by unmodified pullulan. The unexpected formation of flower-like structure was performed when using 1:2 molar ratio of Na_2SeO_3 to cysteine. The formation mechanism of the microflowers was tentatively identified as anisotropic hierarchical growth. The microflowers exhibited effective drug adsorption for doxorubicin which was three times higher than that for the doxorubicin loaded spherical SeNPs/FA-CP and showed more potent activity against cancer cells while showing less toxicity against normal cells. The data demonstrated that the microflower SeNPs/FA-CP could be a candidate anticancer drug template in drug delivery systems. To enhance drug loading capacity and create universal drug loading template for drug delivery application, the β -cyclodextrin was conjugated on FA-CP (CD-FA-CP) and use for stabilization of SeNPs (SeNPs/CD-FA-CP). The maximum loading capacity of doxorubicin of the microflower SeNPs/CD-FA-CP was four times higher than the capacity of microflower stabilized by FA-CP. In addition, others guest molecules; curcumin and methylene blue could be loaded into SeNPs/CD-FA-CP hybrid microflower. These finding showed that the SeNPs/CD-FA-CP microflowers can be used as universal template for any guest molecules especially hydrophobic drugs. Thus, this work presents an alternative way for using SeNPs/pullulan derivative as a carrier-based drug delivery system for cancer treatment.

Department: Department of Chemistry

Student's Signature

Field of Study: Chemistry

Advisor's Signature

Academic Year: 2018

ACKNOWLEDGEMENTS

This research could not be successful without the valuable advice of my advisor. I am highly thankful to Prof. Nongnuj Muangsin for supporting, assistance, guidance, motivation and good suggestion for solving a problem through the completion of my doctoral study. I really appreciate all her contributions of time and opinion to make my Ph.D. experience productive and stimulating. Without her supports, I would have been unimaginable this thesis could be completed and achieved. It is a great honor for me to be a member in Nongnuj's laboratory.

I would like to express my appreciation to the members of my committee: Assoc. Prof. Vudhichai Parasuk, Prof. Thawatchai Tuntulani, Assoc. Prof. Nuanphan Chantarasiri and Asst. Prof. Thitiphan Chimsook for their valuable advice comments, suggestions and assessing this research. Further I would like to thank Development and Promotion of Science and Technology Talents Project (DPST) Scholarships for financial support during my doctoral study. Without these facilities and sponsorship, I would not be possible to conduct this research.

I really grateful to my family for their all along encourage, understanding, and greatest support and my friends for every spirit.

Finally, I would like to thank myself for my super power to send me pass many challenging and difficult experiences. I really grew up and can be held up a big smile on my face.

Punnida Nonsuwan

TABLE OF CONTENTS

	Page
ABSTRACT (THAI).....	iii
ABSTRACT (ENGLISH).....	iv
ACKNOWLEDGEMENTS	v
TABLE OF CONTENTS	vi
LIST OF TABLES.....	ix
LIST OF FIGURES.....	x
CHAPTER 1.....	1
INTRODUCTION.....	1
1.1 Research background	1
1.2 Research objectives	3
1.3 The expected beneficial outcomes	4
CHAPTER 2.....	5
LITERATURE REVIEWS.....	5
2.1 Nanoparticles (NPs) and nanomaterials (NMs)	5
2.1.1 Types of nanomaterials.....	5
2.1.2 Nanoparticles in biomedical applications.....	7
2.1.3 SeNPs and the application for drug delivery	11
2.2 Polysaccharide pullulan, its functionalization and applications	13
2.2.1 The properties of pullulan.....	14
2.2.2 The functionalization of pullulan and its applications.....	15
2.3 Polysaccharide stabilized nanoparticles.....	17

2.4 The control of the shape and morphology.....	19
CHAPTER 3.....	23
MATERIALS AND METHODS	23
3.1 Materials.....	23
3.2 Synthesis and characterization of pullulan derivative	23
3.2.1 Synthesis and characterization of folic acid decorated cationic pullulan (FA-CP).....	23
3.2.2 Synthesis and characterization of β -cyclodextrin conjugated FA-CP (CD- FA-CP).....	25
3.3 Synthesis and characterization of SeNPs stabilized by pullulan and derivatives	26
3.4 Drug loading and release study.....	27
3.5 Cytotoxicity study.....	28
3.6 Detection of apoptotic/necrotic cells (annexin-V/propidium iodide assay)	29
3.7 Determination of intracellular Se concentration.....	29
3.8 Cellular uptake assays by confocal laser scanning microscope.....	30
CHAPTER 4.....	31
RESULTS AND DISCUSSION.....	31
4.1 Synthesis and characterization of FA-CP	32
4.2 Synthesis and characterization of SeNPs stabilized by FA-CP	38
4.2.1 Effect of cysteine concentration.....	40
4.2.2 Spherical structure of SeNP/FA-CP.....	42
4.2.2.1 Effect of FA-CP concentration.....	42
4.2.2.2 Effect of type of stabilizer	45
4.2.2.3 In vitro cytotoxicity.....	50

4.2.2.4 Intracellular Se concentration	51
4.2.3 Microflower structure of SeNPs/FA-CP	53
4.2.3.1 Effect of FA-CP concentration.....	53
4.2.3.2 Possible mechanism for the formation of SeNPs stabilized by FA-CP hybrid flower.....	55
4.2.3.3 Anticancer drug loading and release studies of SeNPs/FA-CP hybrid flower.....	63
4.3 Synthesis and characterization of CD-FA-CP.....	70
4.4 Synthesis and characterization of SeNPs stabilized by CD-FA-CP	75
4.4.1 Effect of cysteine concentration.....	75
4.4.2 The use of SeNPs/CD-FA-CP microflower as a template for universal guest molecules loading.....	79
4.4.3 In vitro release of doxorubicin from SeNPs/CD-FA-CP@DOX.....	81
4.4.4 <i>In vitro</i> cytotoxicity study.....	83
4.4.5 <i>In vitro</i> cellular uptake study	84
CHAPTER 5.....	87
CONCLUSION	87
5.1 Conclusion	87
5.2 Suggestion for future work	89
REFERENCES	90
APPENDIX.....	103
VITA.....	106

LIST OF TABLES

Table 1. The degree of quaternization of cationic pullulan	37
Table 2. The degree of substitution of folic acid on cationic pullulan	37
Table 3. Particle size of SeNPs stabilized by pullulan and derivatives and their zeta potential.....	49
Table 4. The T_g and T_m of FA-CP and CD-FA-CP.....	75
Table 5. Fitting results of doxorubicin-release model of SeNPs/CD-FA-CP microflowers.....	83

LIST OF FIGURES

Figure 1 Schematic of drug loading options in targeted drug delivery [27].	11
Figure 2 Pullulan structure.	15
Figure 3 Schematic model of the Se-HBP nanocomposites during the formation process [1].	19
Figure 4 Diagram of possible mechanisms for selenium nanorods [2].	20
Figure 5 The proposed mechanism for the formation of cubic-like SeNPs [3].	21
Figure 6 Schematic presentation of the synthesis of CP (step 1), FA-CP (step 2) and CD-FA-CP (step 3).	34
Figure 7 ^1H NMR spectra of a) pullulan, b) CP and c) FA-CP.	36
Figure 8 FTIR spectra of a) pullulan, b) CP and c) FA-CP.	39
Figure 9 Schematic presentation of the synthesis of SeNPs.	40
Figure 10 SEM images of shape of SeNPs stabilized by FA-CP with molar ratio of Na_2SeO_3 to cysteine a) 1:0, b) 1:1, c) 1:2 and d) 1:4.	41
Figure 11 SEM images of SeNPs stabilized by FA-CP with FA-CP concentration of a) 0%, b) 0.023%, c) 0.045%, d) 0.23%, e) 0.45 and f) 0.91% w/v.	44
Figure 12 SEM images of SeNPs stabilized by a) pullulan, b) CP, c) FA-P d) FA-CP at concentration of 0.23% w/v and e) EDX spectra of SeNPs/FA-CP.	47
Figure 13 TEM images of SeNPs stabilized by a) pullulan, b) CP, c) FA-P and d) FA-CP at concentration of 0.23% w/v.	48
Figure 14 <i>In vitro</i> anticancer activities of SeNPs stabilized by pullulan and derivatives on KB cancer cell and normal cell lines (72 h). Cell viability was determined by a colorimetric MTT assay. Each IC_{50} value represents the mean \pm SD of three independent experiments.	51

Figure 15 Quantitative analysis of Se concentration in KB cells exposed to SeNPs stabilized by pullulan and derivatives for 24 h by ICP-AES method. Each value represents the mean±SD of three independent experiments.....	52
Figure 16 SEM images of shape of SeNPs stabilized by FA-CP with FA-CP concentration of a) 0.023%, b) 0.045%, c) 0.23%, d) 0.43% and e) 0.91% w/v.	54
Figure 17 Schematic representation of the SeNPs stabilized by pullulan derivative inorganic/organic hybrid flowers.....	60
Figure 18 a) EDS spectrum for a representation of the hexagonal plated-sheet. The inset shows an SEM image and corresponding EDS mapping data for hexagonal sheet, b) EDS spectrum for a representative sample of SeNPs stabilized by FA-CP hybrid flower. The inset shows an SEM image and corresponding EDS mapping data for an ensemble of microflowers.....	61
Figure 19 a) TEM images of hybrid microflower of SeNP stabilized by FA-CP at 1:2 molar ratio of Na ₂ SeO ₃ :cysteine, b) SAED pattern of SeNPs stabilized by FA-CP hybrid flower, c) HRTEM of nanosheet of SeNPs stabilized by FA-CP hybrid flower, d) XRD pattern of SeNPs stabilized by FA-CP hybrid flower, c) HRTEM of nanosheet of SeNPs stabilized by FA-CP hybrid flower, and d) XRD pattern of SeNPs stabilized by FA-CP.....	62
Figure 20 Doxorubicin-loaded SeNPs hybrid flower observed by microscopy.....	66
Figure 21 a) The capacity of the doxorubicin-loaded hybrid flower and spherical SeNPs. b) Cumulative drug release (%) of doxorubicin from doxorubicin-loaded hybrid microflowers.	67
Figure 22 a) Cytotoxicity of doxorubicin-loaded hybrid microflower against KB and L292 cells. b) Cell growth photos of KB cells treated with different concentration of doxorubicin-loaded hybrid microflowers.....	68
Figure 23 The percent of apoptosis/necrosis of KB cells analyzed by flow cytometry.	69
Figure 24 The FTIR spectra of a) β-CD and b) CD-OTs.	71
Figure 25 ¹ H NMR of a) β-CD and b) CD-OTs.....	72

Figure 26 Mass spectrum of CD-OTs.....	72
Figure 27 The ^1H NMR spectra of a) FA-CP and b) CD-PA-CP.	73
Figure 28 DSC thermograms of a) FA-CP and b) CD-FA-CP.	74
Figure 29 SEM images of shape of SeNPs stabilized by CD-FA-CP with molar ratio of Na_2SeO_3 to cysteine 1:1 (a and b) and 1:2 (c and d).....	77
Figure 30 EDS mapping data of a) the hexagonal plated-sheet of SeNPs/CD-FA-CP and b) SeNPs/CD-FA-CP microflowers.	78
Figure 31 The capacity of guest molecules-loaded SeNPs/CD-FA-CP.	80
Figure 32 Cumulative drug release (%) of doxorubicin from doxorubicin-loaded SeNPs/CD-FA-CP microflowers.	82
Figure 33 The in vitro cell viability of KB cells incubated with free doxorubicin and doxorubicin-loaded SeNPs/CD-FA-CP microflower at different concentrations of doxorubicin for 72 h.....	84
Figure 34 Confocal laser scanning microscopy images of KB cells incubated for 6 and 12h at 37 °C with doxorubicin-loaded SeNPs/CD-FA-CF hybrid flower.....	86

CHAPTER 1

INTRODUCTION

1.1 Research background

Nanotechnology has grown high interest in cancer treatment and diagnostics. The size and shape of nanoparticles play an important factor of their biological activity especially for cancer [4]. Normally, the small size of nanoparticles is more active than the large size because of high surface area. However, the suitable size and shape is required to treat cancer for the intracellular uptake [5]. Selenium nanoparticles (SeNPs) have gathered a great deal of attention as potential cancer therapeutic agents and drugs carriers [6]. The synthesis of SeNPs is further more attractive because it shows outstanding photoelectric properties, high biological activity, low toxicity and novel remedial properties [7, 8]. Nevertheless, the low selectivity between cancer and normal cell and an easy aggregation of SeNPs greatly obstruct the potential of SeNPs as drug carrier. In our work, we introduced pullulan in the synthetic SeNPs process because of its distinguished properties: water solubility, non-toxicity, biocompatibility and low cost [9-11]. Pullulan can be easily derivatized in order to extend its applications by grafting different chemical structures onto its backbone [12-15]. Pullulan hydroxyls were used in numerous chemical reactions leading to a large number of derivatives. Regarding to drug delivery

applications, the use of pullulan derivatives with nonmetal nanoparticles (NPs) such as SeNPs, as an organic/inorganic hybrid material for cancer treatment has been rarely reported. Therefore, in this work we seek to design the pullulan molecule to provide the desired properties for the control of the shape and morphology of these hybrid materials. Many different studies have reported the use of solely organic materials such as chitosan, dextran and PEG-PCL block co-polymer for cancer treatment application [16, 17]. Although the encapsulation or conjugation of anticancer drugs with the polymers can stabilize and solubilize the drugs, the problems of small release and low loading of anticancer drugs were observed [18, 19]. In addition, inorganic materials and especially metal nanoparticles such as gold, silver and metal oxide (iron oxide and cerium oxide) have received much attention recently due to their use in cancer therapy as drugs delivery vehicles [20, 21] and as anticancer agents [22, 23]. However, the easy aggregation of nanoparticles was the main problem for their use alone. Thus, the combination of organic and inorganic components to form organic/inorganic hybrid materials can address the problems associated with the use of each component by itself.

In this work, we focused on the synthesis of hybrid material using the SeNPs as the inorganic material and pullulan as the organic material. The selectivity and stability of SeNPs should be improved by focusing on the modification of pullulan to stabilize the synthesized SeNPs and specifically target the cancer cells. Previous

studies suggested that the nanoparticles stability can be enhanced by fabrication with positive charge [24], while the selectivity can improve by surface functionalization with targeting molecule such as folic acid [6, 12, 14]. The FA-CP was introduced by quaternization to obtain the positive charge and functionalized folic acid (FA) on the pullulan chain. Furthermore, the β -CD was grafted on FA-CP to create CD-FA-CP functionalization in order to increase drugs loading capacity. The organic/inorganic hybrid material of SeNPs stabilized by pullulan derivatives were fabricated and intend to apply in biomedical applications, especially drug delivery system.

1.2 Research objectives

The aim of the present work is to design the pullulan derivatives and prepare the hybrid organic/inorganic material of SeNPS stabilized by pullulan and its derivatives using in drug delivery system for cancer treatment. The details of these objectives were described as follows:

1. To prepare the functionalized pullulan
2. To synthesize selenium nanoparticles by using pullulan and its derivative as a stabilizer
3. To evaluate an *in vitro* cytotoxicity of the obtained selenium nanoparticles

1.3 The expected beneficial outcomes

New selenium nanoparticles stabilized by pullulan derivatives having effectiveness to treat cancer cells will be obtained and being template for drug transport was explored.



CHAPTER 2

LITERATURE REVIEWS

2.1 Nanoparticles (NPs) and nanomaterials (NMs)

Nanotechnology is a known field of research which produced materials of various types at nanoscale level. Nanoparticles (NPs) are wide class of materials that include particulate substances, which have a size in the range of 10-1000 nm [25, 26] . Recently, the growth of research and applications in used of NPs and NMs has been increased, particularly as applied to biomedical area [27-29]. The types, size, shapes, and toxicity of NPs are and important tool to realize a number of their applications.

2.1.1 Types of nanomaterials

Most current NMs can be broadly organized into various categories depending on their morphology, size and chemical properties [30]. Based on the characteristics such as physical and chemical properties, some of the well-known classes of NPs are given as below.

(i) Carbon-based NMs

Generally, the component of these NMs contains carbon and their morphologies such as hollow tubes, ellipsoids or spheres are found. Fullerenes and

carbon nanotubes (CNTs) represent two major classes of carbon-based NPs. Fullerenes are hollow cages exclusively formed by carbon atoms which possess arranged pentagonal and hexagonal sp^2 hybridized carbon units. The well-known fullerenes consist of C_{60} and C_{70} . They have performed commercial interest because of their electrical conductivity, high strength, structure, electron affinity, and versatility [31]. CNTs take the form of cylindrical structure with 1–2 nm in diameter [32]. Although, CTs are strong, they are not brittle. They can be bent, and when released, they will spring back to their original shape. Their application can be used as actuators [33], nanoprobes and sensors [34], electronic devices [35], and catalysis [36].

(ii) Inorganic-based NMs

These NMs include metal, and nonmetal NPs and NMs. The well-known metal can be synthesized such as Au or Ag NPs. Due to the localized surface plasmon resonance (LSPR) characteristics, these NPs possess unique optoelectrical properties. The metal oxides such as TiO_2 and ZnO NPs, and semiconductors such as silicon and ceramics were developed and getting great attention of researchers due to their use in applications such as catalysis, photocatalysis [37, 38], photodegradation of dyes [39, 40], and electronic devices [41]. Interestingly, pure nonmetal NPs such as selenium nanoparticles (SeNPs) has not extensively studied. Thus, the synthesis of

SeNPs and its application were investigated and the deep information was detailed in section 2.3.1.

(iii) Organic-based nanomaterials

These include NMs made mostly from organic substance, excluding carbon-based or inorganic-based NMs. The noncovalent interactions are utilized for the self-assembly and design of molecules resulting in the transformation of the organic NMs into desired structures such as dendrimers [42], micelles, liposomes and polymer NPs [43].

(iv) Composite-based NMs

It can define as the combination of NPs and other NPs or NPs combined with larger or with bulk materials (e.g., hybrid nanofibers) or more complicated structures, such as a metal-organic frameworks. In addition, the composites may be any combinations of carbon-based, metal-based, or organic-based NMs with any form of metal, ceramic, or polymer bulk materials. The synthesis of these kinds material depends on depending on the required properties for the desired application.

2.1.2 Nanoparticles in biomedical applications

Nanoparticles possess unique properties that are being explored for biomedical and industrial applications. Important biomedical applications of NPs are in biosensors, hyperthermia therapeutic, photoimaging, and targeted drug delivery.

(i) Biosensors

The analysing biological samples were easily test by an analytical device such as biosensors. Biosensors convert chemical, biological or biochemical response into an electrical signal. It composes of three main components; bioreceptor, transducer, and electronic unit (contains the amplifier, processor and display). NPs can be used as bioreceptors which coated with a bioresponsive shell. The bioreceptor recognizes the target analyte/substrate of interest, the transducer then transforms the resulting signal into an electrical signal that is more easily quantified [44].

(ii) Hyperthermia therapeutic

Hyperthermia is a therapeutic technique that applies heat to the diseased or infected site with an increase of temperature to 41-46 °C. The cancerous cells are killed without damaging the healthy cells. This technique is often used in combination with radiotherapy and chemotherapy to enhance the efficiency of therapeutic treatment. Magnetic NPs such as Fe_3O_4 NPs are widely used for investigation due to their tunable magnetic properties and potential as diagnostic [45]. The development of the synthesized Fe_3O_4 NPs with different morphologies and surface chemistries affects the magnetic hyperthermia properties and heating efficiency of Fe_3O_4 based NPs [45, 46].

(iii) Optical imaging

Contrast agents are generally used in these bioimaging techniques in order to identify the organ or tissue of interest as well as identifying healthy tissue from diseased tissue. The most widely used NPs in optical imaging are semiconductor nanocrystals, known as quantum dots. The optical properties depend on the sizes which are unique in their applications to the efficient labelling of biomolecules and tissues. Semiconductor quantum dots are about 100 times brighter than traditional fluorescent, have narrow emission spectra and broader excitation than traditional organic dye molecules. Since the quantum dots share the similar excitation wavelength and the emission is size tunable, multiple color imaging with single excitation. The small size of quantum dots can penetrate deep to tissue/organs and emit the clear signal. Recently, gold nanoparticles (AuNPs) have been the popular choice for near IR emitting nanofluorophores since it is relative biocompatible and easy to synthesize [47, 48]. The surface plasmon resonance is dependent on the size of the NPs. Other types of gold nanomaterials such as gold nanorods and gold nanoshells were also popularly used in bioimaging because of its tunable surface plasmon bands and controllable position of the resonance by varying the synthesis conditions.

(iv) Targeted drug delivery

Besides the size and surface properties, the goal of nanoparticle drug delivery system is to direct the drug to the specific site where the tumor or infection are located. This system help to increase the amount of drug delivered at the site and minimize or avoids drug induced damage to healthy tissues. Therefore, coating specific targeting ligand(s) on the surface of NPs is the most common strategy (Figure 1). These targeting ligands could be in the form of small molecules, peptides, antibodies, and designed proteins [49, 50]. The small organic molecules are the most commonly used as targeting agents due to easy preparation, stability, and control of conjugation chemistry. For example, biotin (vitamin H) has been widely used for conjugation with nanoparticles due to very high affinity for streptavidin [51]. Folic acid (vitamin B9) has excessive affinity for folate receptor and thus has been investigated for targeting many types of cancers where folate receptors are highly expressed [52].

In this research, the modification of NPs surface by the anticancer targeting; folic acid was focused to aim the targeted drug delivery.

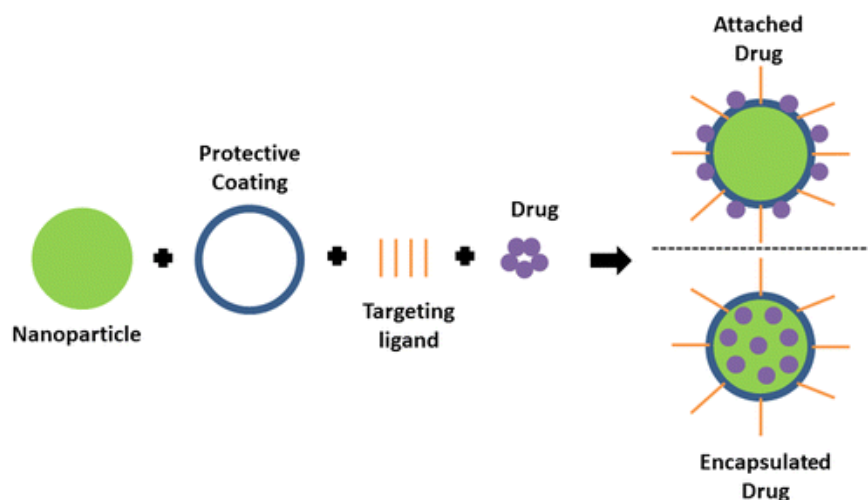


Figure 1 Schematic of drug loading options in targeted drug delivery [27].

2.1.3 SeNPs and the application for drug delivery

Selenium (Se) is an element that is widely used for photoelectrical materials, semiconductor, solar cell, rectifiers, photographic exposure meters, and xerography [53]. Selenium in pharmaceutical was first discovered as a trace of dietary prevented liver necrosis in vitamin E deficient rats [54]. It is also essential for humans to establish more than two dozen selenoproteins that play critical roles in reproduction, thyroid hormone metabolism, DNA synthesis, antioxidant defense systems, and immune function [53, 55].

Recently, SeNPs have been developed for medical diagnostics application. There are many researchers gained the attention in pharmaceutical field. It has been found that selenium can prevent free radicals from damaging cells and tissues and also can reduce the cancer mortality and incidence [7, 56, 57]. To decrease toxic side

effect and dosage of cancer drugs and increase treatment efficacy and specific target location, the surface of SeNPs was fabricated for drug delivery system. Zheng and coworkers, 2011 prepared sialic acid (SA) surface-decorated Se-NPs (SA-Se-NPs) because SA shows ability to bind selectins that exist in the plasma membrane cancer cells [58]. The results show that spherical SA-SeNPs improved cancer-targeting and cell-penetrating abilities. Moreover, the cellular uptake and cytotoxicity of SeNPs in HeLa cells were SA significantly enhanced by SA. Attractively, studies have found that higher positive charge on nanoparticles surface presented stronger affinity for the negatively charged cell membrane, as a result in increasing cellular uptake [59]. Yu and coworker, 2012 suggested that the positive charge of the NH_3^+ group on the outer surface of SeNPs by chitosan decoration can enhance the cellular uptake and cytotoxicity of SeNPs in cancer cell [24]. Moreover, the modified surface nanoparticles by targeting ligand can also help to increase uptake efficiency of nanomaterials. Folic acid (FA) is a targeting ligand for cancer therapy which can bind with folate receptor (FR) overexpressing on membrane in many tumors [60-62]. Pi et al., 2013 reported that folic acid protected/modified selenium nanoparticles (FA-SeNPs) improved the cellular uptake by binding with FR and moved inside the cancer cell by endocytosis process [62]. Those synthesized material targeted the mitochondria of cancer cell and induced apoptosis.

Therefore, the modification of biopolymer chain by positively charge and targeting ligand is an alternative way to both decorate surface and stabilize SeNPs for cancer cell treatment.

2.2 Polysaccharide pullulan, its functionalization and applications

Polysaccharides are carbohydrate polymers in which monosaccharide $((\text{CH}_2\text{O})_n)$ units are covalently joined by an O-glycosidic bond in either a branched or linear configuration. Polysaccharide can be a homopolysaccharide, in which all the monosaccharides are the same, or a heteropolysaccharide in which the monosaccharides vary. Depending on which monosaccharides and which carbons in the monosaccharides are connected, polysaccharides take on a variety of forms. Due to their structure, polysaccharides can have a wide variety of functions in nature. Some polysaccharides serve as stores of energy, as in glycogen (branched polysaccharide of glucose), some for sending cellular messages and others as a structural component providing support to cells and tissues, as in cellulose (linear polysaccharide of glucose).

Polysaccharides are produced from different sources obtained from microorganisms, plants, and animals. Polysaccharides made by microorganisms are secreted from the cell to form a layer over the surface of the organism. Microbial polysaccharides such as xanthan, xylinan, gellan, curdlan, pullulan, dextran, scleroglucan, schizophyllan, and cyanobacterial polysaccharides are available in

commercial using for food, pharmaceutical, and medical applications [63-65]. Polysaccharides in plants such as starch (a polymer of glucose, being found in the form of both amylose and the branched amylopectin) and cellulose are well known plant polysaccharides which used as a storage and support polysaccharide in plants. Chitin, an example of animal polysaccharide, is the exoskeleton of many arthropods, and is the main component of cell walls in fungi, radulas of mollusks etc. The utilization of polysaccharide should consider the structure, properties, production and modification to potentialize its applications. Polysaccharides will therefore become increasingly important in various fields since they possess unique structures and characteristics that are quite different from the synthetic polymers.

2.2.1 The properties of pullulan

Of the many kinds of polysaccharides, pullulan is one of the polysaccharides that have found a wide range of applications in the food, pharmaceutical and other industries. This polymer is consisting of maltotriose units connected by an α (1 \rightarrow 4) glycosidic bond, whereas consecutive maltotriose units are connected to each other by an α (1 \rightarrow 6) glycosidic bond (Figure 2). Pullulan powder is white to off -white, odorless, and tasteless which forms a viscous non-hygroscopic solution when dissolved in water at 5-10%. It is highly soluble in water, dilute alkali, insoluble in alcohol and other organic solvents except dimethylsulphoxide and formamide. As pullulan is highly water soluble, non-toxic, non-mutagenic, non-carcinogenic and

edible [66] so it can be used as a drug carrier and it helps in controlled release of drug in plasma. Furthermore, pullulan has a considerable mechanical strength and other functional properties such as adhesiveness, film formability, enzymatically-mediated degradability [67]. Pullulan is biodegradable, impermeable to oxygen, and is not attacked by the digestive enzymes of the human gut, hence can be used as carrier for oral delivery of drug.

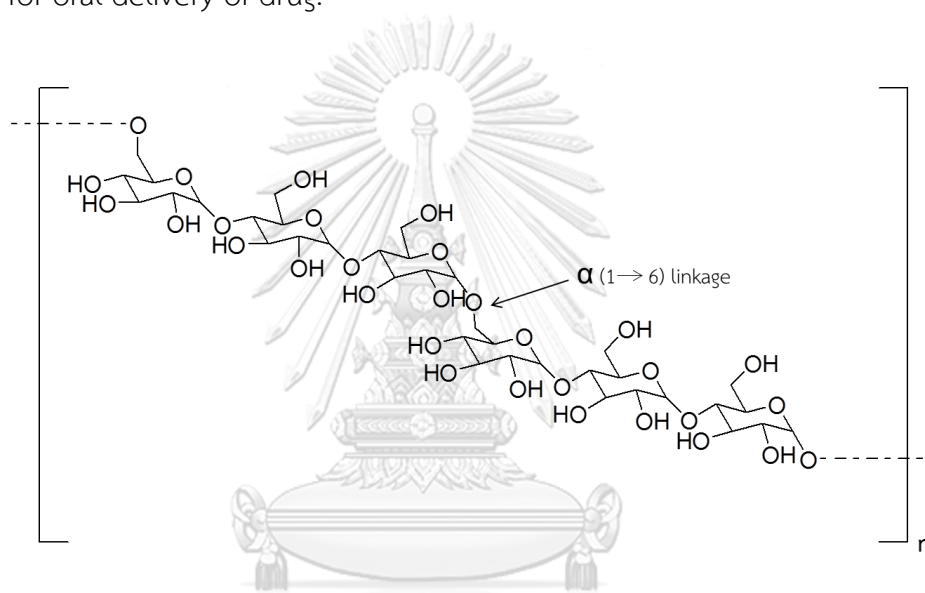


Figure 2 Pullulan structure.

2.2.2 The functionalization of pullulan and its applications

The structural features of the polysaccharides, such as degree and steric configuration of substitutions, linkages of monosaccharides, and molar mass and its distribution play a key role on their physicochemical (e.g. solubility and fluid capability) and bioactive properties [68]. Thus, the modification of native polysaccharides is important to extend their applications in both traditional and

newly explored biomedical areas, such as tissue engineering, controlled drug delivery and release, and wound healing/dressing.

Focusing on pullulan, its structure contains large number of hydroxyl group which is easily to modify, thus the chemically modified to produce derivatives is developed and their applications were also studied by various groups. The derivertization of pullulan with targeting agents was obtained which were used to produce self-organized drug loaded nanogels for receptor mediated cancer cells targeting [69, 70]. Cationic pullulan are reported previously by other groups [15, 71, 72]. For example, Marieta Nichifor et al., 2010 synthesized cationic modified pullulan by chemical modification of the quaternary ammonium reagents. The new cationic polysaccharides have self-assembling properties and potential application as hipolipemic drugs, flocculants, drug delivery systems or antibacterial agents [72]. In addition, graft-copolymerization of pullulan with poly(ethylene glycol) PEG, poly(L-lactide) PLLA and poly(N-isopropylacrylamide) PNIPAAm have been reported [73-75]. As studied by Gheorghe et al, 2008, poly(Nisopropylacrylamide-co-acrylamide) was grafted onto pullulan microspheres in order to generate temperature sensitivity [76]. Then, the pH-sensitive units ($-\text{COOH}$) were introduced by reaction between the remaining $-\text{OH}$ groups of pullulan with succinic anhydride. The grafted pullulan microspheres showed more hydrophilic than pullulan microspheres leading to increase their swelling degree significantly. Thus a pH and temperature sensitive

pullulan microspheres can be prepared for controlled release of drugs. In summary, pullulan is a unique polysaccharide that can be functionalized to obtain the desirable properties and was allowed to be utilized in many different ways with a variety of potential industrial and medical applications.

2.3 Polysaccharide stabilized nanoparticles

An easy aggregation and agglomeration of nanoparticles became the significant problem that has recently been recognized because of some toxicity conducting. Many types of NPs are aggregated in aqueous biological matrices, such as in phosphate buffered saline and cell culture media, due to the high ionic strength and neutral pH. Thus, the use of polysaccharides as a stabilizing agent was explored for the prevention of NPs aggregation [77-79].

The well-known polysaccharide, chitosan has been used as a protecting polymer for the preparation NPs [78, 80-82]. Since the use of chitosan as reducing and stabilizing agents to prepare AuNPs was reported by Huang [78, 80], many groups have incorporated chitosan into AuNPs preparation and applications. For example, Zhu and Radhakumary detailed the preparation of AuNPs with chitosan as a reducing agent and stabilizer of the gold salt through thermal method [83]. Yong Jin et al., 2013 created an efficient route for the preparation of AuNPs in chitosan which was reduced by atmospheric plasma at room temperature [81]. The synthesized process took only minutes and produced high stability. Pullulan and its derivatives were

developed for synthesized AuNPs [84, 85]. It used as a reducing/stabilizing/capping agent of AuNPs with prolonged stability. Monodispersed AuNPs@pullulan can be utilized in drug delivery application due to high cellular uptake, biocompatibility and non-cytotoxicity.

In this work, the stabilized SeNPs was focused due to an easy aggregation. To increase the stability of SeNPs, the stabilizer is required in the chemical reduction methods based on solution-phase procedures. Zhang and coworkers, 2004 introduced the use of renewable raw materials to be a stabilizer for SeNPs to obtain biocompatible, biodegradable, non-toxic and environmental friendly SeNPs [53]. SeNPs were synthesized by reducing selenious acid solution with ascorbic acid in the presence of polysaccharides, such as chitosan (CS), konjac glucomannan (KGM), acacia gum (ACG), and carboxymethyl cellulose (CMC). The dispersed particles were stable for more than 6 months in the polysaccharide solutions. Moreover, Zhang and coworkers synthesized the SeNPs by using natural hyperbranched polysaccharide (HPB) as the stabilizer and capping agent [1]. They suggested that the spherical SeNPs formed nanocomposites (Se-HPB) by binding with HPB as shown in Figure 3 and were stable for over one month.

Regarding drug delivery applications, the use of pullulan and derivatives with SeNPs for cancer treatment has not been reported. Therefore, in this work we seek

to design the pullulan molecule to provide the desired properties for prevent an aggregation of SeNPs.

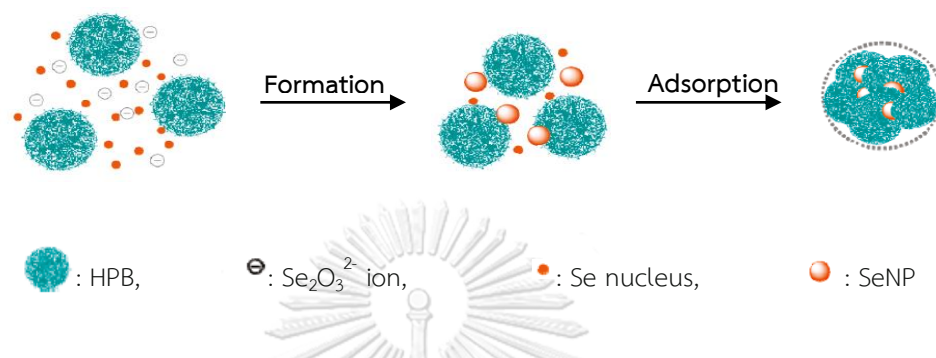


Figure 3 Schematic model of the Se-HBP nanocomposites during the formation process [1].

2.4 The control of the shape and morphology

One of important goals in nanoparticle synthesis is the control of particle size, shape and morphology because many applications of nanomaterials derive from properties that are strongly influenced by the size and shape of the particles. Capping agents play a power role in the synthesis of NPs. It can stabilize and functionalize NPs to control morphology, size and protecting the surface thereby preventing aggregation. Many commercial surfactants can be used as capping agents but most of them are hazardous to the environment since there are difficult to remove and degrade [86, 87]. Therefore, different types of molecules such as

biomolecules (e.g. amino acid) and polysaccharides that could act or be used as classified green capping agents have been discussed with their potential role.

Chen et al., 2009 studied the controlled synthesis of selenium nanospheres and nanorods using L-cysteine acted as both the reducing agent and soft template under mild solution method [2]. They suggested that the different reactant concentration ratios, reaction times, and ultrasonication effect on morphologies and crystalline phases of the products. The morphologies and crystalline phases of SeNPs were not changed by varying the concentration ratio of L-cysteine to selenious acid, but different in diameter. In addition gray rod like t-Se was produced when extended the ultrasonication time. A model of “sphere breaking-oriented aggregation-growth” is suggested to explain the possible formation mechanism of selenium nanorods. First, the spherical SeNPs were formed by the action of L-cysteine. Second, the selenium nanospheres were broken to the smaller size when prolonged the ultrasonication time and then some nanoparticles arranged in a direction by oriented aggregation. The high energy on its surface induced an annular edge of particles the initiation spot, and further directional growth to form rod-like product (Figure 4).

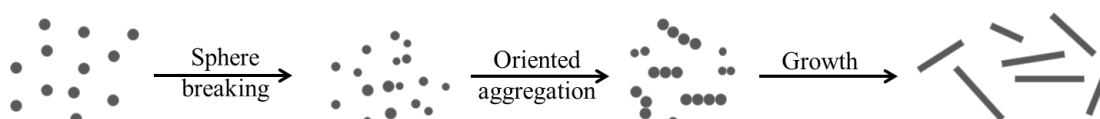


Figure 4 Diagram of possible mechanisms for selenium nanorods [2].

Green synthesis of selenium nanoparticles was prepared. Kong et al., 2014 prepared spherical SeNPs from the reduction of selenious acid by ascorbic acid with the stabilization of gum arabic (GA) to prevent aggregation. GA with the large number of terminal hydroxyl group can attach to the SeNP surface in order to be like a capping agent that making GA-SeNPs remained stable for at least 30 days [88]. The nanoparticles show the size in the range of 30-50 nm. Recently, the cubic-like structure of selenium nanoparticles was reported by controlling the shape of SeNPs with the stabilizing agent which was a functionalized molecule [3]. The assembly process of SeNPs into cubic-like structures when the SeNPs were stabilized with folic acid-gallic acid-N,N,N-trimethyl chitosan (FA-GA-TMC) was carried out. This assembly was attributed to intermolecular interactions, including electrostatic interactions, π - π stacking and hydrogen bonding among the nearest particles to achieve the lower energetically attachment, leading to the formation of cubic-like structures. The proposed mechanism for the formation of cubic-like SeNPs was shown in Figure 5.

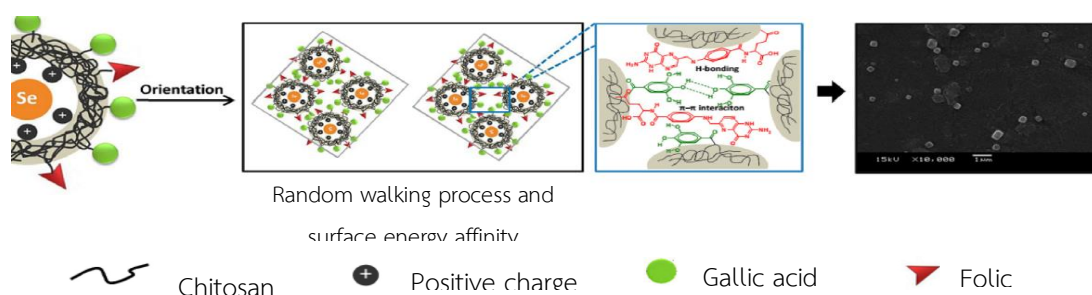


Figure 5 The proposed mechanism for the formation of cubic-like SeNPs [3].

In this work, the fabrication of SeNPs stabilized by pullulan derivatives was reported. The size, shape, and morphology of the synthesized SeNPs are studied and the results are described in Chapter 4.



CHAPTER 3

MATERIALS AND METHODS

3.1 Materials

Pullulan with average molecular weight, Mw, of 50–70 kDa and (3-chloro-2-hydroxypropyl) trimethyl ammonium chloride (Quat-188) were provided by TCI, Japan. Folic acid, N,N-Dicyclohexylcarbodiimide (DCC), 4-Dimethylaminopyridine (DMAP), sodium selenite, L-cysteine hydrochloride and MTT (3-(4,5-dimethylthiazol-2-yl)-2,5-diphenyltetrazolium bromide) dye were purchased from Sigma-Aldrich Co., USA. Cellulose dialysis tubing (Membrane Filtration Products, Inc., USA) with the molecular weight cutoff of 12–14 kDa was used to purify all modified pullulan samples. The doxorubicin hydrochloride anticancer drug was obtained from Beijing Packbuy M&C Co., Ltd.

3.2 Synthesis and characterization of pullulan derivative

3.2.1 Synthesis and characterization of folic acid decorated cationic pullulan (FA-CP)

The cationic pullulan (CP) was synthesized by dissolving 1 g of pullulan in 10 mL deionized (DI) water. NaOH solution (0.25 g in 3.5 mL) was added to the pullulan solution and continuously stirred for 30 min at 60 °C. Then, Quat-118 (0.25, 0.5, and

0.7 g) used as the quaternizing agent was added dropwise into the reaction mixture and allowed the reaction at 60 °C for 24 h. The mixture was neutralized before dialysis with distilled water for 2 days and the dialyzed solution was then concentrated under vacuum using a rotary evaporator. The CP product was collected and dried at 60 °C in an oven.

To synthesize FA-CP, 1 g of CP was dissolved in 30 mL of DMSO under stirring at room temperature until the clear solution was produced. FA (50, 200, and 500 mg) was activated in 5 mL DMSO with 60 mg of DCC and 20 mg of DMAP for 60 min at room temperature. The FA solution was added into the pullulan solution and the reaction proceeded at room temperature for 24 h. The mixture was dialyzed against a phosphate buffer with pH 7.4 for 3 days and then dialyzed continually against DI water for several days. The dialyzed solution was then concentrated and dried for several days at 60 °C in an oven. The synthesized products were characterized by Fourier-transform infrared spectroscopy (FTIR), ¹H nuclear magnetic resonance spectroscopy (NMR), and differential scanning calorimeter (DSC).

FTIR analysis was conducted using Nicolet6700 FT-IR spectrophotometer in the range of 4000-400 cm⁻¹ to investigate the functional groups of synthesized products. ¹H NMR was performed using 400 MHz NMR spectrometer (Varian Mercury 400 MHz Spectrometer) by dissolving the sample in deuterium dioxide (D₂O) to confirm the structure of products. The ¹H NMR spectra were used to determine the

degree of quaternization (%DQ) of pullulan and the degree of substitution (%DS) of FA by comparing the ratio of the areas under the proton peaks using Equation (1) for the %DQ [89] and Equation (2) for the %DS of FA [90].

$$\%DQ = \left[\frac{\text{methyl proton}}{\text{anomeric proton}} \times \frac{1}{9} \right] \times 100 \quad (1)$$

$$\%DS_{FA} = \left[\frac{\text{phenyl proton}}{\text{anomeric proton}} \times \frac{1}{2} \right] \times 100 \quad (2)$$

DSC (Seiko SII Exstar6000) was used to determine the thermal transition of modified samples. The experiment was done under N₂ gas atmosphere from 35 to 250 °C at a heating rate 10 °C/min.

3.2.2 Synthesis and characterization of β-cyclodextrin conjugated FA-CP (CD-FA-CP)

6-O-Monotosyl-6-deoxy-β-cyclodextrin (CD-OTs) was synthesized by following the method that was reported by Tripodo et. al., 2013 [91]. In brief, 35.2 mL (88 mmol) of aqueous 2.5 N NaOH was added into a suspension of 10 g (8.8 mmol) of β-CD in 90 mL DI water. After 30 min, 2.52 g (13.22 mmol) of p-toluenesulfonyl chloride was added and continuously stirred for 5 h at room temperature (400 rpm, magnetic stirrer). After reaction, the solution was filtered to remove the residual p-toluenesulfonyl chloride and neutralized by using HCl. In this step, the white precipitation of CD-OTs was observed and collected on filter paper. After washing

with 3x30 mL water and 30 mL acetone, the product was dried at 60 °C in an oven. The synthesized product was characterized by ^1H NMR, FTIR and mass spectrometry.

One gram of FA-CP was dissolved in 10 mL DI water and NaOH solution (0.25 g in 5.0 mL DI water) was then added to the FA-CP solution. The solution was left for 30 min at 60 °C, then the suspension of CD-OTs (0.5 g in 10 mL DI water) was added dropwise into the reaction mixture and continually stirred at 60 °C for 24 h. The mixture was neutralized by using HCl before dialysis with distilled water for several days using a dialysis membrane (molecular weight cut-off 12-14 kDa). The product of CD-FA-CP was collected and dried at 60 °C in oven. The synthesized product was characterized by ^1H NMR and DSC.

3.3 Synthesis and characterization of SeNPs stabilized by pullulan and derivatives

The SeNPs were synthesized by using pullulan and its derivatives as a stabilizer. In brief, 0.5 mL of 0.5% (w/v) pullulan or derivatives and 0.5 mL of 25 mM Na_2SeO_3 were mixed by stirring at 60 °C for 15 min. Cysteine hydrochloride solution (125 mM, 0.10 mL) was then added dropwise into the mixture which the molar ration of Na_2SeO_3 to cysteine was 1:1 at this condition. The reaction was stirred for 1 h and the synthesized SeNPs were rapidly cooled down by putting in water at room temperature. The samples were characterized by scanning electron microscope

(SEM), transmission electron microscopy (TEM), dynamic light scattering (DLS), zeta potential, and X-ray diffraction (XRD).

In this study, the effect of the Na₂SeO₃ to cysteine molar ratio (1:0, 1:1, 1:2 and 1:4), type of stabilizers (P, PQ, FA-CP and CD-FA-CP), and the stabilizer concentration (0.023, 0.045, 0.23, 0.45, and 0.91% w/v) were evaluated to study their ability to control the size and morphology of SeNPs.

3.4 Drug loading and release study

In this work doxorubicin was used as a model anticancer drug. Doxorubicin aqueous solution (50 μL, 1 mg/mL) was added into the synthesized SeNPs solution. The mixture was stirred gently for 24 h at room temperature and was then collected by centrifugation. The loading capacity was investigated by fluorescence spectroscopy at the excitation wavelength of 480 nm. The loading content was calculated according to Wang et al., 2014 [92]:

$$\text{Loading capacity (mg/g sample)} = \left[\frac{m-CV}{W} \right] \times 100 \quad (3)$$

where m (mg) is the total amount of doxorubicin added into the solution, C (mg/mL) and V (mL) are the doxorubicin concentration and volume of the supernatant, respectively, and W (g) is the weight of the stabilized SeNPs.

The release behavior of doxorubicin was studied by dissolving doxorubicin - loaded SeNPs in 1 mL of phosphate buffered saline (PBS, pH 7.4) and then

transferring the obtained mixture into dialysis bags. The prepared sample was immersed in 29 mL of buffer solution and incubated at 37 °C. The concentration of doxorubicin in the released buffer was detected by fluorescence spectroscopy as previously described.

In this study, other drugs; curcumin, and methylene blue were used to investigate the ability of SeNPs stabilized by CD-FA-CP as the universal template drug loading. The loading capacity was investigated by UV-Vis spectroscopy at the wavelength of 430 and 663 nm for curcumin and methylene blue, respectively.

3.5 Cytotoxicity study

Cancer cells or normal cells are seeded in 96-well tissue culture plates at a concentration of 5,000 cells/well and incubated at 37 °C for 24 h incubation. Medium containing different concentrations of samples were added to the cells, followed by 72 h incubation. Cell viability is determined by measuring the ability of cells to converse 3-(4,5-dimethyl thial-2-yl)-2,5-diphenyltetrazolium bromide (MTT) to a purple formazan dye. After incubation, 10 μ L/well of MTT solution (5 mg/mL) is added and incubated for 4 h. The medium is removed and replaced with DMSO (150 μ L/well) to dissolve the formazan salt formed. The color intensity of the formazan solution, which is indicated to the number of viable cells, is measured at 540 nm using a multimode microplate reader.

3.6 Detection of apoptotic/necrotic cells (annexin-V/propidium iodide assay)

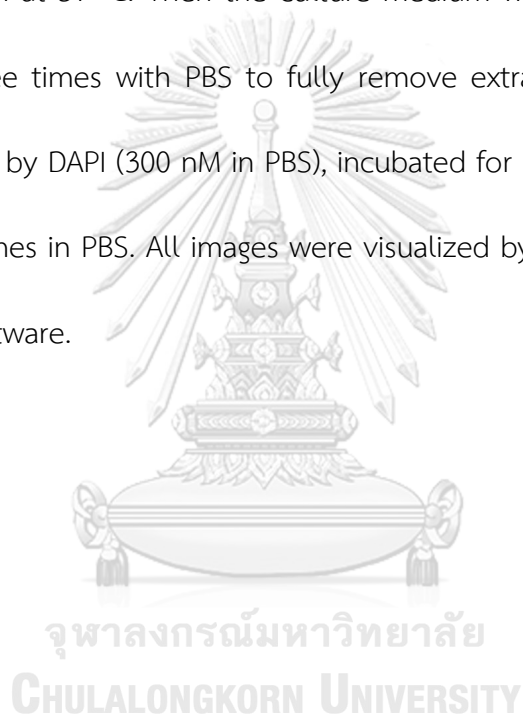
KB cells were treated with different concentration doxorubicin-loaded SeNPs and incubated for 24 h (according to the cell viability assay). Apoptotic/necrotic cells were detected by Annexin-V/propidium iodide (PI) assay according to the manufacturer's instructions (ImmunoTools, Germany). Briefly, after the treatment, the cells were washed with PBS and re-suspended in 100 μ L of binding buffer (10 mM HEPES pH 7.4, 140 mM NaCl, 2.5 mM CaCl_2) and incubated with 5 μ L of Annexin V-FITC and 5 μ L of PI at room temperature in the dark for 30 min. Then, 400 μ L of the binding buffer was added and the cells were analyzed using a FC500 flow cytometer (Beckman Coulter, USA). FlowJo V10 analysis software was used to calculate the percentages of apoptotic/necrotic cells (Annexin-V+/PI+).

3.7 Determination of intracellular Se concentration

Intracellular Se concentration was determined by the ICP-OES method [24]. Briefly, KB cells were seeded into 6-well plates at 10^6 cells/well (5 mL) and allowed to attach for 24 h. SeNPs stabilized by pullulan and derivatives was added and incubated for 24 h at 37°C. At the end of the incubation, the medium was removed from the wells and the cells were rinsed three times with PBS to remove the nanoparticles outside the cells. The collected cells were digested with 2 mL of concentrated nitric acid and 1 mL of H_2O_2 for 3 h. The digested solution was reconstituted to 10 mL with Milli-Q H_2O and used for ICP-OES analysis.

3.8 Cellular uptake assays by confocal laser scanning microscope

Confocal laser scanning microscope (CLSM, Olympus FV1000, Tokyo, Japan) was used to observe the cellular uptake of doxorubicin-loaded SeNPs stabilized by CD-FA-CP (SeNPs/CD-FA-CP@DOX). KB cells which had been cultured in a confocal dish were incubated with SeNPs/CD-FA-CP@DOX at doxorubicin concentration with 2 μM for 6 and 12 h at 37 °C. Then the culture medium was removed and the cells were washed three times with PBS to fully remove extracellular doxorubicin. The cells were stained by DAPI (300 nM in PBS), incubated for 5 min and then rinsed the sample several times in PBS. All images were visualized by CLSM and analyzed with image analysis software.



CHAPTER 4

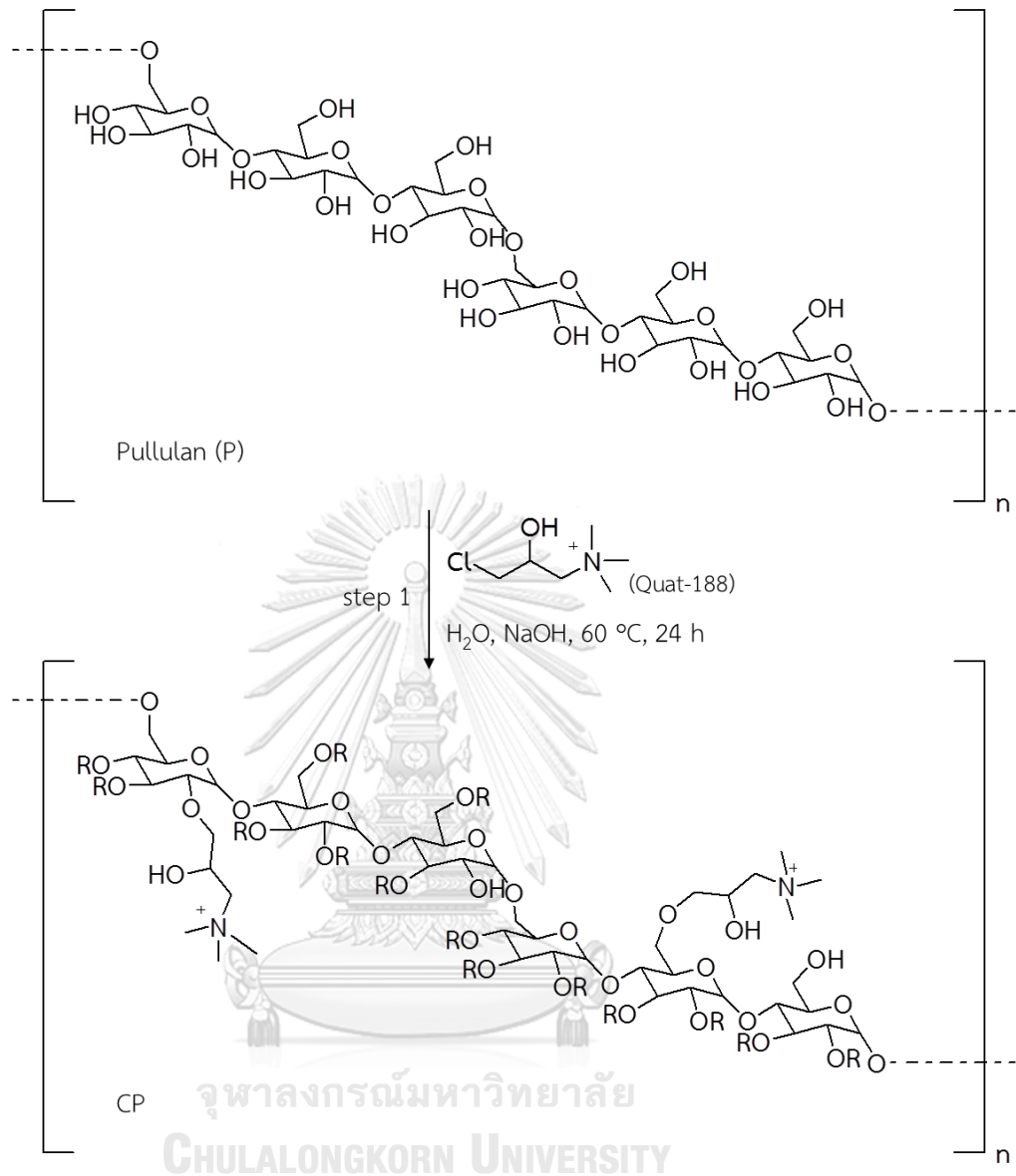
RESULTS AND DISCUSSION

Nanotechnology has raised high expectation in cancer treatment and diagnostics, and SeNPs have exhibited a great attention as potential cancer therapeutic agents and drugs carriers [24, 93, 94]. Recently, the use of SeNPs as carriers of pharmaceutical agents to enhance their anticancer was reported [93]. However, the limitation in drug delivery system which is low cellular uptake, lack of targeting and easy aggregation of SeNPs still existed. To solve these problems, in this research, the decoration of SeNPs with the aim of increase the cellular uptake, enhancement the selective killing abilities against cancer cells and preventing aggregation was focused. The pullulan derivatives were chemically designed to be a stabilizer for the preparation of SeNPs by introduction the positive charge and cancer targeting molecule such as folic acid (FA) for increasing cellular uptake and use as a cancer-targeted drug delivery system for doxorubicin. In addition, the functionalized pullulan chain with β -cyclodextrin was done to increase drug loading capacity. Herein, two major types of pullulan derivatives; folic acid decorated cationic pullulan (FA-CP) and β -cyclodextrin conjugated folic acid decorated cationic pullulan (CD-FA-CP) were synthesized and use as stabilizer for SeNPs.

Part A: the use FA-CP derivative as a stabilizer

4.1 Synthesis and characterization of FA-CP

Polysaccharides are biomaterials which are widespread in nature. Their structures, functionalities, and properties make them attractive molecules for various applications, particularly the biomedical area. In order to use polysaccharides for specific purposes, it is sometimes preferable to design their partial structures by chemical functionalization to establish the desirable properties. In this work, pullulan derivatives; CP and FA-CP were synthesized which depicted in step 1 and 2 of Figure 6. The positive charge was conjugated to produce cationic pullulan, CP and FA-CP was obtained when FA was decorated on CP.



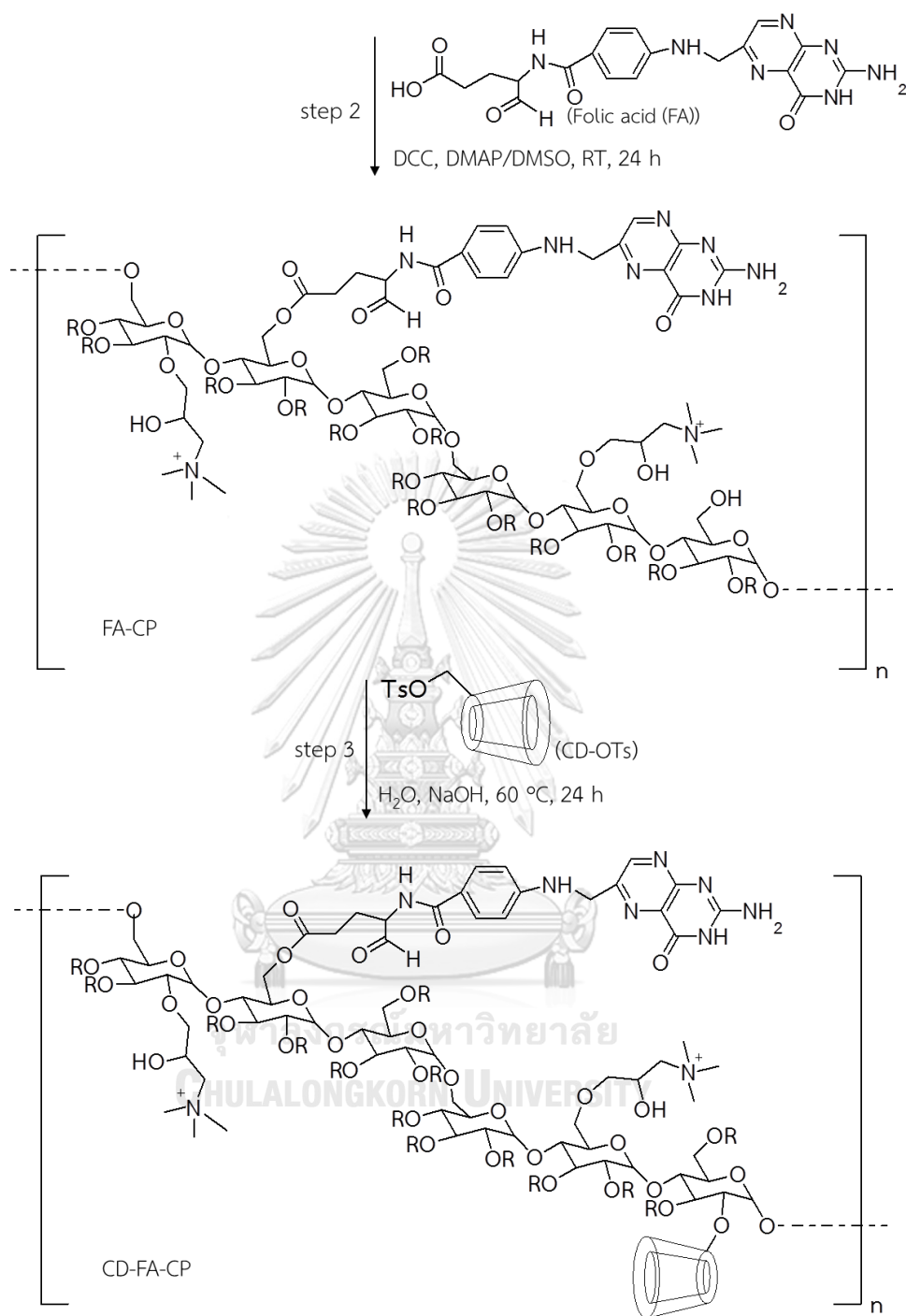


Figure 6 Schematic presentation of the synthesis of CP (step 1), FA-CP (step 2) and CD-FA-CP (step 3).

The structure of polysaccharide pullulan consists of three α -1,4-linked D-glucopyranose units (maltotriose) that are repeatedly linked by α -1,6-glycosidic bonds. The spectrum of original pullulan (Figure 7a) showed the three distinct resonances at 5.22, 5.17 (α -1 \rightarrow 4-Glc), and 4.76 ppm (α -1 \rightarrow 6-Glc) which were corresponded to anomeric protons of pullulan [95, 96]. Figure 7b, the CP product from quaternization of pullulan revealed a new proton peak at 4.25 and 3.03 ppm assigned to the methine proton and the methyl proton from Quat-188, respectively [72]. The existence of FA molecule in FA-CP derivative was confirmed by the weak resonance signals of aromatic protons of FA which were appeared at 6.7-7.6 ppm [97, 98] with the changing of coupling constant from original FA (Figure 7c). In addition, the degree of quaternization (DQ) of CP and the degree of substitution (DS) of FA on CP were determined from the ^1H NMR spectra. According to Equation (1), the DQ with different concentration of Quat-188 using was summarized in Table 1. An increasing of quaternizing agent tends to increase the DQ because there are more molecules of Quat-188 to substitute on pullulan. However, the limitation of Quat-188 amount was observed when increase the amount of Quat-188 to 0.7 g/1 g of pullulan. The reason behind that maybe due to the steric hindrance provided by high amount of molecule itself to limit the mobility of other molecules close to the reaction site [99]. Thus, the CP with the range of 11.2-16.6 %DQ was chosen for the preparation of FA-CP. The DS of FA (DS_{FA}) which was calculated by Equation (2) was showed in

Table 2. Similarly, the increasing of FA amount provided an increased trend of DS_{FA} . The pullulan derivative with 3.7-6.7 % DS_{FA} was selected because higher amount of FA did not significantly increase % DS_{FA} . Therefore, the FA-CP with 11.2-16.6 %DQ and 3.7-6.7 % DS_{FA} was used for further experiments.

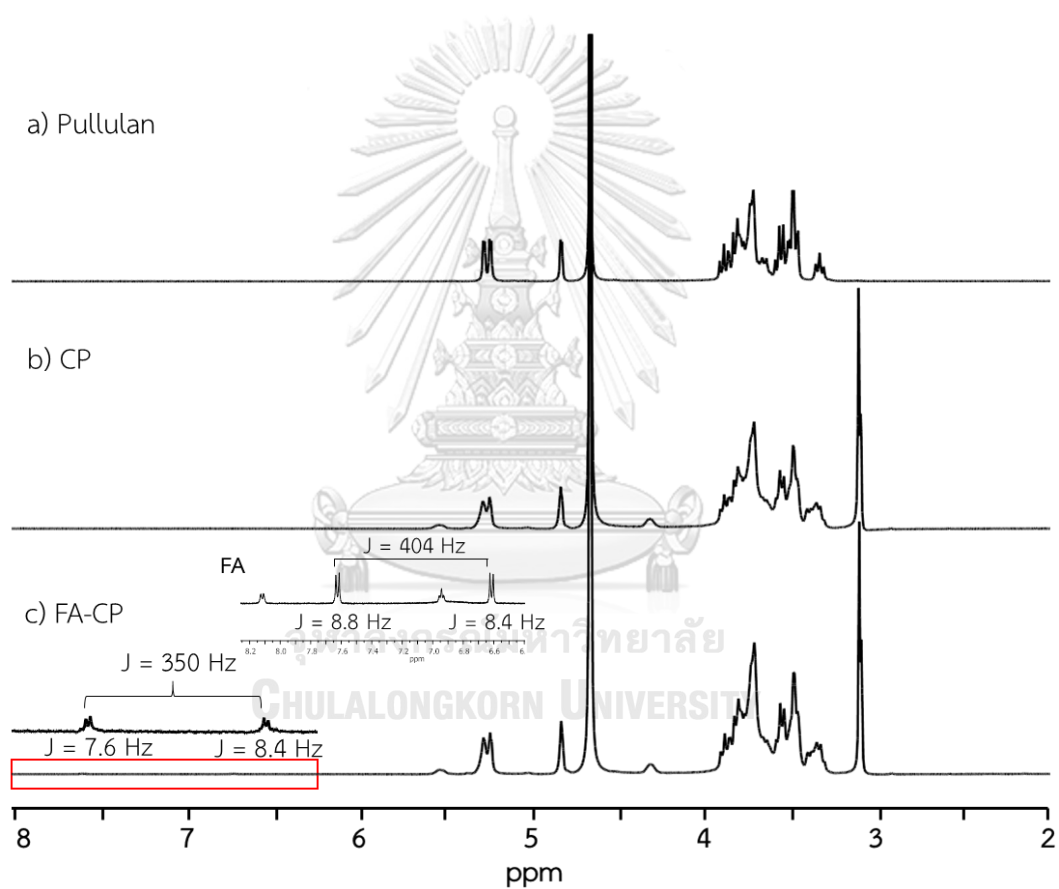


Figure 7 ^1H NMR spectra of a) pullulan, b) CP and c) FA-CP.

Table 1. The degree of quaternization of cationic pullulan

Amount of Quat-188 (g)/1 g of pullulan	Range of %DQ*
0.25	3.9-6.3
0.50	11.2-16.6
0.70	8.7-13.5

* Three times experiment

Table 2. The degree of substitution of folic acid on cationic pullulan

Amount of FA (mg)/1 g of CP	Range of %DS _{FA} *
50	0
200	3.7-6.7
500	6.5-9.3

* Three times experiment

IR spectra from Figure 8a and b confirmed the linkage between pullulan and Quat-188 as revealed by the C–O bond at 1640 cm^{-1} . The intensity at 1477 cm^{-1} is attributed to C–H stretching in the methyl group of ammonium from Quat-188. Moreover, the vibration at 1576 cm^{-1} was assigned to the N–H bond of quaternary

amine. The IR spectrum of FA-CP presenting in Figure 8c showed a new absorbance peak at 1602 cm^{-1} of aromatic C=C and 1483 cm^{-1} of C-C stretching in the aromatic ring of FA [95]. It can be concluded that the quaternization of pullulan and the derivatization of pullulan by FA were successful.

4.2 Synthesis and characterization of SeNPs stabilized by FA-CP

In the preparation process, SeNPs were synthesized using pullulan and derivatives as the stabilizer; 0.5 mL of 0.5% (w/v) pullulan derivatives and 0.5 mL of 25 mM Na_2SeO_3 are mixed by stirring at $60\text{ }^\circ\text{C}$ for 15 min. Then, 0.10 mL of cysteine is added dropwise into the mixture, and the pH of the solution decreased from 9.0 to 3.5. After the addition of cysteine to the colorless SeO_3^{2-} solution, the color of the solution suddenly changed to orange due to the formation of SeNPs (Figure 9). The mixture was allowed to remain at $60\text{ }^\circ\text{C}$ for 60 min and was then rapidly cooled down to room temperature.

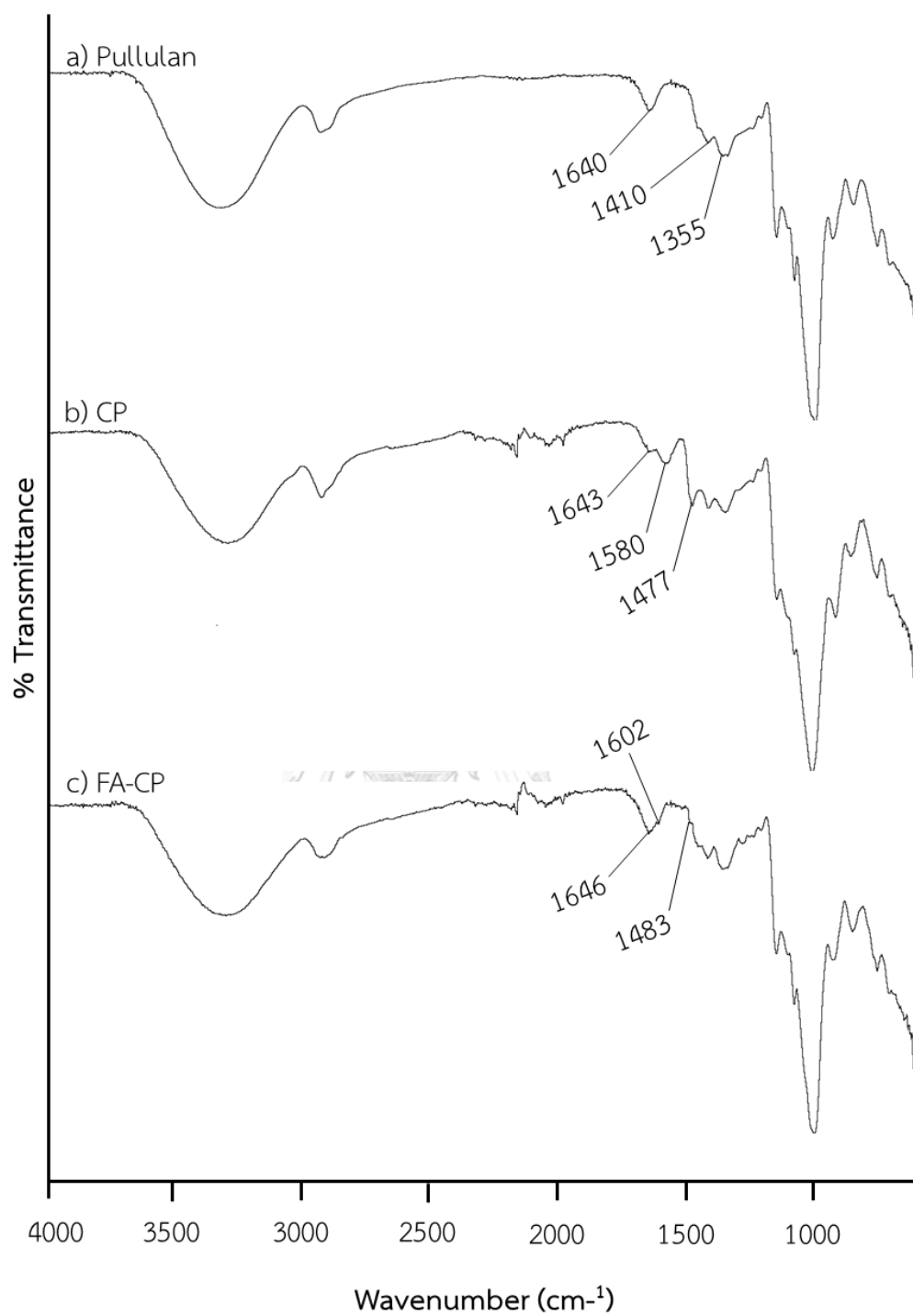


Figure 8 FTIR spectra of a) pullulan, b) CP and c) FA-CP.

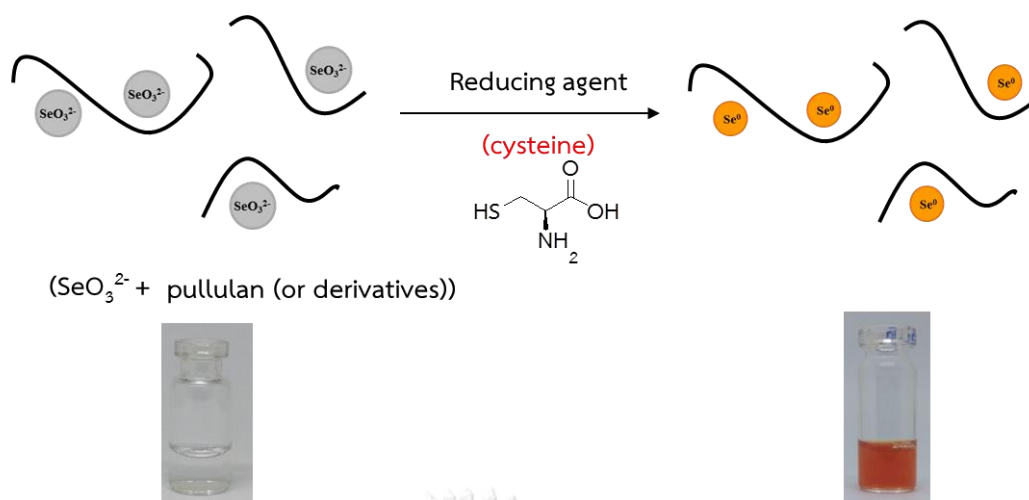


Figure 9 Schematic presentation of the synthesis of SeNPs.

4.2.1 Effect of cysteine concentration

Figure 10a-d reflects the effect of different concentration ratios of sodium selenite to L-cysteine (1:0, 1:1, 1:2, and 1:4, respectively) on the morphology of selenium when using FA-CP as a stabilizer. The prepared nanoselenium presented a spherical structure with the ratio of 1:1 (Figure 10b). Without L-cysteine, the SeNPs cannot form and the unshapable mixture of sodium selenite and stabilizer was performed as shown in Figure 10a. Instead, microflowers appeared when the concentration ratio of Na_2SeO_3 to cysteine was 1:2 (Figure 10c), suggesting that the formation of nanosheets to form microflowers required the presence of a high amount of cysteine. Upon the increase in the molar ratio to 1:4, aggregation was immediately observed instead of a clear orange solution of SeNPs. This is due to an acceleration of

oxidation-reduction when high concentration of reducing agent, cysteine was added.

It might be allowing the aggregation of the critical nuclei of Se to happen [2].

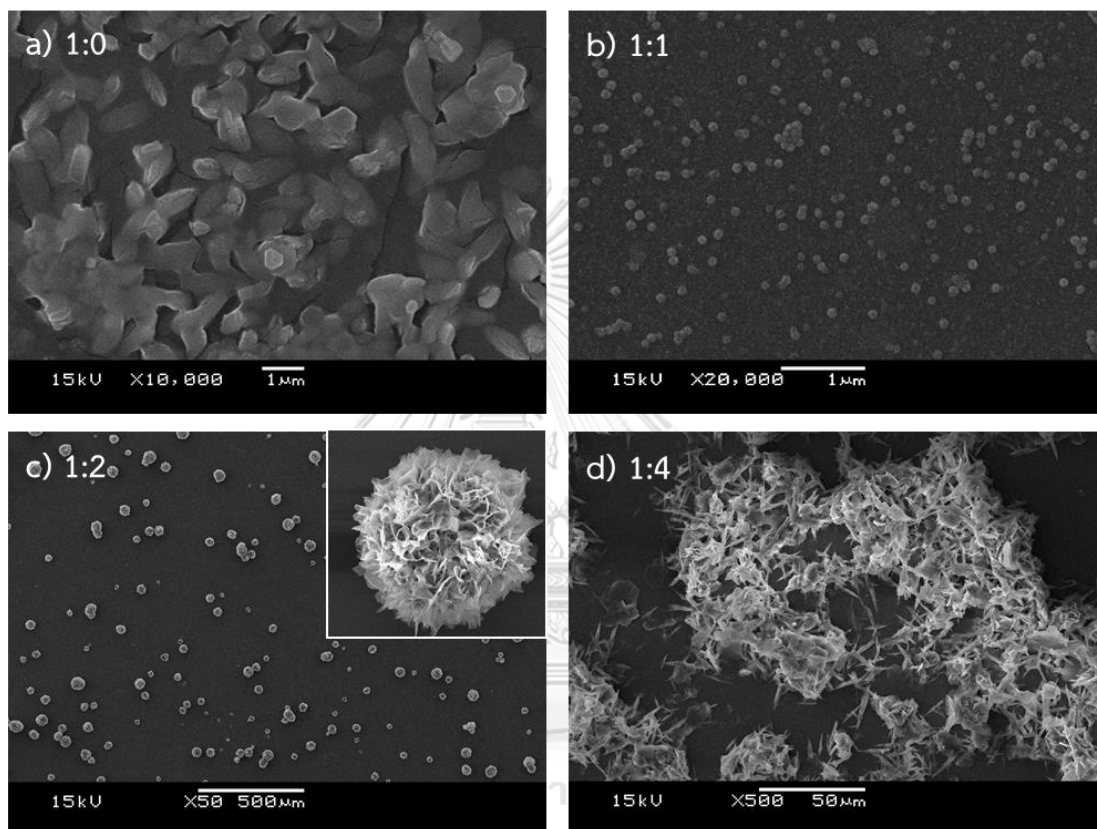


Figure 10 SEM images of shape of SeNPs stabilized by FA-CP with molar ratio of Na_2SeO_3 to cysteine a) 1:0, b) 1:1, c) 1:2 and d) 1:4.

Regarding to the results, the cysteine concentration affects the morphology of SeNPs stabilized by FA-CP (SeNPs/FA-CP). The spherical and microflower structure are the majority shape to perform. Therefore, the detailed study of each structure was informed.

4.2.2 Spherical structure of SeNP/FA-CP

4.2.2.1 Effect of FA-CP concentration

Biomacromolecules are well known to function as stabilizers for controlling inorganic nucleation, growth and self-assembly [88, 100, 101]. In this case, functionalized pullulan, FA-CP was act as a stabilizing agent to protect an aggregation of SeNPs. The concentration of FA-CP was varied to investigate the shape and morphology of SeNPs when the molar ratio of sodium selenite to L-cysteine of 1:1 was chosen. Figure 11a-f showed SEM images of SeNPs prepared under different FA-CP concentrations (0% to 0.91% w/v). SEM images of SeNPs without stabilizer revealed the aggregation of SeNPs to form the large particles shown in Figure 11a. These results indicate that the reduction and stabilization of SeNPs with cysteine resulted in unstable particles, which formed rapidly grew and aggregated into larger particles because of a lack of adequate protection on the surface of the nanoparticles [102]. At a low concentration of FA-CP (0.023% and 0.045% w/v), the spherical nanoselenium with some aggregation was detected. In addition, low distribution of particles was clearly observed (Figure 11b and c) due to small amount

of stabilizer to protection its surface. When the concentration of stabilizer was increased to 0.23% w/v, the shape of the nanoparticles was observed as a uniform spherical structure with high distribution (Figure 11d). At the concentration of FA-CP higher than 0.23% (0.45% and 0.91% w/v), the aggregation was carried out which presented in Figure 11e and f. These large structures were assembled by several particles, resulting in a branched-structure appearance. At higher concentrations of stabilizer, the $\pi - \pi$ stacking interaction, and hydrogen bonding of FA-CP were considered as the major forces leading to aggregation for balancing the surface energy of SeNPs.



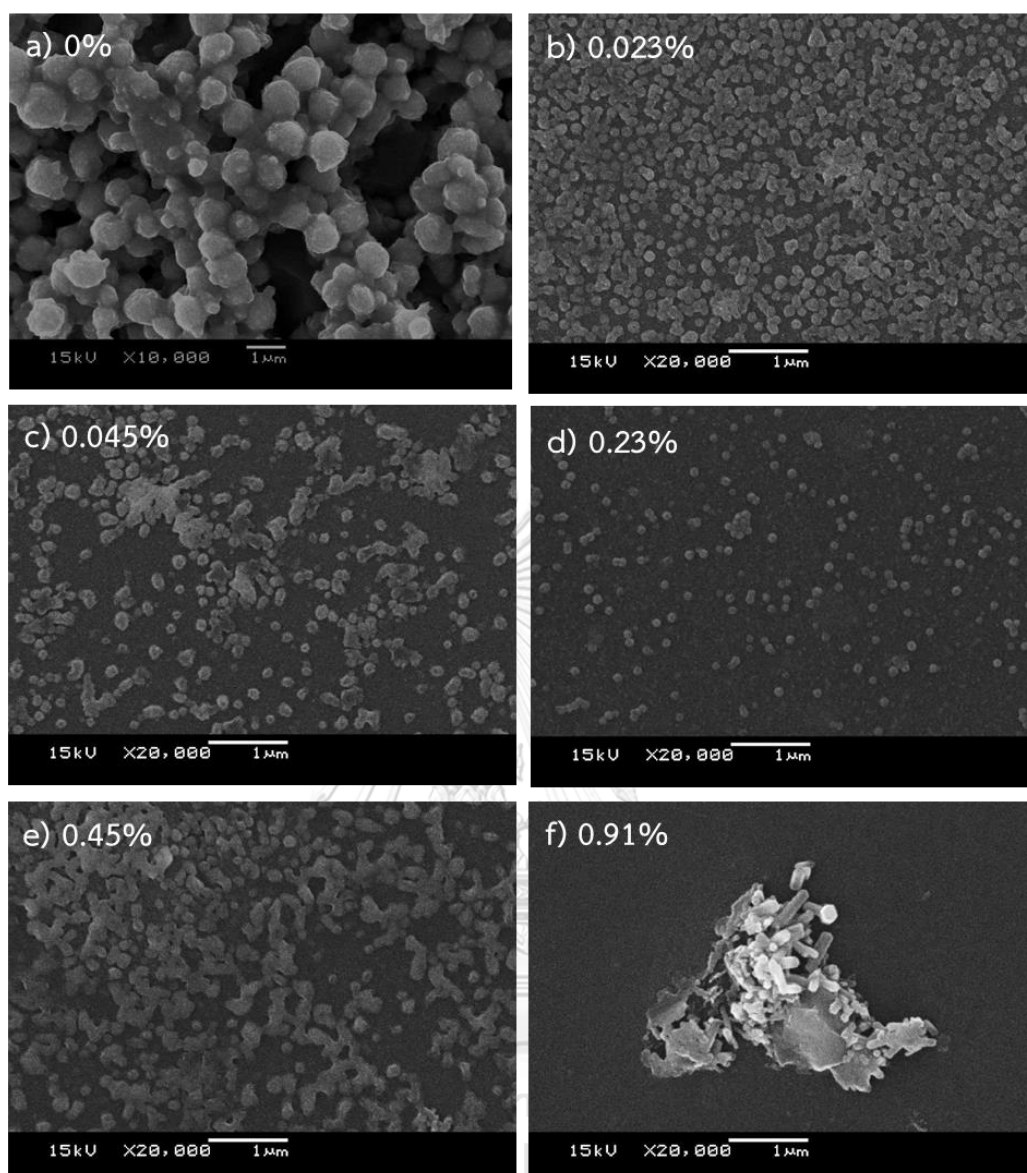


Figure 11 SEM images of SeNPs stabilized by FA-CP with FA-CP concentration of a) 0%, b) 0.023%, c) 0.045%, d) 0.23%, e) 0.45 and f) 0.91% w/v.

4.2.2.2 Effect of type of stabilizer

The concentration of FA-CP of 0.23% w/v was chosen for comparison with others stabilizer in the synthesis of SeNPs. The morphology of SeNPs stabilized by pullulan (SeNPs/P), CP (SeNPs/CP), FA-P (SeNPs/FA-P), and FA-CP (SeNPs/FA-CP) were characterized by SEM and TEM which shown in Figure 12a-d and Figure 13a-d. The spherical structure of SeNPs was observed in all types of stabilizer but exhibited difference in size which clearly seen from TEM images (Figure 13a-d) corresponding to the unimolecular structure of nanoparticles. The size of SeNPs stabilized by pullulan and derivatives was summarized in Table 3. The order of the sizes of the SeNPs that investigated by TEM from small to large is SeNPs/FA-CP, SeNPs/FA-P, SeNPs/P and SeNPs/CP. We supposed that the main effect of the stabilizer on particle size is because of the steric effect and intermolecular forces [103]. A possible explanation may be that the positively charged of cationic pullulan (%DQ = 11.2-16.6) is higher than pullulan and FA-P (%DS_{FA} = 3.7-6.7) and thus some parts of positive charge exhibited a stronger electrostatic repulsion resulting in the increase in size of nanoparticle. However, the presence of smallest size of SeNPs/FA-CP may be due to the reason that the decorated surface of SeNPs contains both of positively charge (from Quat-188) and negatively charge (from FA) which can create the electrostatic interaction between them. The nanoparticles were come closer leading to decreasing in size. In addition, the SEM images exhibited larger size of nanoparticles, indicating

that the pullulan and pullulan derivatives were probably incorporated into SeNPs [24] and enveloped the nanoparticles which were consistent with the result of SEM-EDX of SeNPs/FA-CP. An elemental composition analysis employing SEM-EDX showed the presence of signals from the Se atoms together with C atom signal and O atom signal from FA-CP (Figure 12e). Si, Na, Mg and Ca were also presented and they were from the coated glass substrates. The particles size from DLS technique reported the bigger size of SeNPs/CP and SeNPs/FA-P compared with the size from SEM. A possible reason may be that the swelling of CP and FA-P which surrounded SeNPs in aqueous phase [104]. However, swelling effect of SeNPs/P and SeNPs/FA-CP was negligible. The significance of zeta potential can be related to the synthesized products. In this study, we found that the value of the zeta potential of the SeNPs/CP was +5.43 mV and that of SeNPs/FA-P was -12.87 mV (Table 3) which suggest that the positive-charged trimethyl ammonium and negative charged FA were exposed on the outside surface of SeNPs.

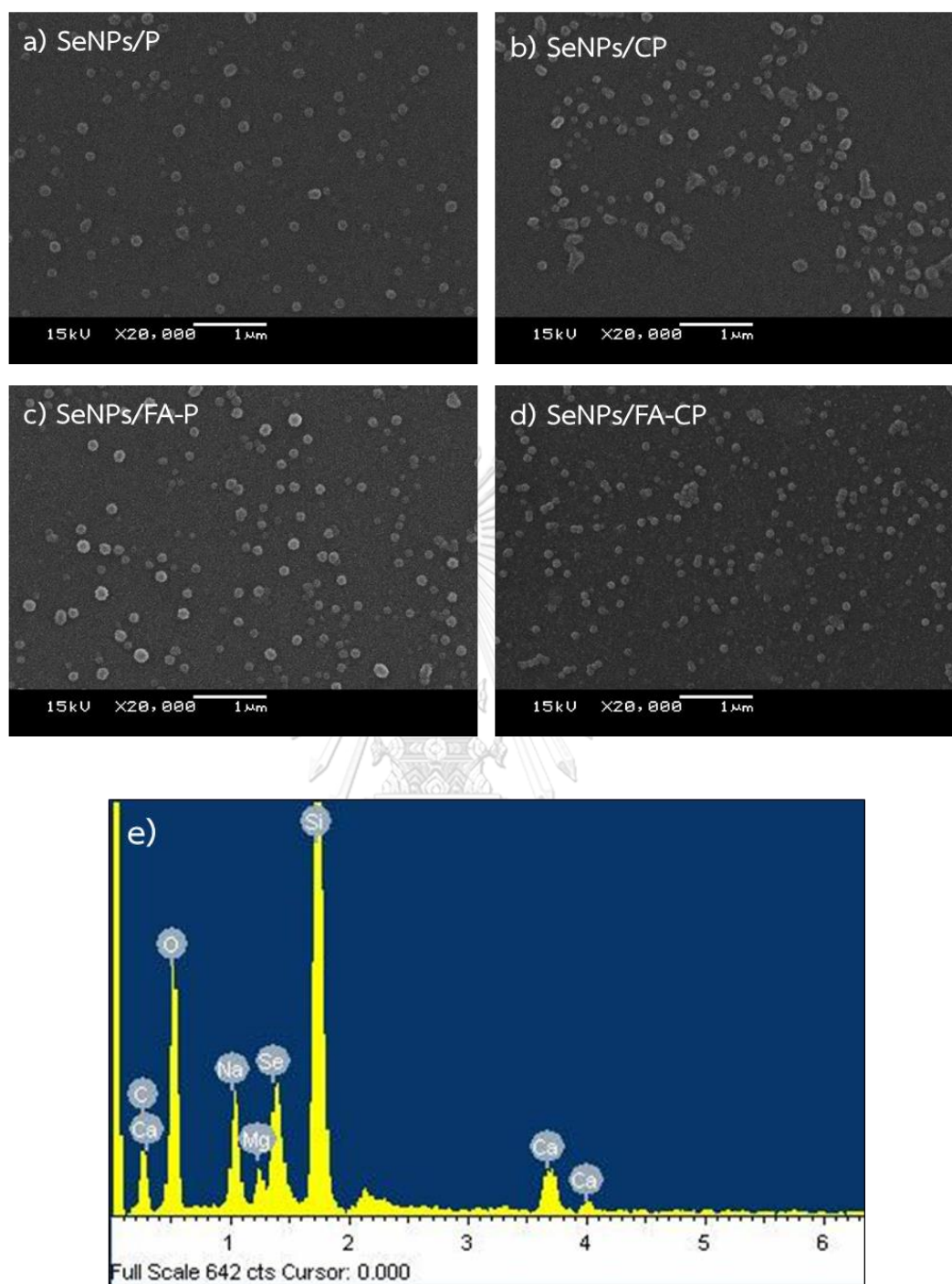


Figure 12 SEM images of SeNPs stabilized by a) pullulan, b) CP, c) FA-P d) FA-CP at concentration of 0.23% w/v and e) EDX spectra of SeNPs/FA-CP.

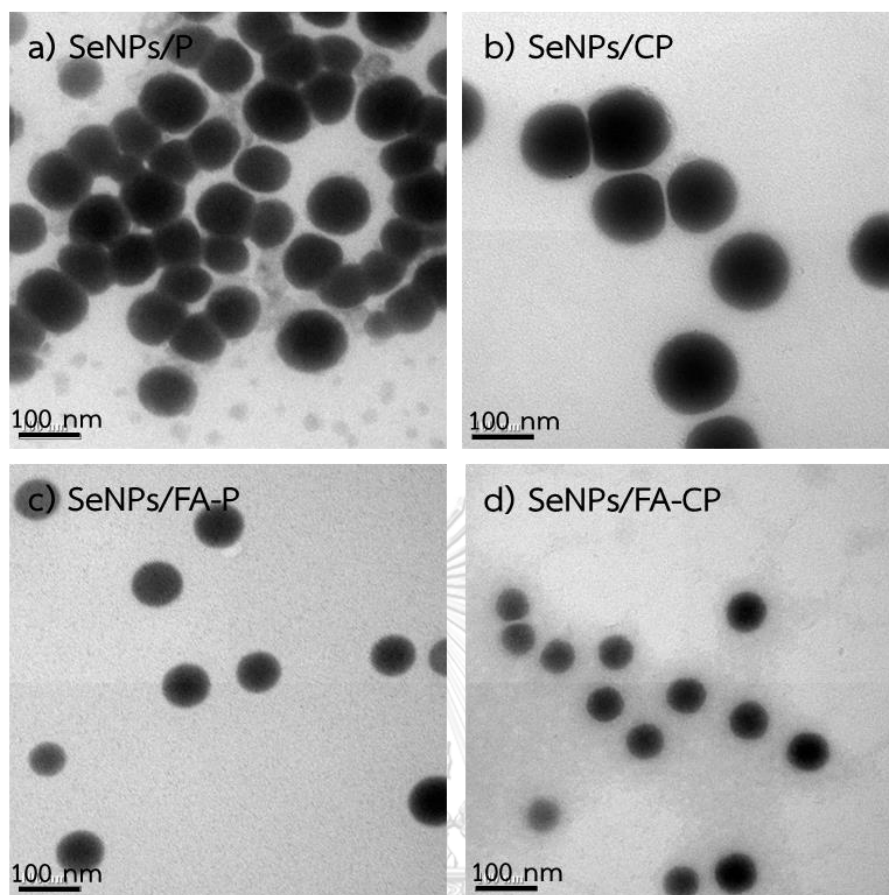


Figure 13 TEM images of SeNPs stabilized by a) pullulan, b) CP, c) FA-P and d) FA-CP at concentration of 0.23% w/v.

Table 3. Particle size of SeNPs stabilized by pullulan and derivatives and their zeta potential

Material	Diameter (nm)	Diameter (nm)		Pdl	Zeta potential (mV)
		by TEM	by SEM		
SeNPs/P	72.17±11.5	139.26±20.34	164.17±1.71	0.156	-1.18±0.105
SeNPs/CP	108.06±14.65	153.99±28.53	257.30±13.44	0.351	5.43±0.721
SeNPs/FA-P	70.64±9.41	155.28±18.15	302.00±16.67	0.426	-12.87±0.533
SeNPs/FA-CP	55.82±6.80	112.19±11.32	141.83±1.10	0.148	-0.25±0.052

4.2.2.3 In vitro cytotoxicity

The in vitro cytotoxic effects of SeNPs stabilized by pullulan and derivatives were experimented against human cancer cell line, KB (cervical carcinoma) and normal cell line, L929 by means of MTT assay. As shown in Figure 14, cellular uptake of SeNPs stabilized by pullulan and derivatives showed growth inhibition against KB with IC_{50} values of SeNPs/P, SeNPs/CP, SeNPs/FA-P and SeNPs/FA-CP ranging from 26.1 to 58.8 μ M. However, SeNPs/FA-CP presented the lowest IC_{50} (26.1 μ M) comparison with other stabilizer. Despite this potency, SeNPs/FA-CP showed lower cytotoxicity normal cells (L929) with an IC_{50} value of 52.8 μ M (Figure 14) which was higher than that in KB cancer cell line. On the other hand, SeNPs/P, SeNPs/CP and SeNPs/FA-P did not show much difference IC_{50} between cancer cell and normal cell. These results suggest that SeNPs/FA-CP possess good selectivity between cancer and normal cells.

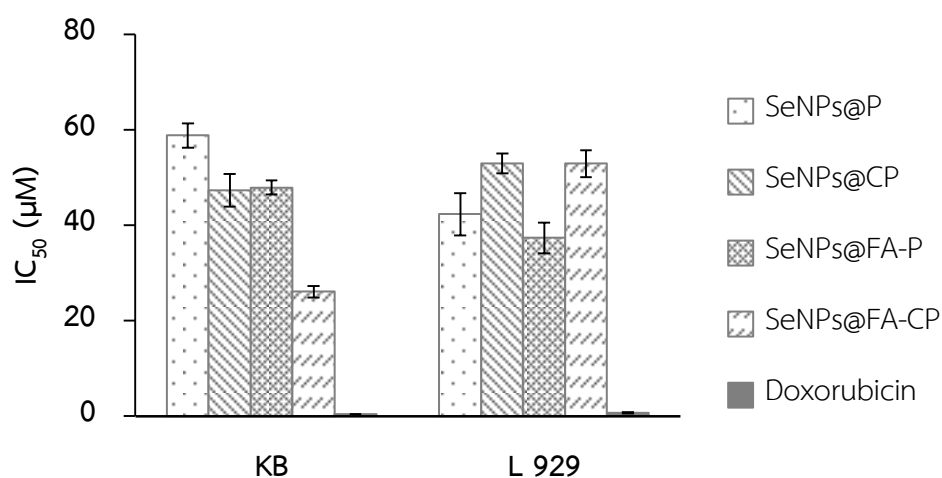


Figure 14 *In vitro* anticancer activities of SeNPs stabilized by pullulan and derivatives on KB cancer cell and normal cell lines (72 h). Cell viability was determined by a colorimetric MTT assay. Each IC_{50} value represents the mean \pm SD of three independent experiments.

4.2.2.4 Intracellular Se concentration

The cellular uptake of SeNPs/P, SeNPs/CP, SeNPs/FA-P and SeNPs/FA-CP in KB cell line and treated for 24 h by using ICP-OES analysis was examined. As shown in Figure 15, KB cells treated with 12.5 μ M SeNPs/FA-CP had significantly increased Se concentrations ($1.41 \mu\text{g}/10^6$ cells) comparing with unmodified pullulan, SeNPs/P ($0.37 \mu\text{g}/10^6$ cells). In addition, it was higher than treated with SeNPs/CP and SeNPs/FA-P which obtained 0.93 and $0.64 \mu\text{g}/10^6$ cells, respectively. The results suggest that the smaller size, the positive surface charge and FA, cancer targeting surface decoration contributed to the enhanced cellular uptake of SeNPs/FA-CP, compared with SeNPs, in others stabilizer.

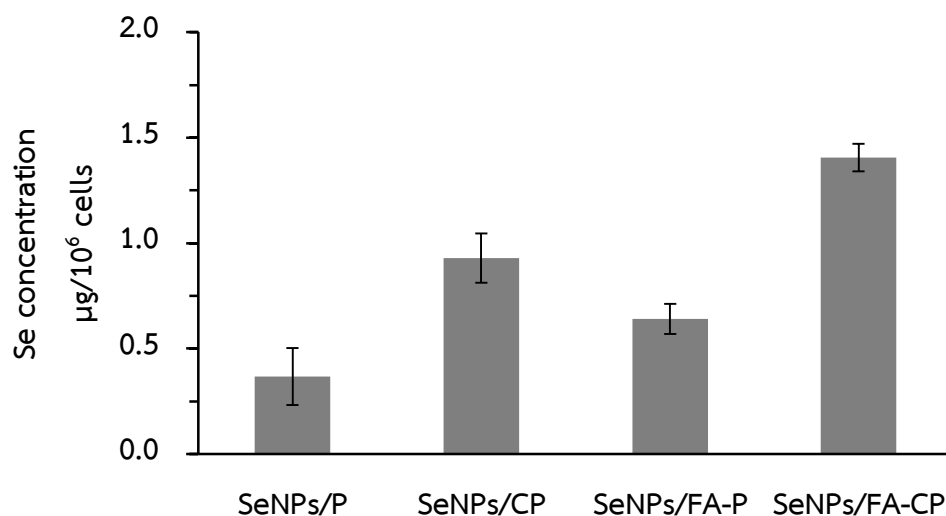


Figure 15 Quantitative analysis of Se concentration in KB cells exposed to SeNPs stabilized by pullulan and derivatives for 24 h by ICP-AES method. Each value represents the mean \pm SD of three independent experiments.

The spherical shape of SeNPs has been a beloved structure for the synthesis of nanoselenium which was widely reported for cancer treatment applications due to the intense attention attracted by SeNPs as potential cancer therapeutic agents and drugs carriers [105, 106]. In this research, I expect to obtain the spherical SeNPs; however, the unexpected selenium microflowers were observed when verified the concentration of cysteine affecting the synthesis of SeNPs. Therefore, the shape-controlled synthesis of SeNPs hybrid flower can extend our understanding of the emerging structure property that can improve the performance of the materials for various applications and in particular in the pharmaceutical field.

4.2.3 Microflower structure of SeNPs/FA-CP

4.2.3.1 Effect of FA-CP concentration

Regarding to section 4.2.1, 1:2 molar ratio of Na_2SeO_3 to cysteine could induce the flower-like structure. An increase in the concentration of FA-CP to 0.023%, 0.045%, 0.23%, 0.45% and 0.91% w/v was further studied for the formation of microflowers while preserving the Na_2SeO_3 to cysteine molar ratio to be 1:2. As shown in Figure 16a and b, the formation of the flowery morphology was difficult under FA-CP concentration lower than 0.023% w/v due to the lack of polymer content for plated sheets production; this lead to the formation of incomplete hybrid flowers. An increase in the FA-CP concentration to 0.23% and 0.45% w/v resulted in the generation of hierarchical structures (Figure 16c and d) with insignificant differences of layer thickness (Figure 16f and g). In addition, for the concentration of 0.91% w/v FA-CP, the fusion of hybrid flower with other structures was observed as shown in Figure 16e, which outer surface of microflower was covered by the FA-CP fiber. The fiber was formed due to the high amount of the added pullulan derivative. As described above, the structure of FA-CP contains two features: the positive charge from the $\text{N}^+(\text{CH}_3)_3$ of quaternized pullulan and the hydrophobic regions comprised by the phenyl rings of folic acid. For high of FA-CP concentrations, the amount of the hydrophobic components was also high, providing the hydrophobic interaction with $\pi - \pi$ stacking and cationic-dipole interaction

[107]; consequently, the fiber was formed as a nonwoven three-dimensional architecture (inset in Figure 16e) and some parts of the fiber were wrapped around the microflower.

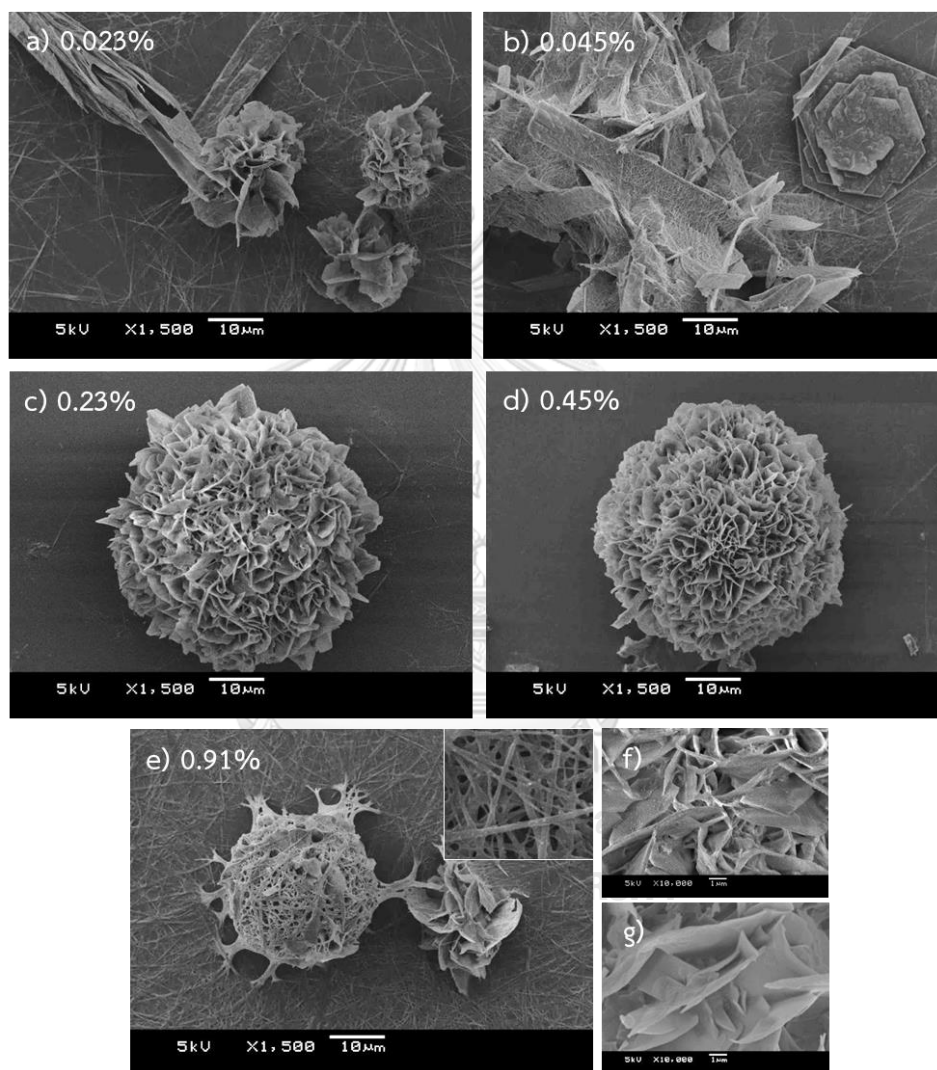


Figure 16 SEM images of shape of SeNPs stabilized by FA-CP with FA-CP concentration of a) 0.023%, b) 0.045%, c) 0.23%, d) 0.43% and e) 0.91% w/v.

4.2.3.2 Possible mechanism for the formation of SeNPs stabilized by FA-CP hybrid flower

In the past decade, various kinds of SeNPs morphology have been reported. The formation of the SeNPs as nanospheres, nanorods, and cubic-like structure were reported. Zhang et al. (2010) studied the fabrication of SeNPs using natural hyperbranched polysaccharide (HPB) as the stabilizer and the capping agent [1]. The Se^{4+} ions were reduced to elemental selenium (Se^0), and then the selenium atoms aggregated into selenium particles. The Se-HPB nanocomposites were formed by binding with HPB, resulting in the formation of a uniform and spherical morphology. The experiment for the dynamic growth of Se nanorods was displayed by Chen et al., 2009 [2]. They suggested that the spherical amorphous Se particles were formed first, and then rapidly changed into rod-shaped by controlling the ultrasonic time.

Recently, selenium nanoparticles with a cubic-like structure were reported to be synthesized by controlling the shape of SeNPs with a functionalized molecule used as the stabilizing agent [3]. The folic acid-gallic acid-N,N,N-trimethyl chitosan (FA-GA-TMC) was synthesized and stabilized SeNPs. The assembly process of SeNPs into cubic-like structures was carried out by intermolecular interactions including electrostatic interactions, $\pi - \pi$ stacking and hydrogen bonding among the nearest particles lowering the energy through attachment and leading to the formation of cubic-like structures.

Nevertheless, the SeNPs hybrid flowers have not been reported, and therefore, an understanding of the formation mechanism of the SeNPs hybrid flower is highly required. The formation mechanism of SeNPs hybrid flower is unclear because no work has been reported on this structure. However, the growth mechanism of organic-inorganic hybrid flower from the related publications can help to better understand the present system. Suber and Plunkett (2010) first accidentally discovered the hybrid nanoflower and confirmed that the copper (II) ions, Cu^{2+} (inorganic component) and protein (organic component) create a new type of particle via their interactions [108]. The protein molecules form complexes with the Cu^{2+} , and these complexes become nucleation sites for the primary crystals of copper phosphate. Interaction between the protein and Cu^{2+} then leads to the growth of the particles in micrometer sized flower petal-shaped features. In addition, silk protein/copper hybrid flowers were successfully prepared [109]. Protein molecules formed complexes with the Cu^{2+} ions through the coordination of amino acid backbone, leading to the growth of nanosheets. Furthermore, nucleation and the subsequent growth of the copper phosphate nanocrystals were generated on the surfaces of the thin nanosheet petals, consequently forming thicker and layered petals. The growth process proceeded to form full multilayer flower structures. Moreover, they suggested that the chloride ions (Cl^-) played an important role for the growth of hybrid flower-like structures by domination of the crystallization process of copper phosphate and control the preferred orientation of the protein to

induce the nucleation and the crystalline grains of copper phosphate. The hybrid flowers with other inorganic and organic component were studied subsequently. Flower-like chitosan/calcium pyrophosphate hybrid microflowers were introduced by Wang et al. (2014) [92]. Chitosan (CS) and tripolyphosphate (TPP) were used to fabricate a gel complex and acted as a template to support rapid nucleation of $\text{Ca}_2\text{P}_2\text{O}_7$ crystals. An anisotropic growth of Ca^{2+} on CSTPP nanocomplexes leads to the formation of hybrid microflowers.

To validate the proposed mechanism of hybrid flowers of SeNPs stabilized by FA-CP, the functionalized pullulan, FA-CP, was mixed with Na_2SeO_3 at 60 °C for 15 min. The intermolecular linkages between the positively charged of FA-CP and negatively charged SeO_3^{2-} ions were formed. The SeNPs stabilized by FA-CP were generated after the addition of L-cysteine hydrochloride via the oxidation-reduction reaction, Se^{4+} was reduced to Se^0 by cysteine as can be observed by the change of the solution color from colorless to orange. The Se nuclei were bound to the FA-CP positive charge [3] and L-cysteine with the carboxyl group [2] thus inhibiting the crystal growth and stabilizing the SeNPs due to the hindrance effect. The formation mechanism of the SeNPs hybrid flowers was tentatively proposed as shown in Figure 17. The SeNPs stabilized by FA-CP were formed and induced the formation of hexagonal sheets (step 1) through simple intermolecular interactions such as electrostatic interaction, $\pi - \pi$ interaction, hydrogen bonding, and van der Waals

forces. The assembly process of hexagonal sheets proceeded to form multilayer structures and anisotropic growth continued to create full bloom flower as shown in steps 2, 3, 4 and 5. During the oxidation-reduction process, the mercapto group of L-cysteine was susceptible to oxidation to give the disulfide derivative cysteine. This is proposed to play an important structural role for the arrangement of the hexagonal plated sheet by generating the interaction with the FA-CP derivative that stabilized SeNPs distributed in the interior of the sheet. Therefore, it can be suggested that the functionalized FA-CP molecules not only stabilized the SeNPs but also forced the hexagonal sheet formation via intermolecular interactions between the neighboring of SeNPs stabilized by FA-CP and disulfide derivative cysteine. These hypotheses were preliminarily confirmed by energy-dispersive X-ray spectroscopic (EDS) mapping analysis (Figure 18). The data showed the hexagonal arrangement of sulfur atoms (white spot) and the dissipation of the SeNPs stabilized by FA-CP were observed (red spot). In addition, it was proposed that the chloride ion (Cl^-) was a key factor for the generation of electrostatic interactions with some positively charged parts of FA-CP to form petals as was clearly seen in the green spot of the inset of Figure 18a. The anisotropic growth of a huge number of hexagonal sheets resulted in full bloom flowers [13]. The EDS spectra for the hexagonal sheet and the SeNPs hybrid flower shown in Figure 18a and b indicated that the SeNPs hybrid flowers were composed of C, O, Se, S, and Cl, as expected for hybrid flower formation. Si, Na, and Ca were also observed and the coated glass substrates were assigned as the origin of these

elements. A representative SEM image with the corresponding EDS mapping data are shown in the insets of Figure 18a and b. The general morphologies of the SeNPs hybrid microflowers were also determined by transmission electron microscopy (TEM) as shown in the TEM image of a single microflower in Figure 19a. We can observe that the SeNPs in the size range of 20–50 nm were distributed on the sheet. This showed that the sheets of the SeNPs hybrid flowers became more compact and intense to form blooming flowers. However, the spherical SeNPs stabilized by FA-CP were observed. Moreover, the crystal structure of SeNPs hybrid flowers was determined by the XRD technique. The XRD pattern of the synthesized products indicated the nano-crystalline nature of the SeNPs [110-112] (Figure 19d), revealing the formation of diffraction rings in the SAED patterns, attributed to the (100), (101), and (110) reflections of nanocrystals [110, 113, 114] (Figure 19b). In the HRTEM analysis of single nanosheets, the (100) set of planes with the 0.330 nm interplanar distance [113] was predominantly observed as shown in Figure 19c.

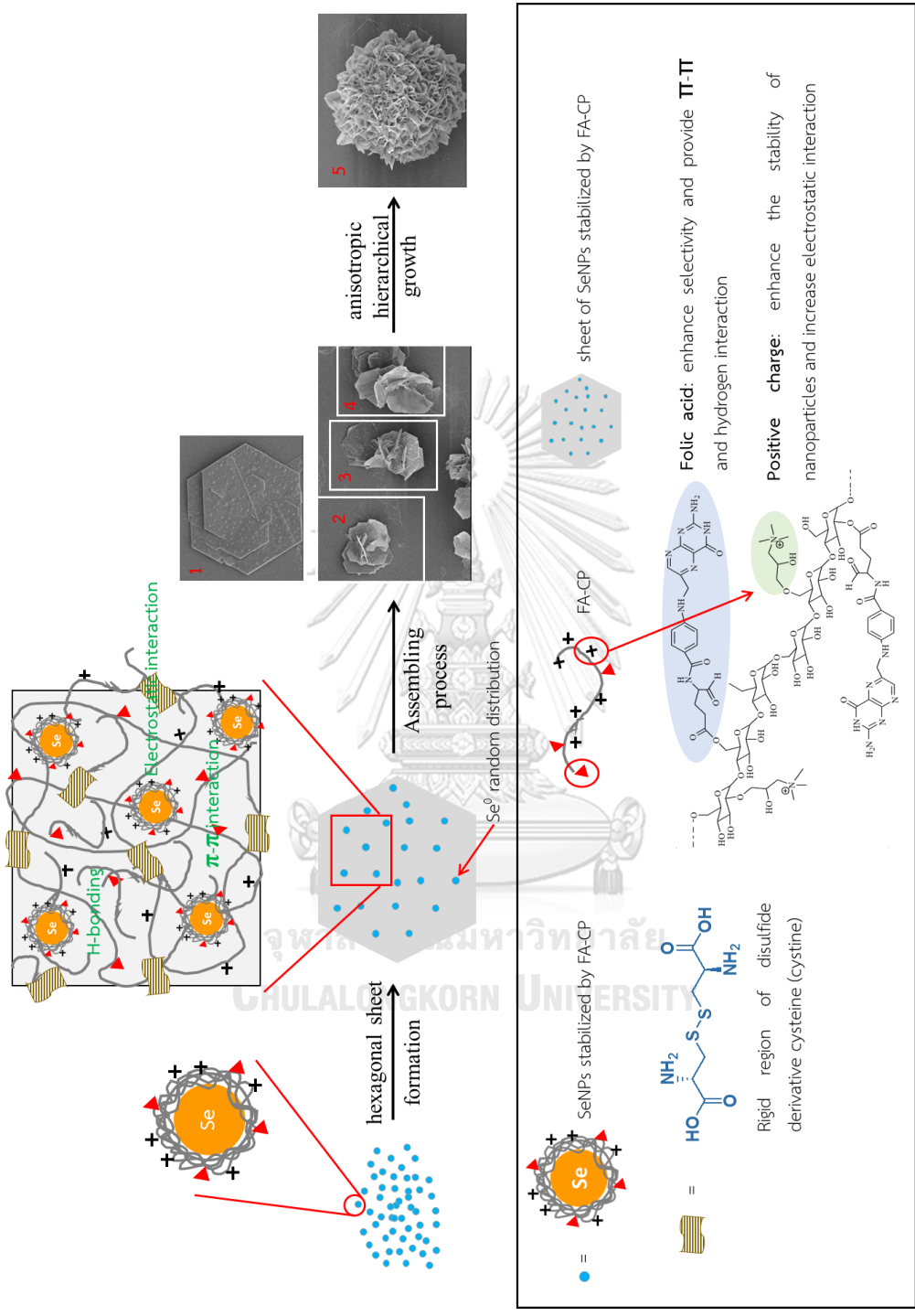


Figure 17 Schematic representation of the SeNPs stabilized by pullulan derivative inorganic/organic hybrid flowers.

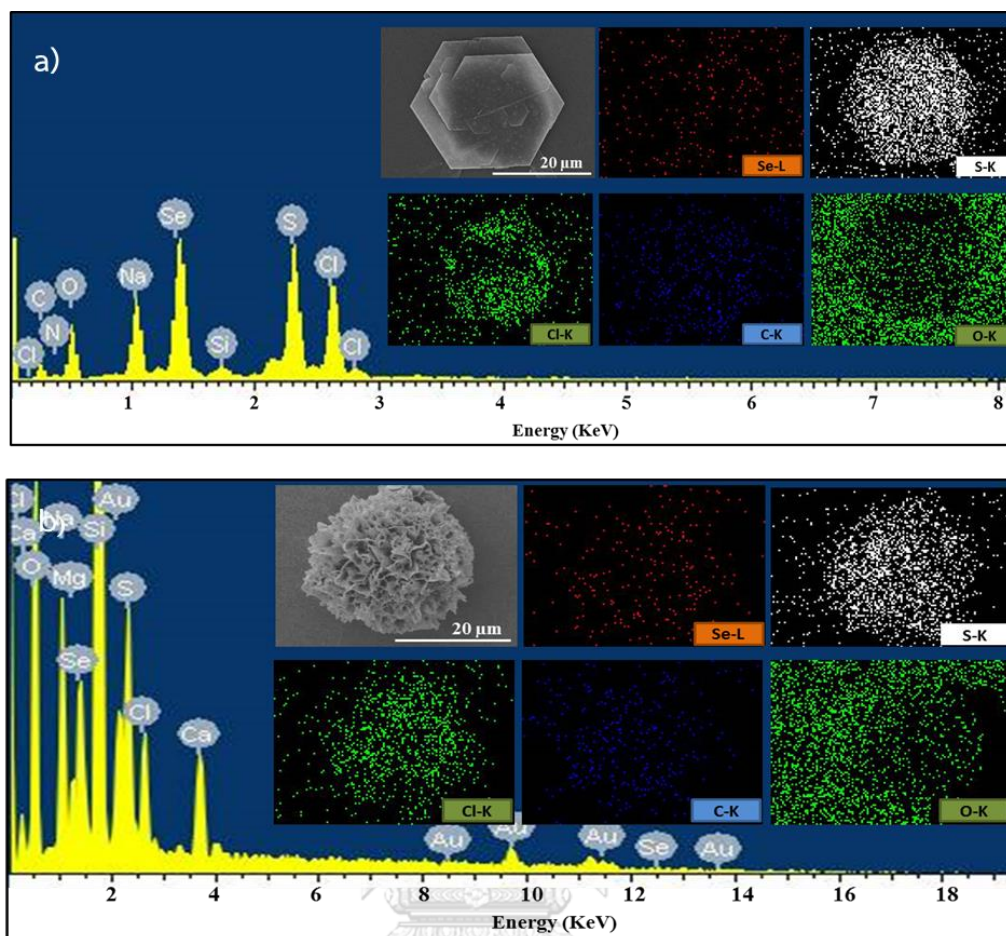


Figure 18 a) EDS spectrum for a representation of the hexagonal plated-sheet. The inset shows an SEM image and corresponding EDS mapping data for hexagonal sheet, b) EDS spectrum for a representative sample of SeNPs stabilized by FA-CP hybrid flower. The inset shows an SEM image and corresponding EDS mapping data for an ensemble of microflowers.

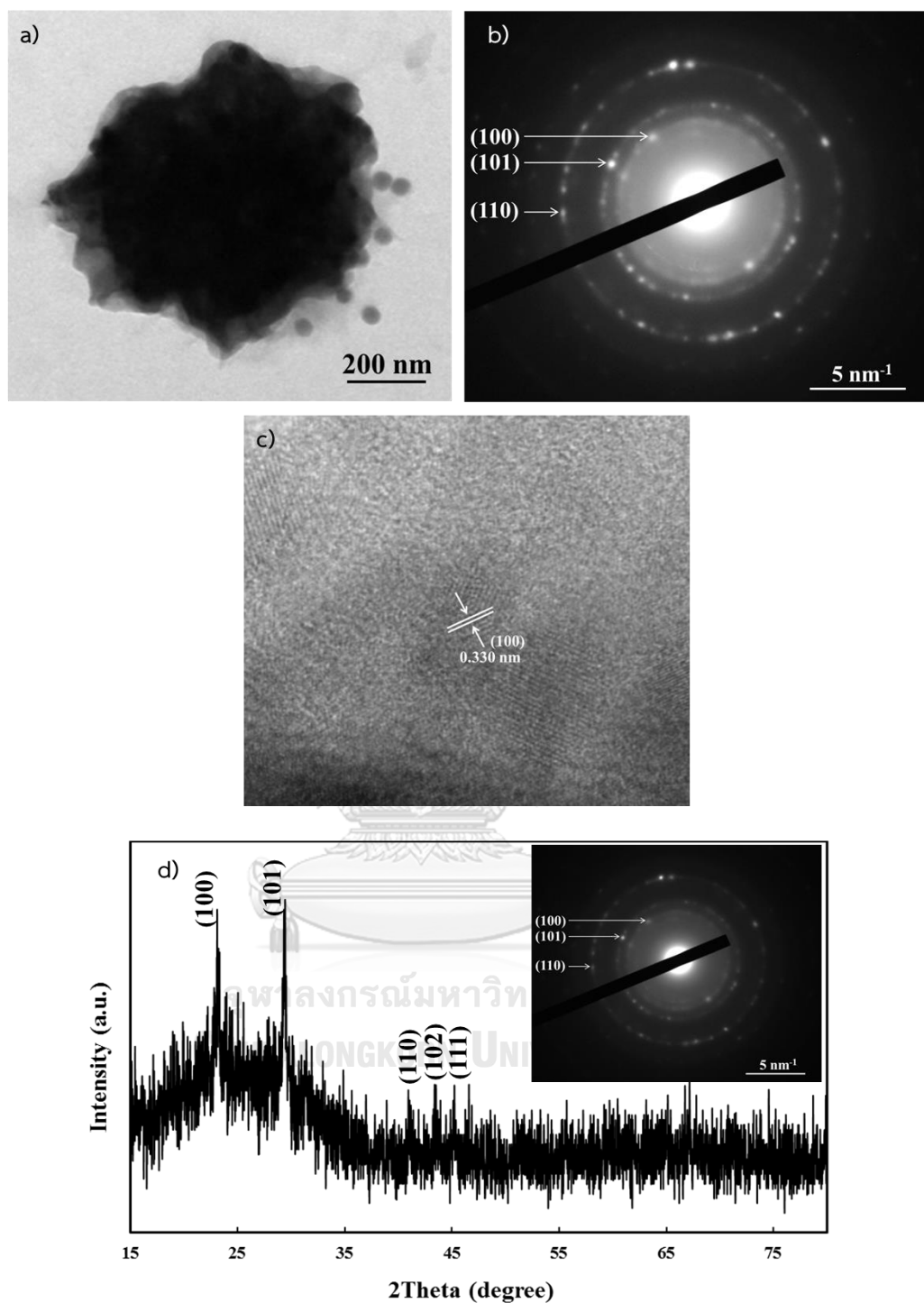


Figure 19 a) TEM images of hybrid microflower of SeNP stabilized by FA-CP at 1:2 molar ratio of Na_2SeO_3 :cysteine, b) SAED pattern of SeNPs stabilized by FA-CP hybrid flower, c) HRTEM of nanosheet of SeNPs stabilized by FA-CP hybrid flower, and d) XRD pattern of SeNPs stabilized by FA-CP.

4.2.3.3 Anticancer drug loading and release studies of SeNPs/FA-CP hybrid flower

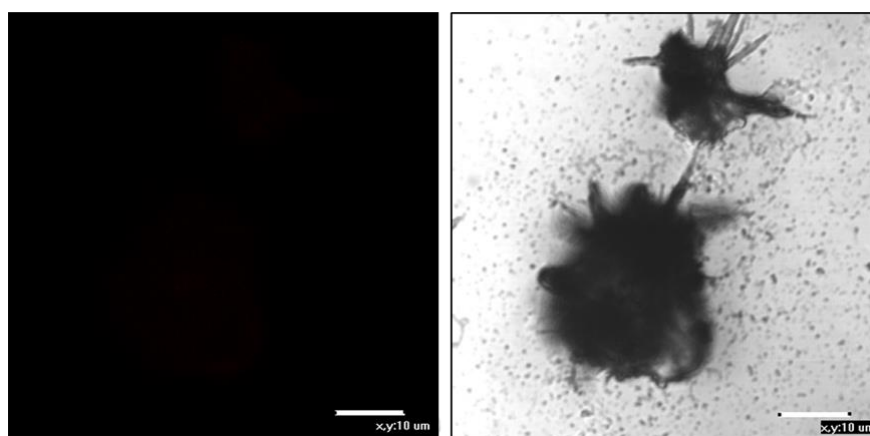
The SeNPs hybrid flower was used as a template for anticancer drug loading because of the high surface area of the flower-like structure [92, 115]. To investigate the drug loading ability of the hybrid flower microstructures, the doxorubicin anticancer drug was used as the model drug. The fluorescence image of doxorubicin-loaded SeNPs hybrid flower (SeNPs/FA-CP@DOX) confirmed that doxorubicin was absorbed on the hybrid flower (Figure 20). Fluorescence spectroscopy was used to carry out doxorubicin loading measurements at the excitation wavelength of 480 nm. The maximum drug-loading capacity of doxorubicin was 142.2 mg/g of FA-CP which was three times higher than the capacity of the doxorubicin loaded spherical SeNPs (53.8 mg/g of FA-CP) when using an equal concentration of Se (Figure 21a). This was likely due to the electrostatic interaction, hydrophobic interactions, or diffusion of model drug to the SeNPs hybrid flower. Figure 21b shows the doxorubicin release performance of the prepared SeNPs/FA-CP@DOX in PBS. It can be seen that the cumulative amount of released doxorubicin reaches a plateau of 68.3% after 10 h. At the first hour, 35.95% of cumulative release was obtained, possibly due to the release of doxorubicin adsorbed on the outer surface of the microflowers. Then, the system exhibited sustained drug release behavior until reaching a plateau. These results suggested that the novel SeNPs hybrid flower stabilized by pullulan derivative

was able to act as a drug template in a drug delivery system. The doxorubicin-loaded SeNPs microflower was further used to study the cytotoxicity toward the KB cancer cell line. The in vitro cytotoxic effects of doxorubicin-loaded SeNPs microflower against the KB (cervical carcinoma) human cancer cell line were examined by an MTT assay. Cells cytotoxicity against KB with the IC_{50} values of $0.060 \mu\text{M}$ (Figure 22a) was found, indicating that the doxorubicin-loaded SeNPs microflower caused 50% inhibition of cell viability at the concentration of $0.060 \mu\text{M}$. This value was calculated using the doxorubicin concentration. The cell growth photos of KB cells treated with different concentration of SeNPs/FA-CP@DOX are shown in Figure 22b, and the decrease in the number of cells and morphological changes of the cells can be observed for higher concentration. Despite this potency, the doxorubicin-loaded SeNPs microflower showed lower cytotoxicity against normal cells (L929) with the IC_{50} value of $0.23 \mu\text{M}$ which was higher than that obtained for the KB cancer cell line (Figure 22a). It can be suggested that the doxorubicin-loaded SeNPs microflower exhibited more potent activity against cancer cells, while it showed less toxicity against normal cells. To determine whether the reduction in cell viability of the KB cells treated with SeNPs/FA-CP@DOX was caused by induction of apoptosis or necrosis, we performed AnnexinV-FITC and propidium iodide (PI) staining after treating the KB cells for 24 h with the concentrations of 0.058 and $0.19 \mu\text{M}$ of SeNPs/FA-CP@DOX. The apoptotic rate of KB cells was increased with the increasing dosage of SeNPs/FA-CP@DOX, in which the late-stage apoptotic rates of KB cells with

0.19 μM of SeNPs/FA-CP@DOX was 10.3% (Figure 23). In addition, the necrosis rate was also increased to 12.9%. This suggested that SeNPs/FA-CP@DOX induced late apoptosis and/or necrosis in KB cells. However, the early- and late-stage apoptotic rates of KB cells treated with doxorubicin only reached 0.52% and 4.64%, respectively and the highest induction of 55.8% was arrested in the necrosis rate. Therefore, SeNPs/FA-CP@DOX exhibits greater ability to induce the apoptosis of KB cells than doxorubicin alone.



a) Unloaded doxorubicin



b) Loaded doxorubicin

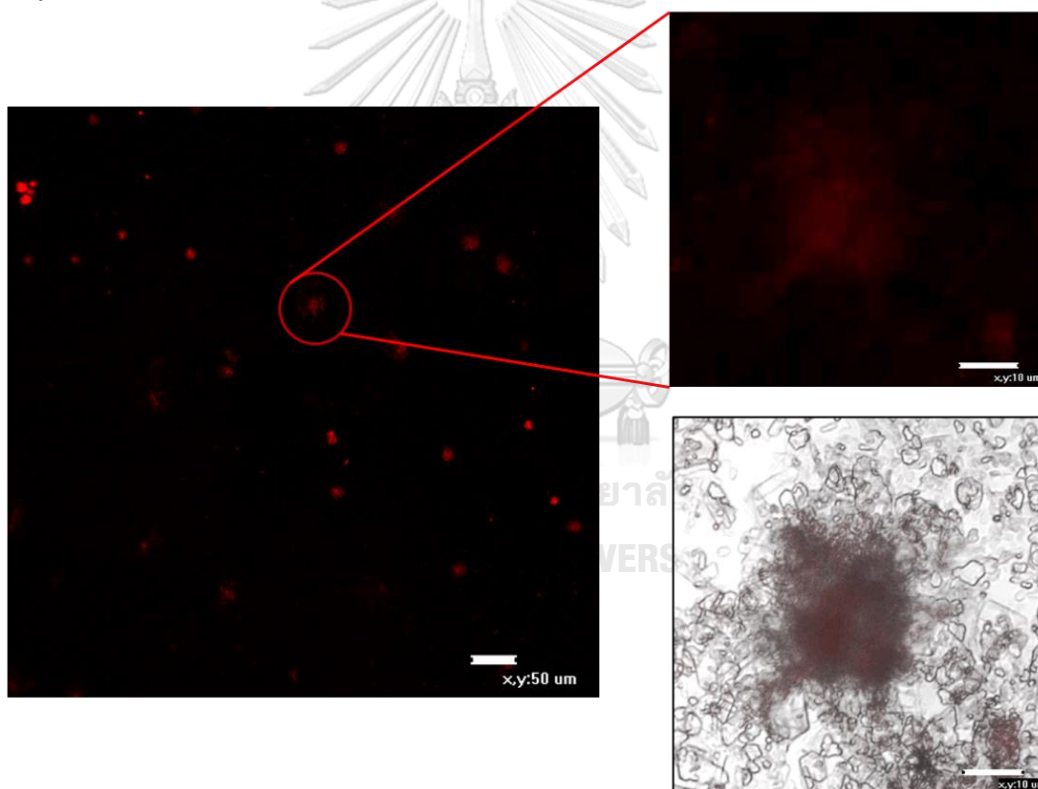


Figure 20 Doxorubicin-loaded SeNPs hybrid flower observed by microscopy.

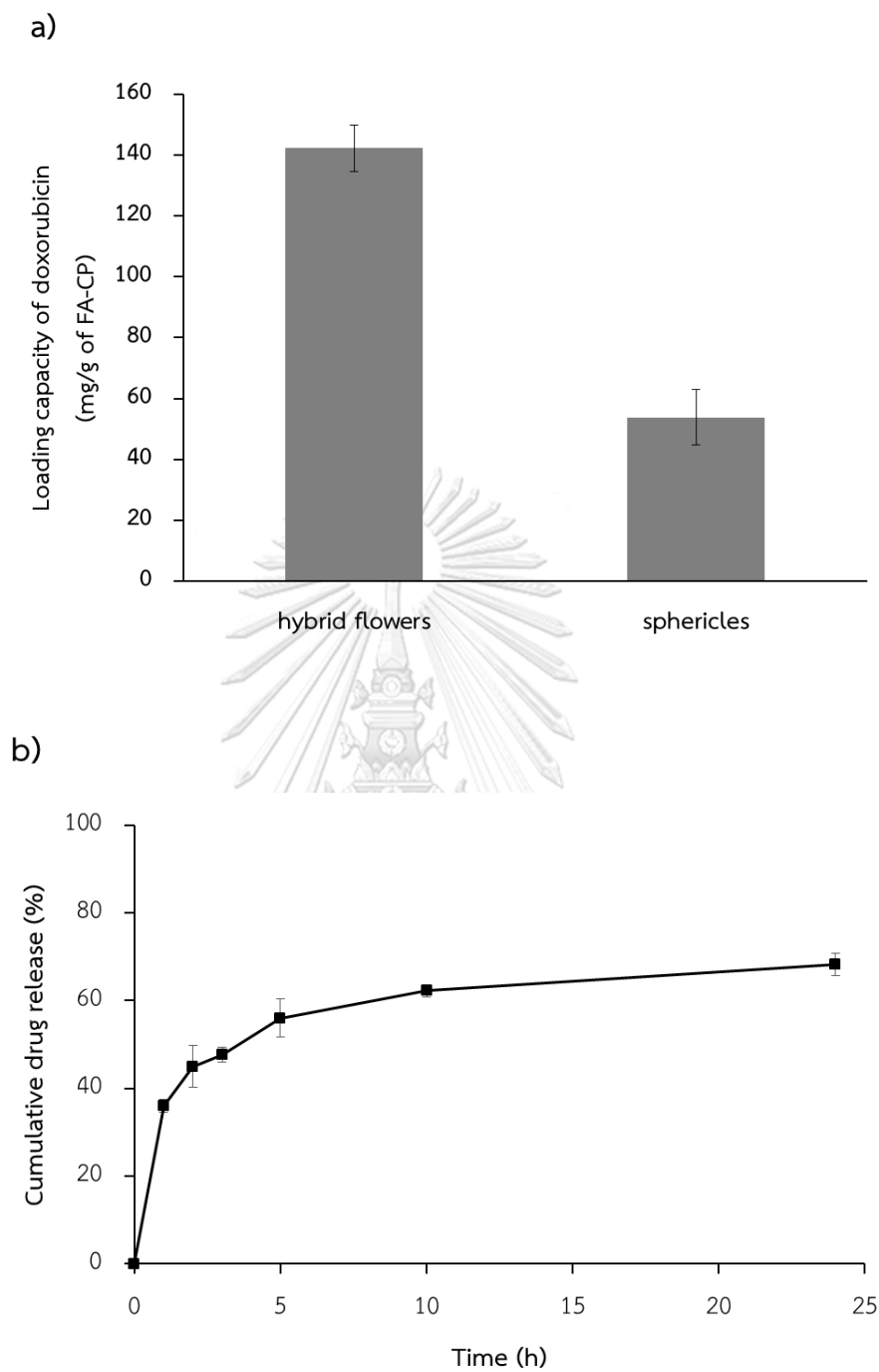


Figure 21 a) The capacity of the doxorubicin-loaded hybrid flower and spherical SeNPs. b) Cumulative drug release (%) of doxorubicin from doxorubicin-loaded hybrid microflowers.

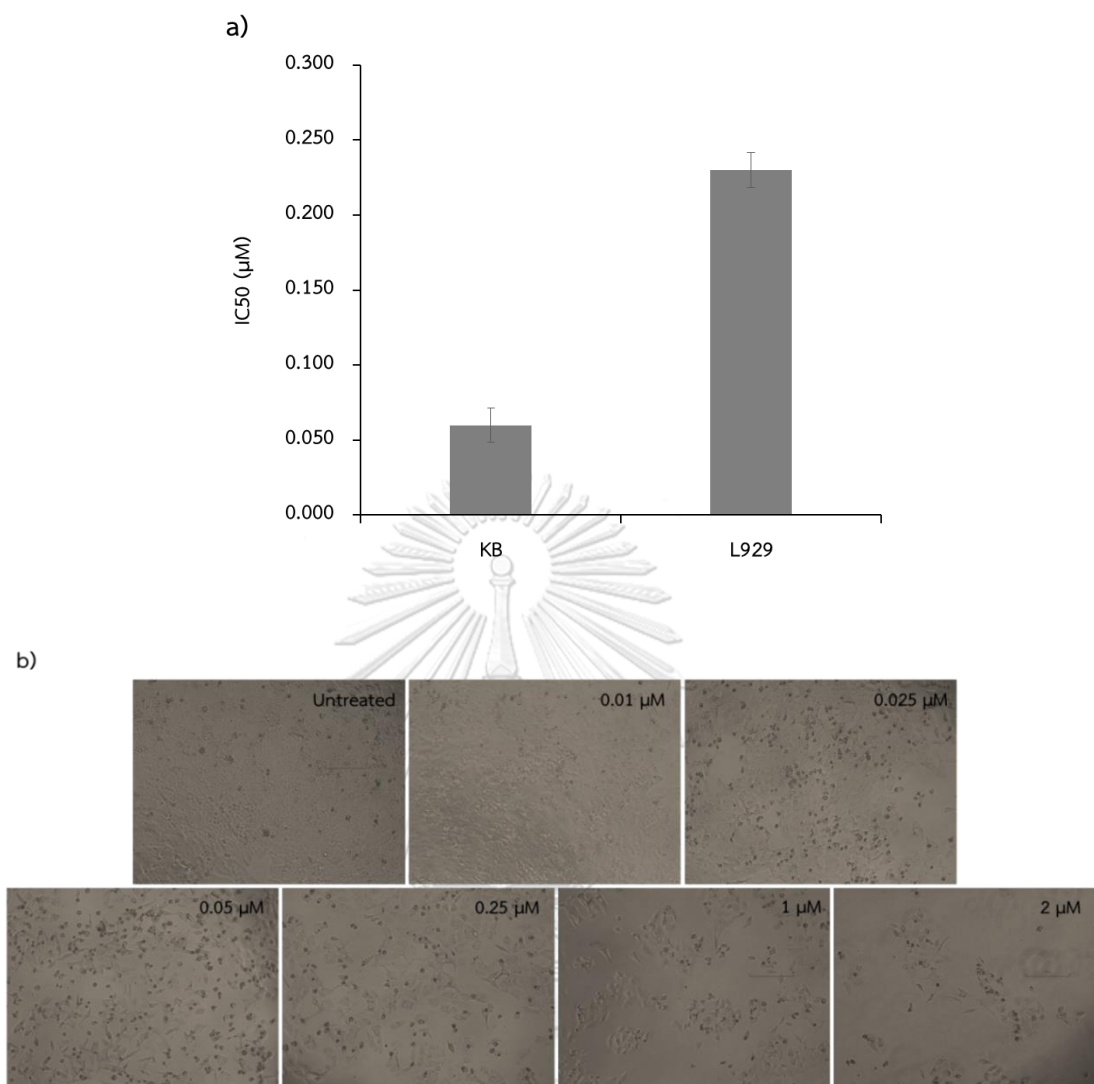


Figure 22 a) Cytotoxicity of doxorubicin-loaded hybrid microflower against KB and L929 cells. b) Cell growth photos of KB cells treated with different concentration of doxorubicin-loaded hybrid microflowers.

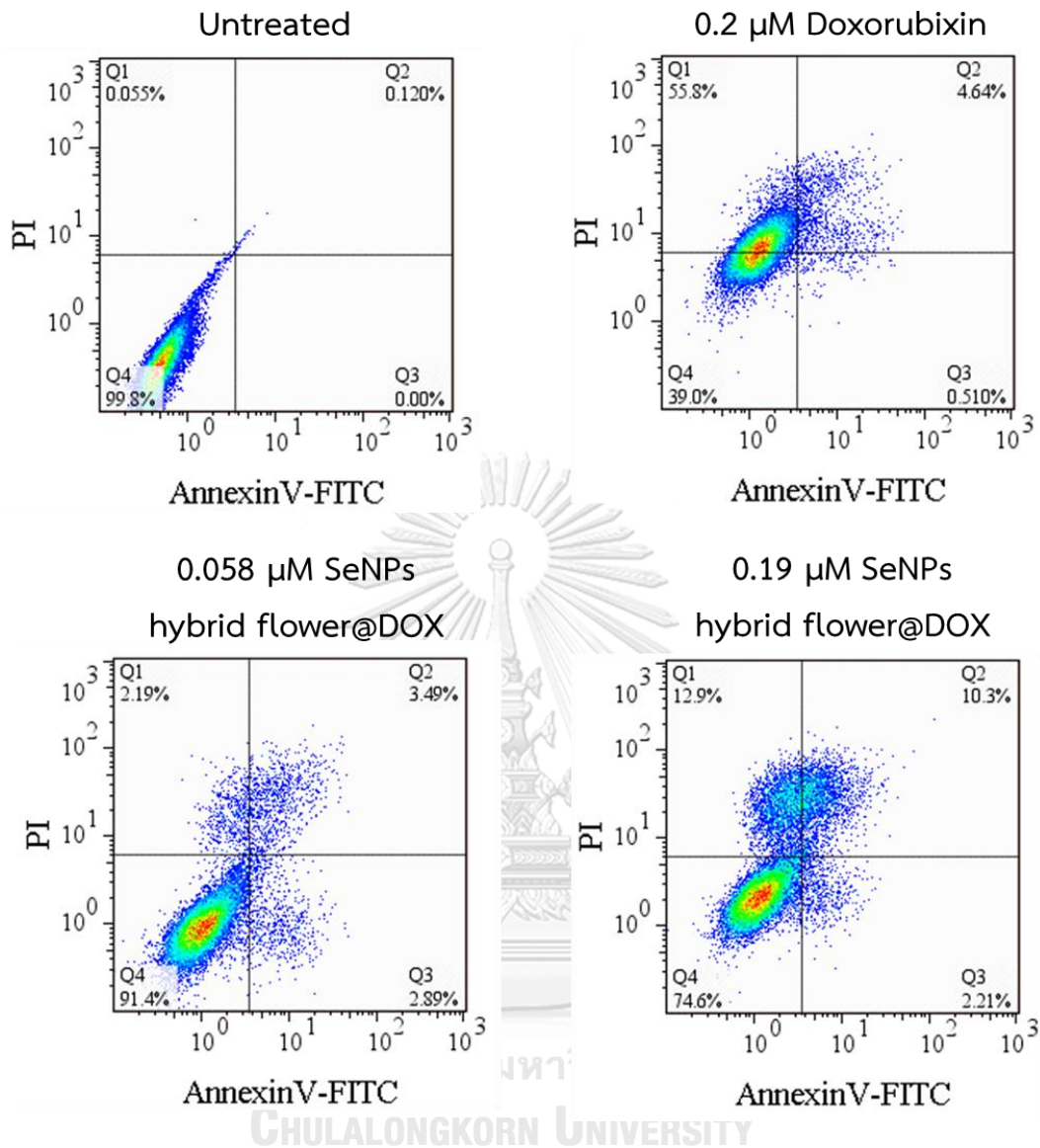


Figure 23 The percent of apoptosis/necrosis of KB cells analyzed by flow cytometry.

Part B: the use CD-FA-CP derivative as a stabilizer

In this part, CD-FA-CP was synthesized which presented in step 3 of Figure 6. The β -CD decorated FA-CP was developed to enhance the drug-loaded capacity.

4.3 Synthesis and characterization of CD-FA-CP

6-O-Monotosyl--cyclodextrin (β -CD-OTs) is one of the most important intermediates in the production of substituted β -CD, Therefore, the functionalization of FA-CP with β -CD was prepared through an intermediate, β -CD-OTs. The conjugation of β -CD with p-toluenesulfonyl groups was confirmed by FTIR based on the peaks at 1236 and 815 cm^{-1} which contributed to Ph-SO₂-R and Ph-SO₂-O-R, respectively (Figure 24). These two peaks were not exhibit in β -CD or p-toluenesulfonyl chloride and could be assigned to substitution of tosyl groups. In addition, the ¹H NMR spectrum (Figure 25) exhibited the characteristic peaks of aromatic proton at 7.71 and 7.40 ppm and the new peak of proton signal appeared around 4.74 ppm which belong to the H-1* of substituted β -CD was observed. Based on the integral ratios of the anomeric proton (H-1) and the multiplet at 4.47–4.39 ppm (OH-6), it showed 6.60:5.49, which were approximately calculated to be 7:6 [116]. It was confirmed that only one of the seven primary hydroxyl groups of β -CD was tosylated. It is strongly confirmed by the degree of tosylation (%DT) which was investigated by ¹H NMR spectrum (Equation 3). It found to be less than 1, suggesting that monotosylation at primary hydroxyl of β -CD was carried out [117, 118].

Furthermore, Mass spectrometry (MS) (Figure 26) revealed a molecular weight of the molecular ion $[M+Na]^+$ of $1311.388 \text{ g mol}^{-1}$ [91], which absolutely agreed with the calculated value for mono-functionalized β -CD.

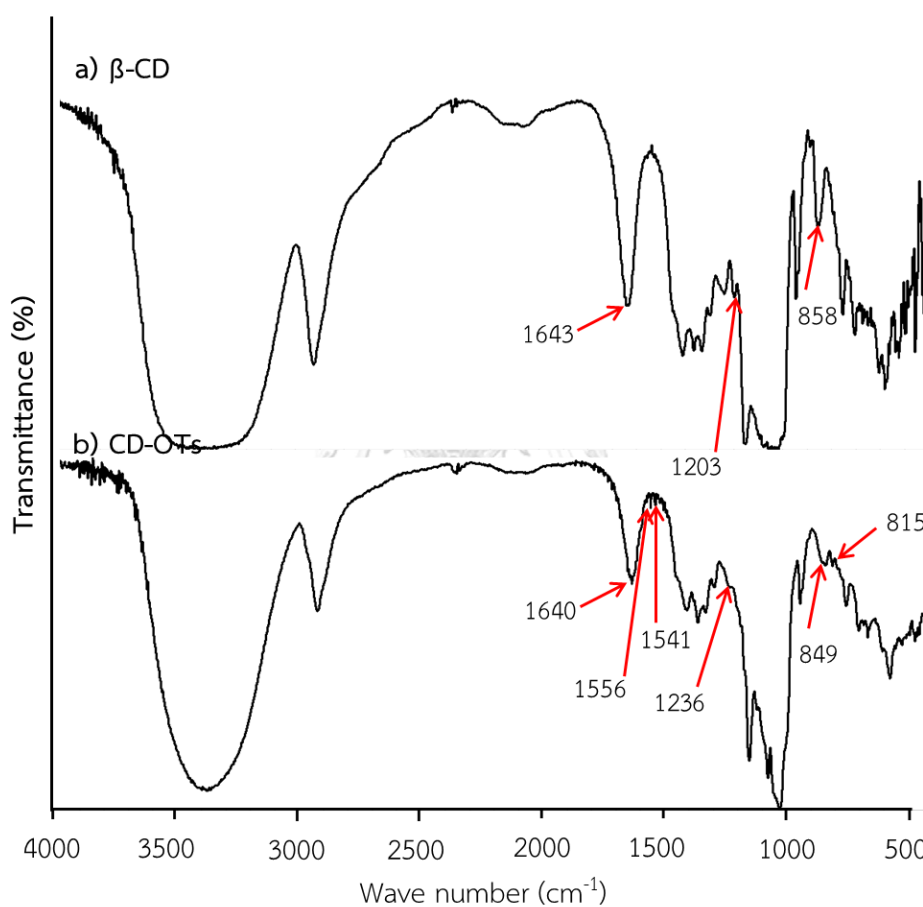


Figure 24 The FTIR spectra of a) β -CD and b) CD-OTs.

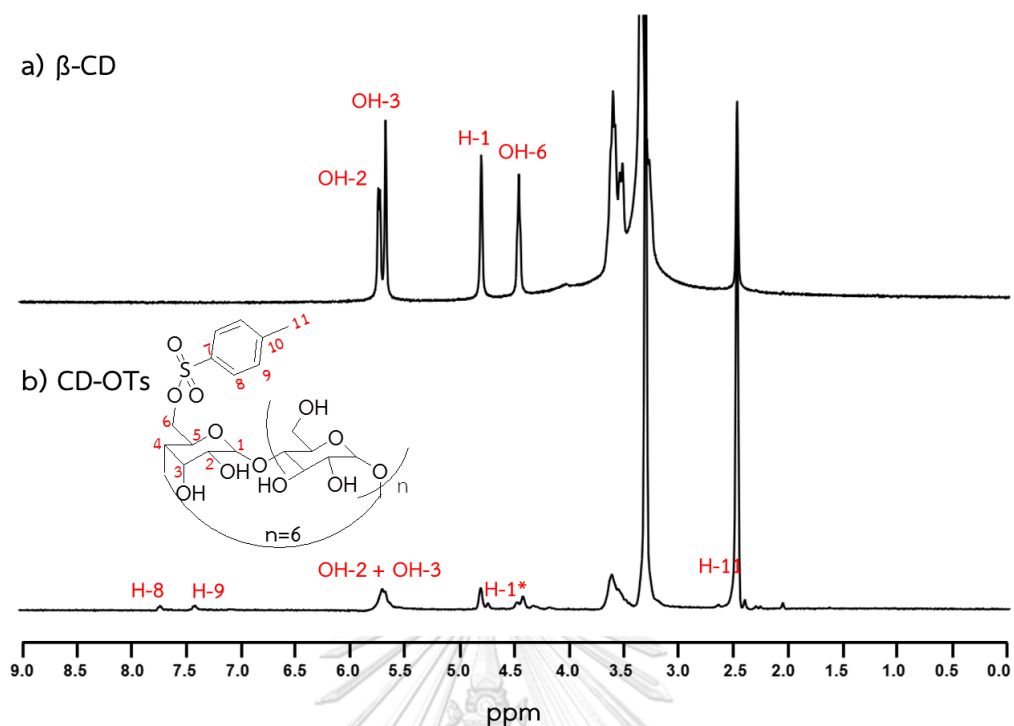


Figure 25 ^1H NMR of a) β -CD and b) CD-OTs.

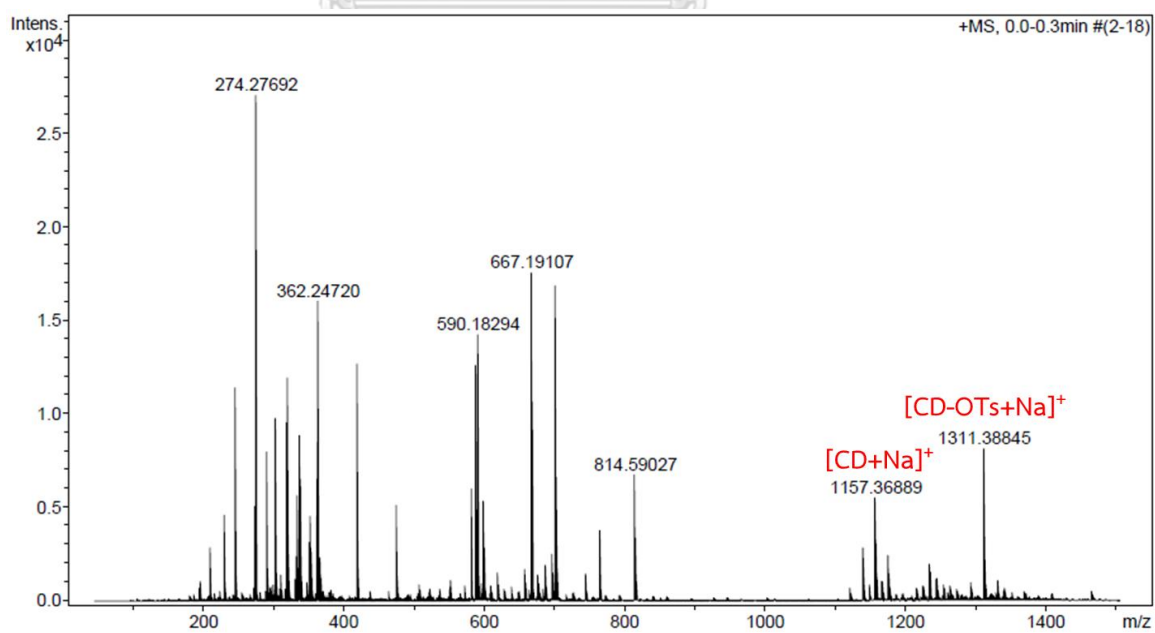


Figure 26 Mass spectrum of CD-OTs.

Afterwards, the β -CD-OTs was grafted with FA-CD (CD-FA-CP) by nucleophilic displacement of tosyl groups as shown in step 3, Figure 6. The ^1H NMR of CD-FA-CP performed the shifted signal at 6.75-7.7 (Figure 27b) which was the phenyl proton signal from FA part. It was likely to suggest that the some parts of FA molecule can interact with cyclodextrin to form inclusion [119] leading to the shift of NMR signal.

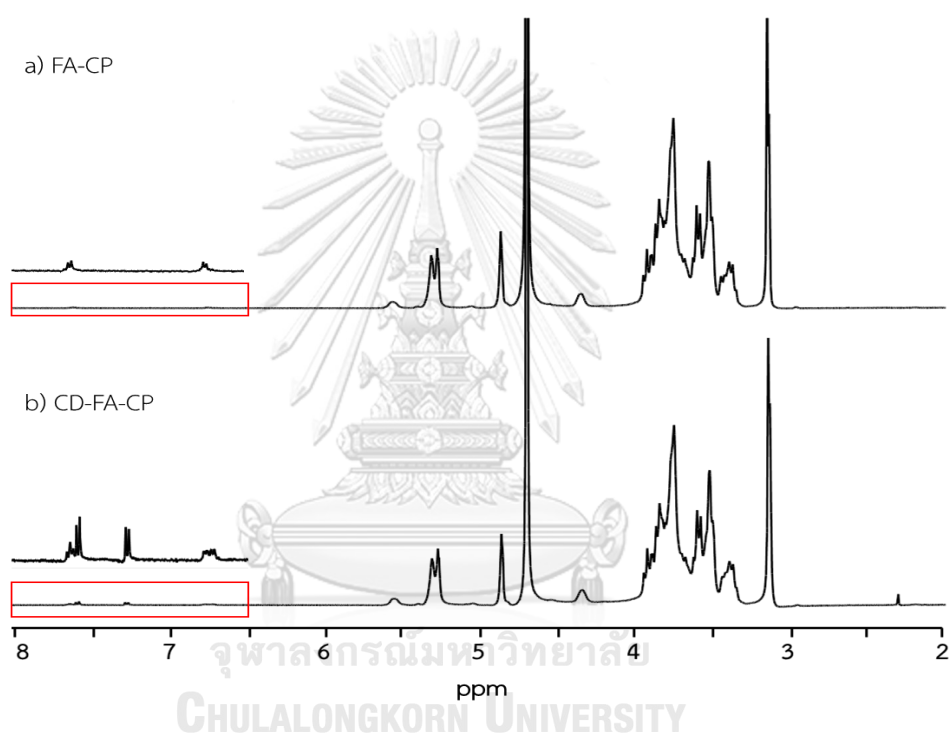


Figure 27 The ^1H NMR spectra of a) FA-CP and b) CD-PA-CP.

DSC is the most popular thermal technique for polymer characterization. To confirm the synthesized product, the thermal properties of the FA-CP and β -CD grafted FA-CP were evaluated using DSC. Figure 28 shows DSC thermograms of FA-CP and CD-FA-CP which used to detect the glass transition temperature (T_g) and melting temperature (T_m) of samples. The T_g and T_m were summarized in Table 4. An

observation of a relatively endothermic peak at about 60.3 and 104.9 °C is assigned to T_g and T_m of FA-CP, respectively. This peak was shifted to higher T_g of 75.0 °C and T_m of 135.9 °C when the functionalization of FA-CP with β -CD. This is maybe because the majority of the chains of CD-FA-CP are in more a crystalline state due to the presence of β -CD to induce the intermolecular interaction. From all of results confirmed the successful preparation of CD-FA-CP.

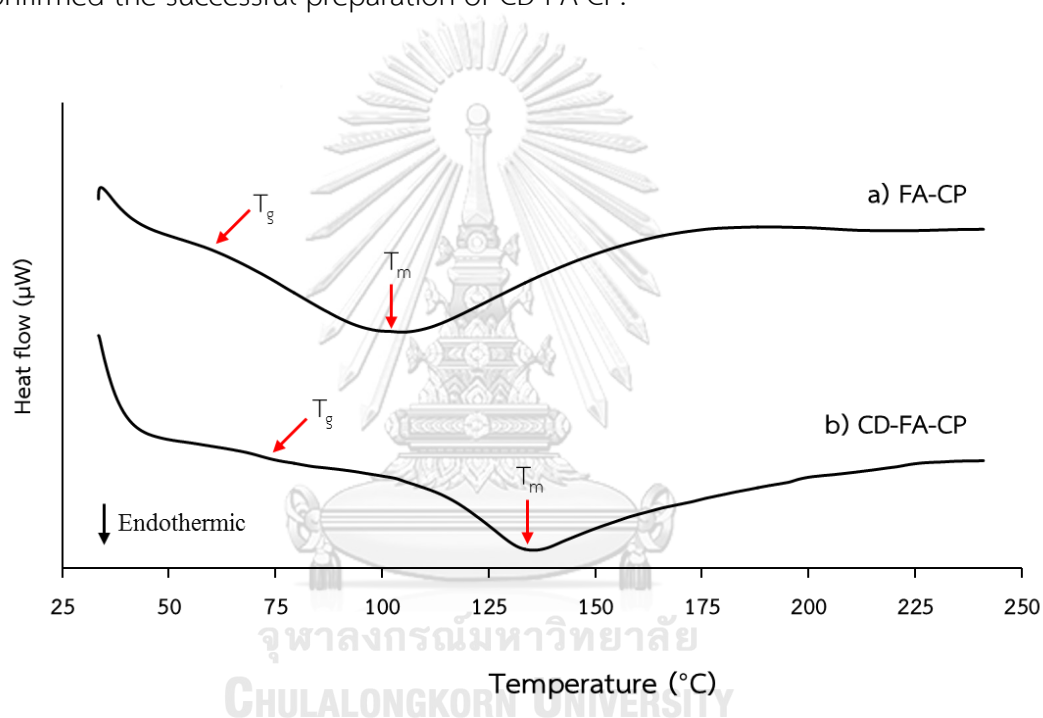


Figure 28 DSC thermograms of a) FA-CP and b) CD-FA-CP.

Table 4. The T_g and T_m of FA-CP and CD-FA-CP

Materials	T_g (°C)	T_m (°C)
FA-CP	60.3±1.1	104.9±0.1
CD-FA-CP	74.9±0.2	135.9±0.1

4.4 Synthesis and characterization of SeNPs stabilized by CD-FA-CP

4.4.1 Effect of cysteine concentration

The results from section 4.2.1 suggested that the concentration of cysteine impacted the morphology of SeNPs in the presence of FA-CP which presented spherical structure with the molar ratio of Na_2SeO_3 to cysteine was 1:1 and microflowers appeared when the molar ratio was 1:2. Thus, the 1:1 and 1:2 molar ratio of Na_2SeO_3 to L-cysteine were studied when using 0.23% of CD-FA-CP as a stabilizer. Interestingly, the hierarchical microflowers growth of SeNPs/CD-FA-CP hybrid system could be observed in both of molar ratio which revealed in Figure 29a-d and the precipitation products were obtained (inset in Figure 29b). The morphology of SeNPs stabilized by FA-CP and CD-FA-CP with the molar ratio of 1:1 was totally different. It was changed from spherical shape to flowery structure. From the results can be guessed that β -CD conjugated FA-CP was an important part to force the formation of flower. From EDS mapping analysis (Figure 30a and b)

suggested that the process to form SeNPs/CD-FA-CP flower-like structures was likely similar to the formation of SeNPs/FA-CP microflower which was described in section 4.2.3.2. In brief, the disulfide derivative cysteine from the oxidation of L-cysteine arranged the structure to form hexagonal plated sheet which clearly seen the white spot plate of sulfur atoms from EDS mapping (Figure 30a). In addition, the Se atoms were dissipated on that plate (red spot). The intermolecular interactions such as electrostatic interaction, hydrogen bonding, and $\pi - \pi$ stacking help to hold the interior hexagonal structure to be rigidity. The large number of hexagonal sheets were then proceeded to form multilayer structures and anisotropic growth continued to build the full flower [13]. However, there configuration were different from SeNPs/FA-CP microflowers (Figure 16c) with two things. First, the hexagonal plated sheet from FA-CP stabilizer (inset in Figure 18a) seems to be thinner than the plate from stabilization by CD-FA-CP (Figure 30a). The β -CD immobilization might be the part to control the thickness of hexagonal sheet. The presence of β -CD helps to enhance the intermolecular interaction by forming hydrogen bonds between the two β -CD molecules [120] or between β -CD and pullulan chain leading to more compact plated sheet. Hence, the thicker hexagonal sheets were observed. Second, the number of hexagonal sheets to form full bloom flower of SeNPs/FA-CP is greater than SeNPs/CD-FA-CP because of the thin layer of hexagonal sheet as former

mention, consequently the single microflower from SeNPs/FA-CP were denser than SeNPs/CD-FA-CP hybrid flower.

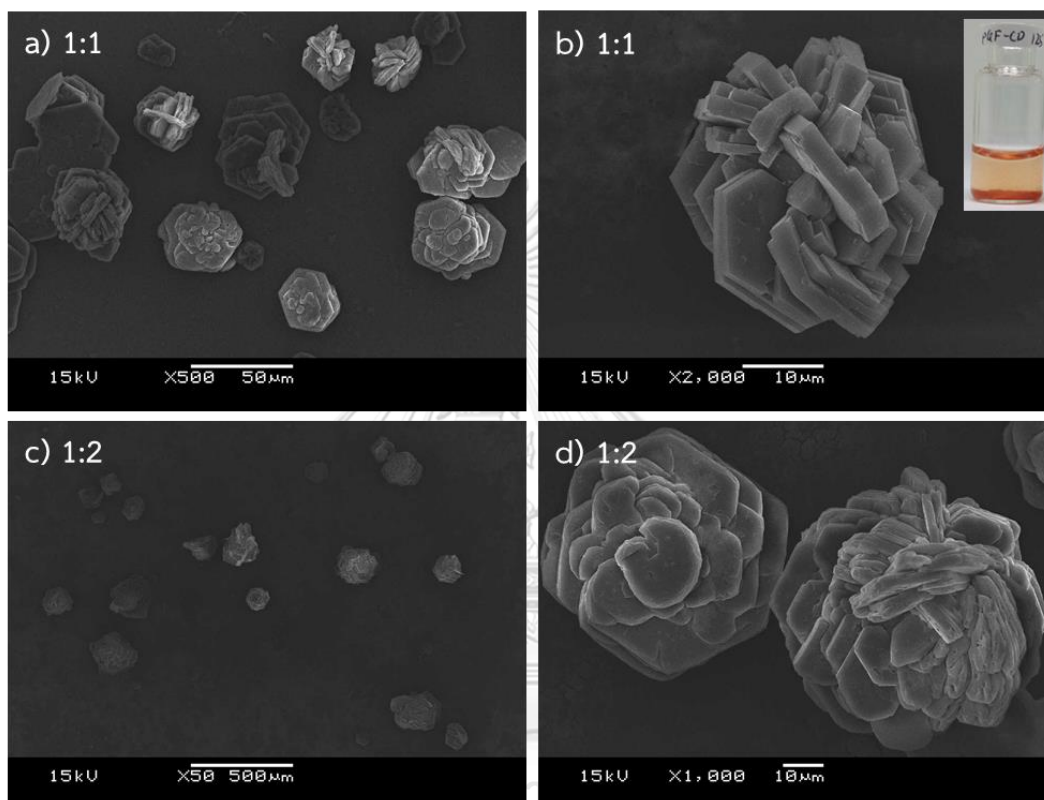


Figure 29 SEM images of shape of SeNPs stabilized by CD-FA-CP with molar ratio of Na_2SeO_3 to cysteine 1:1 (a and b) and 1:2 (c and d).

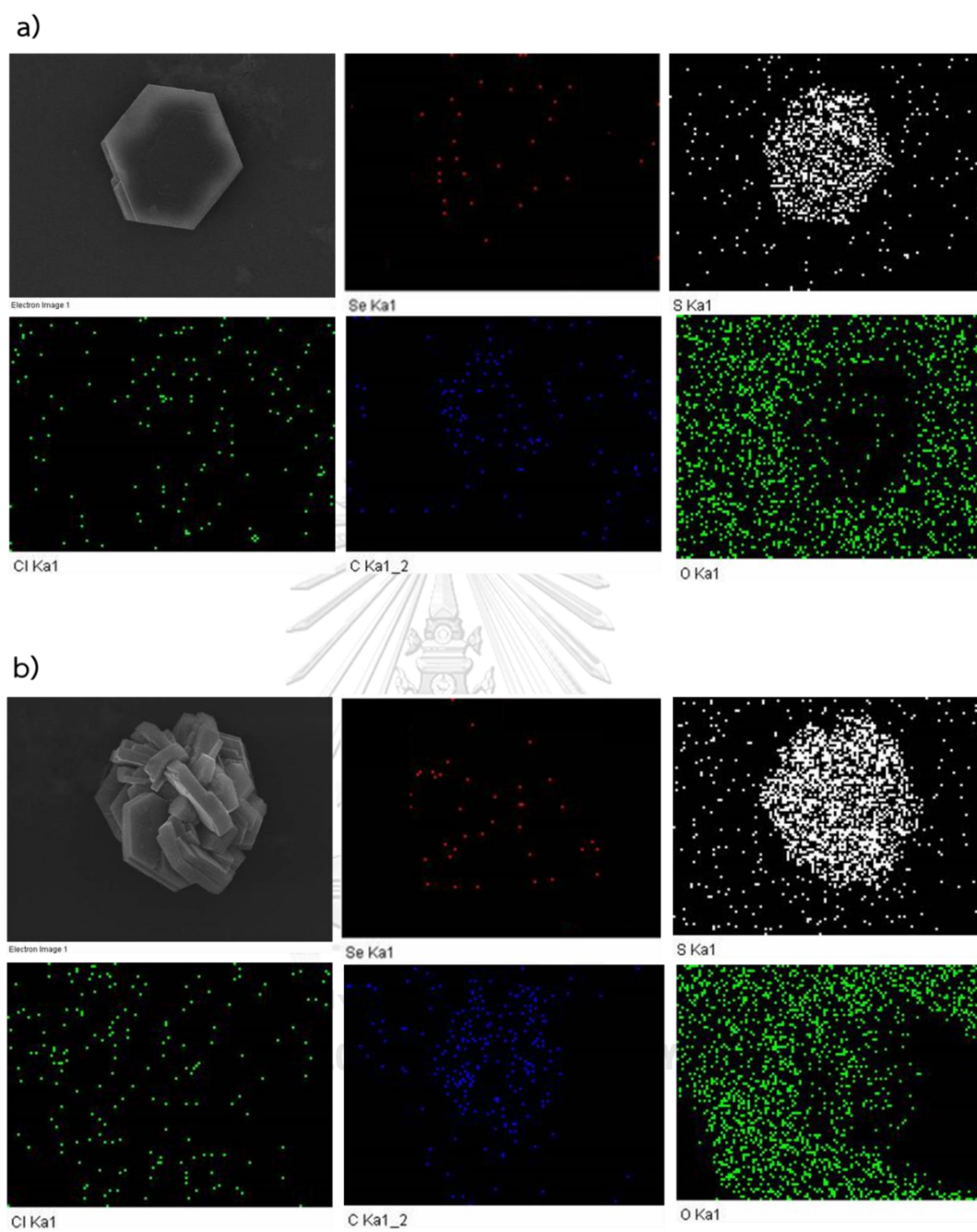


Figure 30 EDS mapping data of a) the hexagonal plated-sheet of SeNPs/CD-FA-CP and b) SeNPs/CD-FA-CP microflowers.

4.4.2 The use of SeNPs/CD-FA-CP microflower as a template for universal guest molecules loading

The design of advanced drug-delivery systems with high bioavailability, high drug-loaded capacity, and more diversity of drugs is a major challenge in pharmaceutical field [121, 122]. The β -CD is widely used for advanced drug delivery systems which used to increase the aqueous solubility, stability, and bioavailability of drugs [123]. The toroidal shape of β -CD shows the dual capability, a hydrophilic exterior and hydrophobic interior that makes β -CD great for encapsulating and releasing various guest molecules or drugs [123, 124]. In this work, three guest molecules; doxorubicin, curcumin, and methylene blue were used to study loaded ability of SeNPs/CD-FA-CP microflower. Doxorubicin loading measurements were carried out using fluorescence spectroscopy at the excitation wavelength of 480 nm while curcumin and methylene blue loading were measured using UV-Vis spectroscopy at wavelength 430 and 663 nm, respectively. The results showed that all of guest molecules at the same added concentration can be loaded into SeNPs/CD-FA-CP microflowers with loading capacity of doxorubicin, curcumin and methylene blue was 647.7 ± 165.2 , 763.3 ± 4.6 , and 99.7 ± 30.2 mg/g of CD-FA-CP, respectively (Figure 31). Therefore, the SeNPs/CD-FA-CP microflowers can be used as a template for any guest molecules especially hydrophobic drugs because not only the adsorption process on the microflower but also inclusion complex forming between guest and cavity of β -CD were cooperate [124]. Inclusion can happen at any

region of the guest molecule and the Intermolecular forces such as Van der Waals forces and hydrophobic interaction play a key role in the temporary entrapment of the guest inside of the host's cavity [125, 126].

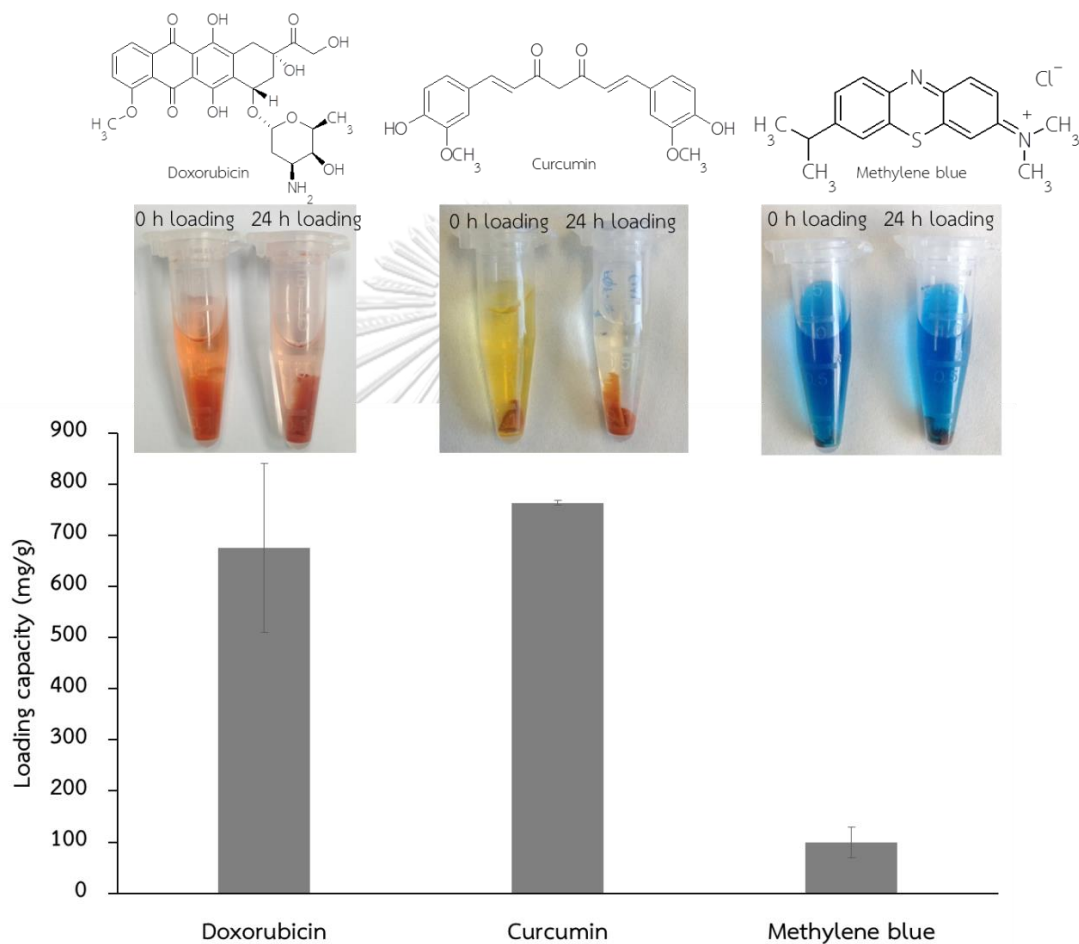


Figure 31 The capacity of guest molecules-loaded SeNPs/CD-FA-CP.

Focusing on doxorubicin-loaded SeNPs/CD-FA-CP microflowers (SeNPs/CD-FA-CP@DOX), the maximum drug-loading capacity was four times higher than the capacity of SeNPs/FA-CP@DOX (142.2 mg/g of FA-CP, Figure 21a) when using an equal concentration of Se. This was likely due to the presence of β -CD to allow

doxorubicin molecule getting into its cavity resulting in an enhancement of drug-loaded capacity. The SeNPs/CD-FA-CP@DOX was chosen for in vitro drug release study.

4.4.3 In vitro release of doxorubicin from SeNPs/CD-FA-CP@DOX

The doxorubicin release curve from of SeNPs/CD-FA-CP@DOX in PBS, pH 7.4 was investigated and the result is presented in Figure 32. It can be seen that the cumulative amount of released doxorubicin tended to increase, however it was released slowly and about 38% of the loaded doxorubicin was released after 288 h. The doxorubicin molecules were not only entrapped in β -CD cavities, but were maybe also absorbed by the surface of microflowers due to π - π stacking between phenyl of FA and doxorubicin, and hydrogen bonding between hydroxyl group of pullulan chain and amino groups of doxorubicin, hence, the release of doxorubicin based on all of them. To obtain more understanding into the mechanism underlying doxorubicin release from SeNPs/CD-FA-CP@DOX, various of kinetic models; Zero-order, First-order, Higuchi and Ritger-Peppas models were used to analyzed the in vitro release data [127, 128]. Comparing to other release kinetic models, Ritger-Peppas model was the model fitting analysis. It presented lowest sum-of-square residuals (SSR) values and showed the highest correlation coefficient (R^2) which displayed the exponent n values of 0.3024 (Table 5 and Appendix). The

results showed that the drug transport mechanism was influenced by drug diffusion, clearly indicating a Fickian diffusion release behaviour ($n < 0.5$) [127, 129].

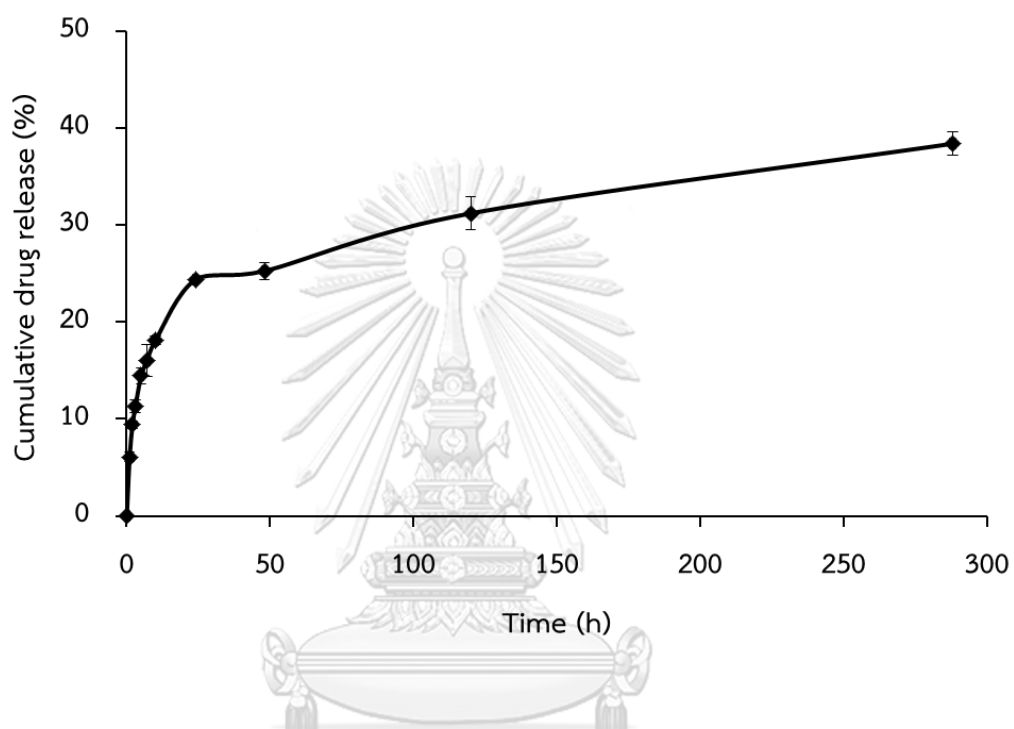


Figure 32 Cumulative drug release (%) of doxorubicin from doxorubicin-loaded SeNPs/CD-FA-CP microflowers.

Table 5. Fitting results of doxorubicin-release model of SeNPs/CD-FA-CP microflowers

Model	Equations	R ²	SSR
Zero order	$Q_t = 0.0957t + 14.596$	0.7269	256.8
First order	$\ln(100-Q_t) = -0.0013t + 4.4464$	0.7793	68.33
Higuchi	$Q_t = 1.8815t^{1/2} + 9.686$	0.8996	97.28
Ritger-Peppas	$\ln Q_t = 0.3024 \ln t + 2.0717$	0.9439	0.164

4.4.4 *In vitro* cytotoxicity study

To evaluate *in vitro* anticancer activities, free doxorubicin and doxorubicin-loaded SeNPs/CD-FA-CP were investigated against KB cell lines at different drug concentrations for 72 h. As shown in Figure 33, cell viability showed a drug concentration-dependent manner against both free doxorubicin and microflowers. SeNPs/CD-FA-CP@DOX showed lower cytotoxicity than that of free doxorubicin. For example, the viability of KB cells was 35% for SeNPs/CD-FA-CP@DOX and 6% for free doxorubicin with 2 μ M doxorubicin. That can be ascribed to the slow release of doxorubicin from the SeNPs/CD-FA-CP microflower at the same doxorubicin concentration [129, 130].

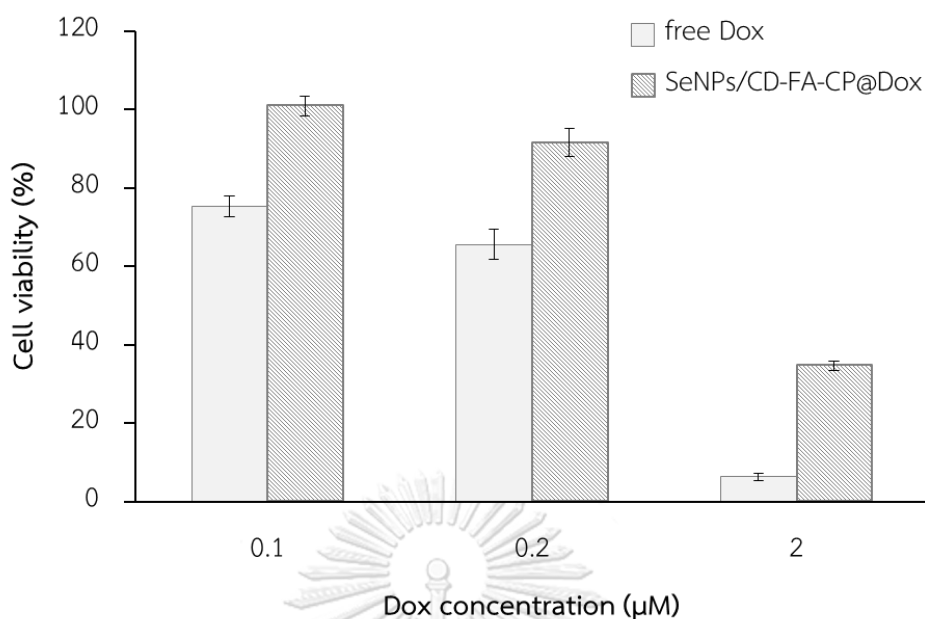


Figure 33 The in vitro cell viability of KB cells incubated with free doxorubicin and doxorubicin-loaded SeNPs/CD-FA-CP microflower at different concentrations of doxorubicin for 72 h.

4.4.5 *In vitro* cellular uptake study

To investigate the intracellular uptake efficiency, doxorubicin-loaded SeNPs/CD-FA-CP hybrid flowers were evaluated using confocal laser scanning microscope (CLSM) (Figure 34). The KB cells were prepared and incubated with SeNPs/CD-FA-CP@DOX at drug dosage of 2 μM and then washed three times with phosphate-buffered saline (PBS) to remove unreacted substances from the cell medium before imaging. As shown in Figure 34a, only the blue fluorescence of DAPI stained nucleus could be clearly observed in the nucleus of KB cells after 6 h of incubation in the untreated SeNPs/CD-FA-CP@DOX. However, KB cell treated with

SeNPs/CD-FA-CP@DOX for 6 h displayed the red fluorescence of doxorubicin in the cytoplasm of KB cells which surrounding blue fluorescence of nucleus (Figure 34b). It was implied that doxorubicin released from SeNPs/CD-FA-CP@DOX had entered the tumor cells and accumulated in cytoplasm but did not internalized to the nucleus. After 12 h incubation, it seems to be that some parts of doxorubicin molecules could internalize to nucleus because of the presence of red fluorescence in nucleus (Figure 34c and d). Therefore, it can be concluded that SeNPs/CD-FA-CP can be used as an alternative drug template and might have potential as anti-tumor drug carriers for cancer therapy.



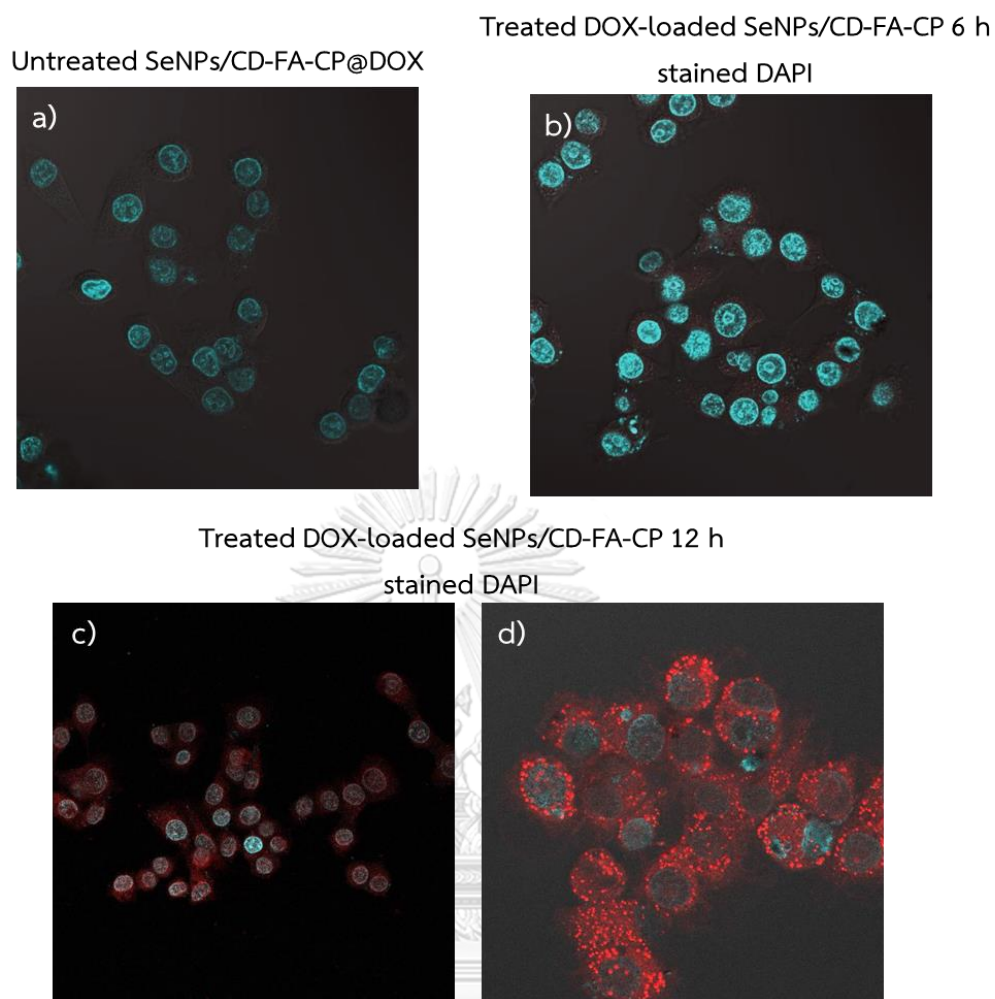


Figure 34 Confocal laser scanning microscopy images of KB cells incubated for 6 and 12 h at 37 °C with doxorubicin-loaded SeNPs/CD-FA-CF hybrid flower.

CHAPTER 5

CONCLUSION

5.1 Conclusion

In this study, the chemical structures of pullulan derivatives; folic acid decorated cationic pullulan (FA-CP) and β -cyclodextrin conjugated FA-CP (CD-FA-CP) were designed. SeNPs were synthesized using pullulan and derivatives as the stabilizer via the reduction of Na_2SeO_3 with freshly prepared L-cysteine. The cysteine concentration strongly affects the morphology of SeNPs stabilized by FA-CP (SeNPs/FA-CP). The spherical and microflower structure were performed when the molar ratio of Na_2SeO_3 :cysteine was 1:1 and 1:2, respectively.

Spherical SeNPs/FA-CP with striking stability was prepared under 1:1 molar ratio of Na_2SeO_3 :cysteine conditions. Pullulan surface decoration with positively charge and cancer targeting molecule significantly enhanced the cellular uptake and cytotoxicity of spherical SeNPs in human cancer cells while exhibiting low toxicity against normal cells. The results suggest that the use of stabilizer with positively charged and cancer targeting molecule could be a simple and attractive approach to achieve selective uptake and anticancer action of nanomaterials in cancer cells.

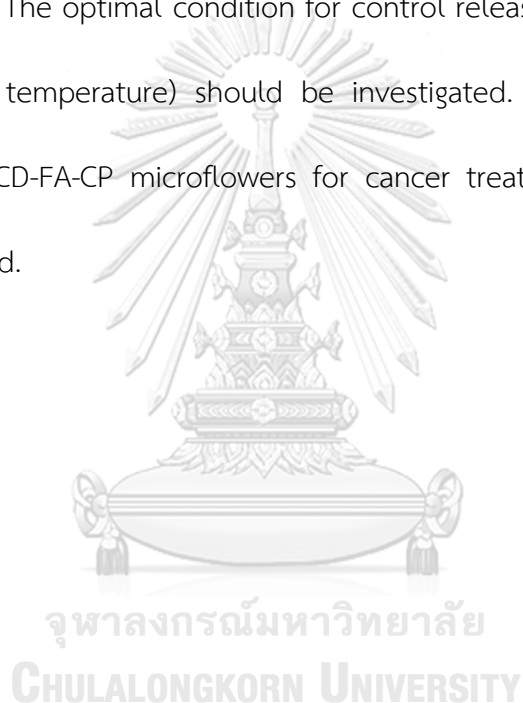
The formation of SeNPs stabilized by the pullulan derivative hybrid microflower could present well-ordered flowery structures by controlling the Na_2SeO_3 to cysteine molar ratio to 1:2 and the FA-CP concentration. The synthesized hybrid flower can be used as a template for enhancement of the anticancer drug loading capacity, showing higher doxorubicin loading than the spherical SeNPs/FA-CP. In addition, doxorubicin-loaded SeNPs microflower exhibited more potent activity against cancer cells, while it showed less toxicity against normal cells. With these merits, the flowerlike structure of SeNPs stabilized by pullulan derivative could be a candidate anticancer drug template in drug delivery systems.

The β -CD decorated FA-CP was developed to enhance the drug-loaded capacity and use for universal drugs. The SeNPs were prepared using CD-FA-CP as a stabilizer. The microflowers of SeNPs/CD-FA-CP were observed in both 1:1 and 1:2 molar ratio due to the presence of β -CD to enhance more intermolecular interaction. Three guest molecules; doxorubicin, curcumin, and methylene blue could be loaded to SeNPs/CD-FA-CP microflower. Compared to doxorubicin loaded SeNPs/FA-CP hybrid flower, the maximum drug-loading capacity of doxorubicin loaded SeNPs/CP-FA-CP was four times higher because of the presence of β -CD to allow doxorubicin molecule getting into its cavity resulting in an enhancement of drug-loaded capacity. It can be concluded that SeNPs/CD-FA-CP microflowers can help to enhance drug loading capacity and be used as a template for any guest molecules especially

hydrophobic drugs because not only the adsorption process on the microflower but also inclusion complex forming between guest and cavity of β -CD were corporate.

5.2 Suggestion for future work

The SeNPs/CD-FA-CP microflowers for being universal template drug loading should be studied by using the variety of drugs or guest molecules to strongly confirm its ability. The optimal condition for control release (e.g. pH, the amount of microflower, and temperature) should be investigated. Furthermore, the animal testing of SeNPs/CD-FA-CP microflowers for cancer treatment or another disease should be explored.



REFERENCES

- [1] Zhang, Y., Wang, J., and Zhang, L. Creation of Highly Stable Selenium Nanoparticles Capped with Hyperbranched Polysaccharide in Water. Langmuir 26(22) (2010): 17617-17623.
- [2] Chen, Z., Shen, Y., Xie, A., Zhu, J., Wu, Z., and Huang, F. l-Cysteine-Assisted Controlled Synthesis of Selenium Nanospheres and Nanorods. Crystal Growth & Design 9(3) (2009): 1327-1333.
- [3] Luesakul, U., Komenek, S., Puthong, S., and Muangsin, N. Shape-controlled synthesis of cubic-like selenium nanoparticles via the self-assembly method. Carbohydrate Polymers 153 (2016): 435-444.
- [4] Qi, L., Xu, Z., Jiang, X., Li, Y., and Wang, M. Cytotoxic activities of chitosan nanoparticles and copper-loaded nanoparticles. Bioorganic & Medicinal Chemistry Letters 15(5) (2005): 1397-1399.
- [5] Chithrani, B.D., Ghazani, A.A., and Chan, W.C.W. Determining the Size and Shape Dependence of Gold Nanoparticle Uptake into Mammalian Cells. Nano Letters 6(4) (2006): 662-668.
- [6] Huang, Y., et al. Selective cellular uptake and induction of apoptosis of cancer-targeted selenium nanoparticles. Biomaterials 34(29) (2013): 7106-7116.
- [7] Tan, L., et al. In vitro study on the individual and synergistic cytotoxicity of adriamycin and selenium nanoparticles against Bel7402 cells with a quartz crystal microbalance. Biosensors and Bioelectronics 24(7) (2009): 2268-2272.
- [8] Yang, F., et al. Surface decoration by Spirulina polysaccharide enhances the cellular uptake and anticancer efficacy of selenium nanoparticles. Int J Nanomedicine 7 (2012): 835-44.
- [9] Bae, B.-c. and Na, K. Self-quenching polysaccharide-based nanogels of pullulan/folate-photosensitizer conjugates for photodynamic therapy. Biomaterials 31(24) (2010): 6325-6335.
- [10] M.R., R. and Sharma, C.P. Pullulan as a promising biomaterial for biomedical applications: A perspective. Trends in Biomaterials & Artificial Organs 20(2)

- (2007): 116-121.
- [11] Sallustio, S., Galantini, L., Gente, G., Masci, G., and La Mesa, C. Hydrophobically Modified Pullulans: Characterization and Physicochemical Properties. The Journal of Physical Chemistry B 108(49) (2004): 18876-18883.
- [12] Lee, S.J., Shim, Y.-H., Oh, J.-S., Jeong, Y.-I., Park, I.-K., and Lee, H.C. Folic-acid-conjugated pullulan/poly(DL-lactide-co-glycolide) graft copolymer nanoparticles for folate-receptor-mediated drug delivery. Nanoscale Research Letters 10 (2015): 43.
- [13] Lee, S.W., Cheon, S.A., Kim, M.I., and Park, T.J. Organic-inorganic hybrid nanoflowers: types, characteristics, and future prospects. Journal of Nanobiotechnology 13(1) (2015): 54.
- [14] Scomparin, A., Salmaso, S., Bersani, S., Satchi-Fainaro, R., and Caliceti, P. Novel folated and non-folated pullulan bioconjugates for anticancer drug delivery. European Journal of Pharmaceutical Sciences 42(5) (2011): 547-558.
- [15] Souguir, Z., Roudesli, S., Picton, E.L., Le Cerf, D., and About-Jaudet, E. Novel cationic and amphiphilic pullulan derivatives I: Synthesis and characterization. European Polymer Journal 43(12) (2007): 4940-4950.
- [16] Dass, C.R. and Choong, P.F. The use of chitosan formulations in cancer therapy. J Microencapsul 25(4) (2008): 275-9.
- [17] Dragojevic, S., Ryu, J.S., and Raucher, D. Polymer-Based Prodrugs: Improving Tumor Targeting and the Solubility of Small Molecule Drugs in Cancer Therapy. Molecules 20(12) (2015): 21750-69.
- [18] Duncan, R. The dawning era of polymer therapeutics. Nat Rev Drug Discov 2(5) (2003): 347-60.
- [19] Hoare, T.R. and Kohane, D.S. Hydrogels in drug delivery: Progress and challenges. Polymer 49(8) (2008): 1993-2007.
- [20] Frezza, M., et al. Novel metals and metal complexes as platforms for cancer therapy. Curr Pharm Des 16(16) (2010): 1813-25.
- [21] Pasut, G. and Veronese, F.M. Polymer-drug conjugation, recent achievements and general strategies. Progress in Polymer Science 32(8) (2007): 933-961.

- [22] Muhammad, N. and Guo, Z. Metal-based anticancer chemotherapeutic agents. Current Opinion in Chemical Biology 19 (2014): 144-153.
- [23] Vinardell, M.P. and Mitjans, M. Antitumor Activities of Metal Oxide Nanoparticles. Nanomaterials (Basel) 5(2) (2015): 1004-1021.
- [24] Yu, B., Zhang, Y., Zheng, W., Fan, C., and Chen, T. Positive Surface Charge Enhances Selective Cellular Uptake and Anticancer Efficacy of Selenium Nanoparticles. Inorganic Chemistry 51(16) (2012): 8956-8963.
- [25] Mohanraj, V. and Chen, Y. Nanoparticles – A Review. Tropical Journal of Pharmaceutical Research 5(1) (2006): 561-573.
- [26] Laurent, S., et al. Magnetic Iron Oxide Nanoparticles: Synthesis, Stabilization, Vectorization, Physicochemical Characterizations, and Biological Applications. Chemical Reviews 108(6) (2008): 2064-2110.
- [27] McNamara, K. and Tofail, S.A.M. Nanoparticles in biomedical applications. Advances in Physics: X 2(1) (2017): 54-88.
- [28] Khan, H.A., Sakharkar, M.K., Nayak, A., Kishore, U., and Khan, A. 14 - Nanoparticles for biomedical applications: An overview. in Narayan, R. (ed.) Nanobiomaterials, pp. 357-384: Woodhead Publishing, 2018.
- [29] Sun, Y., et al. Superparamagnetic PLGA-iron oxide microcapsules for dual-modality US/MR imaging and high intensity focused US breast cancer ablation. Biomaterials 33(24) (2012): 5854-5864.
- [30] Khan, I., Saeed, K., and Khan, I. Nanoparticles: Properties, applications and toxicities. Arabian Journal of Chemistry (2017).
- [31] Astefanei, A., Núñez, O., and Galceran, M.T. Characterisation and determination of fullerenes: A critical review. Analytica Chimica Acta 882 (2015): 1-21.
- [32] Sinnott, S.B. and Andrews, R. Carbon Nanotubes: Synthesis, Properties, and Applications. Critical Reviews in Solid State and Materials Sciences 26(3) (2001): 145-249.
- [33] Ajayan, P.M. and Zhou, O.Z. Applications of Carbon Nanotubes. in Dresselhaus, M.S., Dresselhaus, G., and Avouris, P. (eds.), Carbon Nanotubes: Synthesis, Structure, Properties, and Applications, pp. 391-425. Berlin, Heidelberg: Springer Berlin Heidelberg, 2001.

- [34] Dai, H., Wong, E.W., Lu, Y.Z., Fan, S., and Lieber, C.M. Synthesis and characterization of carbide nanorods. Nature 375 (1995): 769.
- [35] Ye, X.-R., Lin, Y., Wang, C., and Wai, C.M. Supercritical Fluid Fabrication of Metal Nanowires and Nanorods Templated by Multiwalled Carbon Nanotubes. Advanced Materials 15(4) (2003): 316-319.
- [36] Bower, C., Rosen, R., Jin, L., Han, J., and Zhou, O. Deformation of carbon nanotubes in nanotube-polymer composites. Applied Physics Letters 74(22) (1999): 3317-3319.
- [37] Hisatomi, T., Kubota, J., and Domen, K. Recent advances in semiconductors for photocatalytic and photoelectrochemical water splitting. Chemical Society Reviews 43(22) (2014): 7520-7535.
- [38] Ong, C.B., Ng, L.Y., and Mohammad, A.W. A review of ZnO nanoparticles as solar photocatalysts: Synthesis, mechanisms and applications. Renewable and Sustainable Energy Reviews 81 (2018): 536-551.
- [39] Turki, A., Guillard, C., Dapozze, F., Berhault, G., Ksibi, Z., and Kochkar, H. Design of TiO₂ nanomaterials for the photodegradation of formic acid – Adsorption isotherms and kinetics study. Journal of Photochemistry and Photobiology A: Chemistry 279 (2014): 8-16.
- [40] Yang, J., Chen, C., Ji, H., Ma, W., and Zhao, J. Mechanism of TiO₂-Assisted Photocatalytic Degradation of Dyes under Visible Irradiation: Photoelectrocatalytic Study by TiO₂-Film Electrodes. The Journal of Physical Chemistry B 109(46) (2005): 21900-21907.
- [41] Sun, S., Murray, C.B., Weller, D., Folks, L., and Moser, A. Monodisperse FePt nanoparticles and ferromagnetic FePt nanocrystal superlattices. Science 287(5460) (2000): 1989-92.
- [42] da Costa, V.C.P. and Annunziata, O. Formation of Dendrimer Nanoassemblies by Oligomerization-Induced Liquid-Liquid Phase Separation. 33(22) (2017): 5482-5490.
- [43] Rao, J.P. and Geckeler, K.E. Polymer nanoparticles: Preparation techniques and size-control parameters. Progress in Polymer Science 36(7) (2011): 887-913.

- [44] Li, Z., Wang, Y., Wang, J., Tang, Z., Pounds, J.G., and Lin, Y. Rapid and Sensitive Detection of Protein Biomarker Using a Portable Fluorescence Biosensor Based on Quantum Dots and a Lateral Flow Test Strip. Analytical Chemistry 82(16) (2010): 7008-7014.
- [45] Abenojar, E.C., Wickramasinghe, S., Bas-Concepcion, J., and Samia, A.C.S. Structural effects on the magnetic hyperthermia properties of iron oxide nanoparticles. Progress in Natural Science: Materials International 26(5) (2016): 440-448.
- [46] Turcheniuk, K., Tarasevych, A.V., Kukhar, V.P., Boukherroub, R., and Szunerits, S. Recent advances in surface chemistry strategies for the fabrication of functional iron oxide based magnetic nanoparticles. Nanoscale 5(22) (2013): 10729-10752.
- [47] Lee, S., et al. A near-infrared-fluorescence-quenched gold-nanoparticle imaging probe for in vivo drug screening and protease activity determination. Angew Chem Int Ed Engl 47(15) (2008): 2804-7.
- [48] Shang, L., Yin, J., Li, J., Jin, L., and Dong, S. Gold nanoparticle-based near-infrared fluorescent detection of biological thiols in human plasma. Biosensors and Bioelectronics 25(2) (2009): 269-274.
- [49] Liu, R., Kay, B.K., Jiang, S., and Chen, S. Nanoparticle Delivery: Targeting and Nonspecific Binding. MRS Bulletin 34(6) (2011): 432-440.
- [50] Friedman, A.D., Claypool, S.E., and Liu, R. The smart targeting of nanoparticles. Curr Pharm Des 19(35) (2013): 6315-29.
- [51] Pramanik, A.K., Siddikuzzaman, Palanimuthu, D., Somasundaram, K., and Samuelson, A.G. Biotin Decorated Gold Nanoparticles for Targeted Delivery of a Smart-Linked Anticancer Active Copper Complex: In Vitro and In Vivo Studies. Bioconjugate Chemistry 27(12) (2016): 2874-2885.
- [52] Zhao, X., Li, H., and Lee, R.J. Targeted drug delivery via folate receptors. Expert Opin Drug Deliv 5(3) (2008): 309-19.
- [53] Zhang, S.-Y., Zhang, J., Wang, H.-Y., and Chen, H.-Y. Synthesis of selenium nanoparticles in the presence of polysaccharides. Materials Letters 58(21) (2004): 2590-2594.
- [54] Schwarz, K. and Foltz, C.M. Selenium as an integral part of factor 3 against

- dietary necrotic liver degeneration. Journal of the American Chemical Society 79(12) (1957): 3292-3293.
- [55] Brown, K.M. and Arthur, J.R. Selenium, selenoproteins and human health: a review. Public Health Nutr 4(2b) (2001): 593-9.
- [56] Kong, L., et al. The suppression of prostate LNCaP cancer cells growth by Selenium nanoparticles through Akt/Mdm2/AR controlled apoptosis. Biomaterials 32(27) (2011): 6515-6522.
- [57] Luo, H., Wang, F., Bai, Y., Chen, T., and Zheng, W. Selenium nanoparticles inhibit the growth of HeLa and MDA-MB-231 cells through induction of S phase arrest. Colloids and Surfaces B: Biointerfaces 94 (2012): 304-308.
- [58] Zheng, J.-S., et al. Sialic acid surface decoration enhances cellular uptake and apoptosis-inducing activity of selenium nanoparticles. Colloids and Surfaces B: Biointerfaces 83(1) (2011): 183-187.
- [59] He, C., Hu, Y., Yin, L., Tang, C., and Yin, C. Effects of particle size and surface charge on cellular uptake and biodistribution of polymeric nanoparticles. Biomaterials 31(13) (2010): 3657-3666.
- [60] Wang, H., et al. Folate-PEG coated cationic modified chitosan – Cholesterol liposomes for tumor-targeted drug delivery. Biomaterials 31(14) (2010): 4129-4138.
- [61] Zhang, Z., Huey Lee, S., and Feng, S.-S. Folate-decorated poly(lactide-co-glycolide)-vitamin E TPGS nanoparticles for targeted drug delivery. Biomaterials 28(10) (2007): 1889-1899.
- [62] Pi, J., et al. Pathway of cytotoxicity induced by folic acid modified selenium nanoparticles in MCF-7 cells. Appl Microbiol Biotechnol 97(3) (2013): 1051-62.
- [63] Hyon, S.H., Nakajima, N., Sugai, H., and Matsumura, K. Low cytotoxic tissue adhesive based on oxidized dextran and epsilon-poly-L-lysine. J Biomed Mater Res A 102(8) (2014): 2511-20.
- [64] Ahmad, N.H., Mustafa, S., and Che Man, Y.B. Microbial Polysaccharides and Their Modification Approaches: A Review. International Journal of Food Properties 18(2) (2015): 332-347.
- [65] Kar, R., Mohapatra, S., Bhanja, S., Das, D., and Barik, B. Formulation and in vitro

- characterization of xanthan gum-based sustained release matrix tables of isosorbide-5- mononitrate. Iran J Pharm Res 9(1) (2010): 13-9.
- [66] Kimoto, T., Shibuya, T., and Shiobara, S. Safety studies of a novel starch, pullulan: Chronic toxicity in rats and bacterial mutagenicity. Food and Chemical Toxicology 35(3) (1997): 323-329.
- [67] Shingel, K.I. Current knowledge on biosynthesis, biological activity, and chemical modification of the exopolysaccharide, pullulan. Carbohydrate Research 339(3) (2004): 447-460.
- [68] Ngo, D.-H. and Kim, S.-K. Sulfated polysaccharides as bioactive agents from marine algae. International Journal of Biological Macromolecules 62 (2013): 70-75.
- [69] Kim, E.J., Cho, S.H., and Yuk, S.H. Polymeric microspheres composed of pH/temperature-sensitive polymer complex. Biomaterials 22(18) (2001): 2495-2499.
- [70] Keun-Hong, P., Dong-Min, K., and Kun, N. Physicochemical characterization and carcinoma cell Interaction of self-organized nanogels prepared from polysaccharide/biotin conjugates for development of anticancer drug carrier. Journal of Microbiology and Biotechnology 16(9) (2006): 1369-1376.
- [71] Jo, J., Yamamoto, M., Matsumoto, K., Nakamura, T., and Tabata, Y. Liver targeting of plasmid DNA with a cationized pullulan for tumor suppression. J Nanosci Nanotechnol 6(9-10) (2006): 2853-9.
- [72] Nichifor, M., Stanciu, M.C., and Simionescu, B.C. New cationic hydrophilic and amphiphilic polysaccharides synthesized by one pot procedure. Carbohydrate Polymers 82(3) (2010): 965-975.
- [73] Jiao, Y., Fu, Y., and Jiang, Z. The synthesis and characterization of poly(ethylene glycol) grafted on pullulan. Journal of Applied Polymer Science 91(2) (2004): 1217-1221.
- [74] Ouchi, T., Minari, T., and Ohya, Y. Synthesis of poly(L-lactide)-grafted pullulan through coupling reaction between amino group end-capped poly(L-lactide) and carboxymethyl pullulan and its aggregation behavior in water. Journal of Polymer Science Part A: Polymer Chemistry 42(21) (2004): 5482-5487.

- [75] Ghimici, L. and Constantin, M. Novel thermosensitive flocculating agent based on pullulan. Journal of Hazardous Materials 192(3) (2011): 1009-1016.
- [76] Fundueanu, G., Constantin, M., and Ascenzi, P. Preparation and characterization of pH- and temperature-sensitive pullulan microspheres for controlled release of drugs. Biomaterials 29(18) (2008): 2767-2775.
- [77] Amornkitbamrung, L., et al. Polysaccharide stabilized nanoparticles for deacidification and strengthening of paper. RSC Advances 5(42) (2015): 32950-32961.
- [78] Huang, H. and Yang, X. Synthesis of polysaccharide-stabilized gold and silver nanoparticles: a green method. Carbohydrate Research 339(15) (2004): 2627-2631.
- [79] Sanyasi, S., et al. Polysaccharide-capped silver Nanoparticles inhibit biofilm formation and eliminate multi-drug-resistant bacteria by disrupting bacterial cytoskeleton with reduced cytotoxicity towards mammalian cells. Sci Rep 6 (2016): 24929.
- [80] Huang, H. and Yang, X. Synthesis of Chitosan-Stabilized Gold Nanoparticles in the Absence/Presence of Tripolyphosphate. Biomacromolecules 5(6) (2004): 2340-2346.
- [81] Jin, Y., Li, Z., Hu, L., Shi, X., Guan, W., and Du, Y. Synthesis of chitosan-stabilized gold nanoparticles by atmospheric plasma. Carbohydrate Polymers 91(1) (2013): 152-156.
- [82] Esther, J. and Sridevi, V. Synthesis and characterization of chitosan-stabilized gold nanoparticles through a facile and green approach. Gold Bulletin 50(1) (2017): 1-5.
- [83] Radhakumary, C. and Sreenivasan, K. Gold nanoparticles generated through “green route” bind Hg²⁺ with a concomitant blue shift in plasmon absorption peak. Analyst 136(14) (2011): 2959-2962.
- [84] Laksee, S., Puthong, S., Teerawatananond, T., Palaga, T., and Muangsin, N. Highly efficient and facile fabrication of monodispersed Au nanoparticles using pullulan and their application as anticancer drug carriers. Carbohydrate Polymers 173 (2017): 178-191.

- [85] Laksee, S., Puthong, S., Kongkavitoon, P., Palaga, T., and Muangsin, N. Facile and green synthesis of pullulan derivative-stabilized Au nanoparticles as drug carriers for enhancing anticancer activity. Carbohydrate Polymers 198 (2018): 495-508.
- [86] Gittins, D.I., Bethell, D., Schiffrin, D.J., and Nichols, R.J. A nanometre-scale electronic switch consisting of a metal cluster and redox-addressable groups. Nature 408(6808) (2000): 67-9.
- [87] Liu, F.-K., Ko, F.-H., Huang, P.-W., Wu, C.-H., and Chu, T.-C. Studying the size/shape separation and optical properties of silver nanoparticles by capillary electrophoresis. Journal of Chromatography A 1062(1) (2005): 139-145.
- [88] Kong, H., Yang, J., Zhang, Y., Fang, Y., Nishinari, K., and Phillips, G.O. Synthesis and antioxidant properties of gum arabic-stabilized selenium nanoparticles. International Journal of Biological Macromolecules 65 (2014): 155-162.
- [89] Yuan, R., et al. Self-assembled nanoparticles of glycyrrhetic acid-modified pullulan as a novel carrier of curcumin. Molecules 19(9) (2014): 13305-18.
- [90] Varshosaz, J., Hassanzadeh, F., Sadeghi Aliabadi, H., Nayebzadrian, M., Banitalebi, M., and Rostami, M. Synthesis and characterization of folate-targeted dextran/retinoic acid micelles for doxorubicin delivery in acute leukemia. Biomed Res Int 2014 (2014): 525684.
- [91] Tripodo, G., Wischke, C., Neffe, A.T., and Lendlein, A. Efficient synthesis of pure monotosylated beta-cyclodextrin and its dimers. Carbohydrate Research 381 (2013): 59-63.
- [92] Wang, X., et al. Facile One-Pot Preparation of Chitosan/Calcium Pyrophosphate Hybrid Microflowers. ACS Applied Materials & Interfaces 6(16) (2014): 14522-14532.
- [93] Liu, W., et al. Selenium Nanoparticles as a Carrier of 5-Fluorouracil to Achieve Anticancer Synergism. ACS Nano 6(8) (2012): 6578-6591.
- [94] Zhang, Y., Li, X., Huang, Z., Zheng, W., Fan, C., and Chen, T. Enhancement of cell permeabilization apoptosis-inducing activity of selenium nanoparticles by ATP surface decoration. Nanomedicine: Nanotechnology, Biology and Medicine 9(1) (2013): 74-84.
- [95] Fiege, K., Lünsdorf, H., Atarjibarzadeh, S., and Mischnick, P. Cyanoethylation of

- the glucans dextran and pullulan: Substitution pattern and formation of nanostructures and entrapment of magnetic nanoparticles. Beilstein Journal of Organic Chemistry 8 (2012): 551-566.
- [96] Dionísio, M., Braz, L., Corvo, M., Lourenço, J.P., Grenha, A., and Rosa da Costa, A.M. Charged pullulan derivatives for the development of nanocarriers by polyelectrolyte complexation. International Journal of Biological Macromolecules 86 (2016): 129-138.
- [97] Prabakaran, M., Grailer, J.J., Pilla, S., Steeber, D.A., and Gong, S. Folate-conjugated amphiphilic hyperbranched block copolymers based on Boltorn® H40, poly(L-lactide) and poly(ethylene glycol) for tumor-targeted drug delivery. Biomaterials 30(16) (2009): 3009-3019.
- [98] Seow, W.Y., Xue, J.M., and Yang, Y.-Y. Targeted and intracellular delivery of paclitaxel using multi-functional polymeric micelles. Biomaterials 28(9) (2007): 1730-1740.
- [99] Campisi, S., Schiavoni, M., Chan-Thaw, C.E., and Villa, A. Untangling the role of the capping agent in nanocatalysis: recent Advances and perspectives. Catalysts 6(12) (2016): 185.
- [100] Chen, W., Li, Y., Yang, S., Yue, L., Jiang, Q., and Xia, W. Synthesis and antioxidant properties of chitosan and carboxymethyl chitosan-stabilized selenium nanoparticles. Carbohydrate Polymers 132 (2015): 574-581.
- [101] Jia, X., Liu, Q., Zou, S., Xu, X., and Zhang, L. Construction of selenium nanoparticles/ β -glucan composites for enhancement of the antitumor activity. Carbohydrate Polymers 117 (2015): 434-442.
- [102] Guo, L., Tong, F., Liu, H., Yang, H., and Li, J. Shape-controlled synthesis of self-assembly cubic CuO nanostructures by microwave. Materials Letters 71 (2012): 32-35.
- [103] Daniel, M.C. and Astruc, D. Gold nanoparticles: assembly, supramolecular chemistry, quantum-size-related properties, and applications toward biology, catalysis, and nanotechnology. Chem Rev 104(1) (2004): 293-346.
- [104] Rekha, M.R. and Sharma, C.P. Blood compatibility and in vitro transfection

- studies on cationically modified pullulan for liver cell targeted gene delivery. Biomaterials 30(34) (2009): 6655-6664.
- [105] Luo, H., Wang, F., Bai, Y., Chen, T., and Zheng, W. Selenium nanoparticles inhibit the growth of HeLa and MDA-MB-231 cells through induction of S phase arrest. Colloids Surf B Biointerfaces 94 (2012): 304-8.
- [106] Ren, Y., et al. Antitumor activity of hyaluronic acid–selenium nanoparticles in Heps tumor mice models. International Journal of Biological Macromolecules 57 (2013): 57-62.
- [107] Suvannasara, P., Praphairaksit, N., and Muangsin, N. Self-assembly of mucoadhesive nanofibers. RSC Advances 4(102) (2014): 58664-58673.
- [108] Suber, L. and Plunkett, W.R. Formation mechanism of silver nanoparticle 1D microstructures and their hierarchical assembly into 3D superstructures. Nanoscale 2(1) (2010): 128-133.
- [109] Koley, P., Sakurai, M., and Aono, M. Controlled Fabrication of Silk Protein Sericin Mediated Hierarchical Hybrid Flowers and Their Excellent Adsorption Capability of Heavy Metal Ions of Pb(II), Cd(II) and Hg(II). ACS Applied Materials & Interfaces 8(3) (2016): 2380-2392.
- [110] Li, Q. and Yam, V.W.-W. High-yield synthesis of selenium nanowires in water at room temperature. Chemical Communications (9) (2006): 1006-1008.
- [111] Shah, C.P., Singh, K.K., Kumar, M., and Bajaj, P.N. Vinyl monomers-induced synthesis of polyvinyl alcohol-stabilized selenium nanoparticles. Materials Research Bulletin 45(1) (2010): 56-62.
- [112] Wang, Z. and Zhu, S. Rapid growth of t-Se nanowires in acetone at room temperature and their photoelectrical properties. Frontiers of Optoelectronics in China 4(2) (2011): 188-194.
- [113] Ramasamy, P., Manivasakan, P., and Kim, J. Phase controlled synthesis of SnSe and SnSe₂ hierarchical nanostructures made of single crystalline ultrathin nanosheets. CrystEngComm 17(4) (2015): 807-813.
- [114] Srivastava, N. and Mukhopadhyay, M. Green synthesis and structural characterization of selenium nanoparticles and assessment of their antimicrobial property. Bioprocess Biosyst Eng 38(9) (2015): 1723-30.

- [115] Yang, C., Lin, K., and Chang, J. A simple way to synthesize 3D hierarchical HAp porous microspheres with sustained drug release. Ceramics International 41(9, Part A) (2015): 11153-11160.
- [116] Tripodo, G., Wischke, C., Neffe, A.T., and Lendlein, A. Efficient synthesis of pure monotosylated beta-cyclodextrin and its dimers. Carbohydr Res 381 (2013): 59-63.
- [117] Gonil, P., et al. Novel quaternized chitosan containing β -cyclodextrin moiety: Synthesis, characterization and antimicrobial activity. Carbohydrate Polymers 83(2) (2011): 905-913.
- [118] Raoov, M., Mohamad, S., and Abas, M.R. Synthesis and characterization of beta-cyclodextrin functionalized ionic liquid polymer as a macroporous material for the removal of phenols and As(V). Int J Mol Sci 15(1) (2013): 100-19.
- [119] Kun, L., Manshuo, L., Hudie, X., Bin, H., Yulin, Z., and Bo, Y. Inclusion Complexes of Folic Acid with Polyamine-Modified b-Cyclodextrins: Characterization, Solubilization and Inclusion Mode. Asian Journal of Chemistry 25(1855-1860) (2016).
- [120] Diaz-Salmeron, R., Ponchel, G., Gallard, J.-F., and Bouchemal, K. Hierarchical supramolecular platelets from hydrophobically-modified polysaccharides and α -cyclodextrin: Effect of hydrophobization and α -cyclodextrin concentration on platelet formation. International Journal of Pharmaceutics 548(1) (2018): 227-236.
- [121] Caldorera-Moore, M.E., Liechty, W.B., and Peppas, N.A. Responsive Theranostic Systems: Integration of Diagnostic Imaging Agents and Responsive Controlled Release Drug Delivery Carriers. Accounts of Chemical Research 44(10) (2011): 1061-1070.
- [122] Palanikumar, L., et al. Importance of Encapsulation Stability of Nanocarriers with High Drug Loading Capacity for Increasing in Vivo Therapeutic Efficacy. Biomacromolecules 19(7) (2018): 3030-3039.
- [123] Iacovino, R., et al. β -Cyclodextrin Inclusion Complex to Improve Physicochemical Properties of Pipemidic Acid: Characterization and Bioactivity

- Evaluation. International Journal of Molecular Sciences 14(7) (2013): 13022-13041.
- [124] Zhou, H.-Y., Jiang, L.-J., Zhang, Y.-P., and Li, J.-B. β -Cyclodextrin inclusion complex: preparation, characterization, and its aspirin release in vitro. Frontiers of Materials Science 6(3) (2012): 259-267.
- [125] Piñeiro, Á., et al. On the Characterization of Host–Guest Complexes: Surface Tension, Calorimetry, and Molecular Dynamics of Cyclodextrins with a Non-ionic Surfactant. The Journal of Physical Chemistry B 111(17) (2007): 4383-4392.
- [126] Karoyo, A.H., Borisov, A.S., Wilson, L.D., and Hazendonk, P. Formation of Host-Guest Complexes of β -Cyclodextrin and Perfluorooctanoic Acid. The Journal of Physical Chemistry B 115(31) (2011): 9511-9527.
- [127] Dash, S., Murthy, P.N., Nath, L., and Chowdhury, P. Kinetic modeling on drug release from controlled drug delivery systems. Acta Pol Pharm 67(3) (2010): 217-23.
- [128] Ghosal, K., Chandra, A., Rajabalaya, R., Chakraborty, S., and Nanda, A. Mathematical modeling of drug release profiles for modified hydrophobic HPMC based gels. Pharmazie 67(2) (2012): 147-55.
- [129] Hong, S., Li, Z., Li, C., Dong, C., and Shuang, S. β -Cyclodextrin grafted polypyrrole magnetic nanocomposites toward the targeted delivery and controlled release of doxorubicin. Applied Surface Science 427 (2018): 1189-1198.
- [130] Yang, X., Grailer, J.J., Pilla, S., Steeber, D.A., and Gong, S. Tumor-Targeting, pH-Responsive, and Stable Unimolecular Micelles as Drug Nanocarriers for Targeted Cancer Therapy. Bioconjugate Chemistry 21(3) (2010): 496-504.

APPENDIX

Plots for release of doxorubicin from SeNPs/CD-FA-CP microflower

in PBS buffer at pH values of 7.4

Zero order model:	$Q_t = K_0t + C_0$	
First order model:	$\ln Q_t = -K_f t + \ln Q_0$	or $\ln(100-Q_t) = -K_f t + \ln Q_0$
Higuchi model:	$Q_t = K_H t^{1/2} + C_H$	
Ritger-Peppas model:	$Q_t = K_{RP} t^n$	or $\ln Q_t = n \ln t + \ln K_{RP}$

where Q_t is cumulative percentage of the drug released at time t , Q_0 is the initial amount of drug in microflower, K_0 , K_f , K_H , K_{RP} are release rate constants, and C_0 , C_H are respective intercepts with vertical axis.

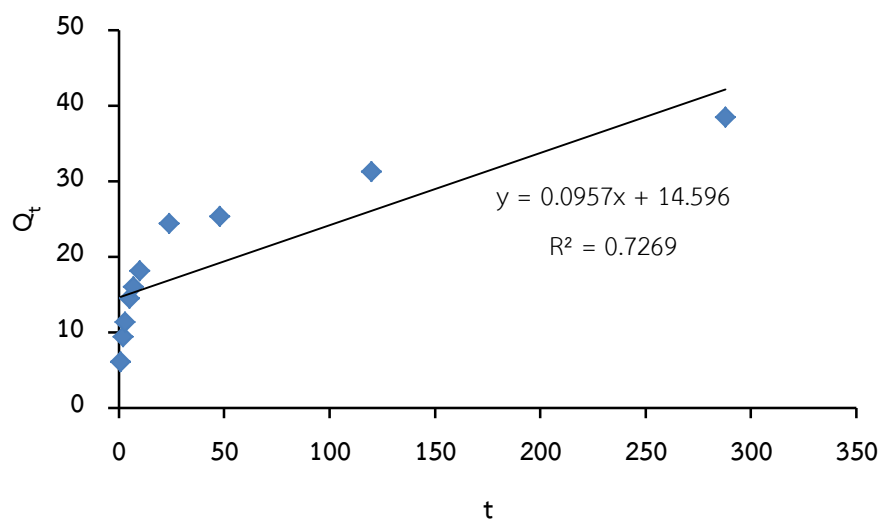


Figure A1 Zero order plots for release of doxorubicin from SeNPs/CD-FA-CP microflower.

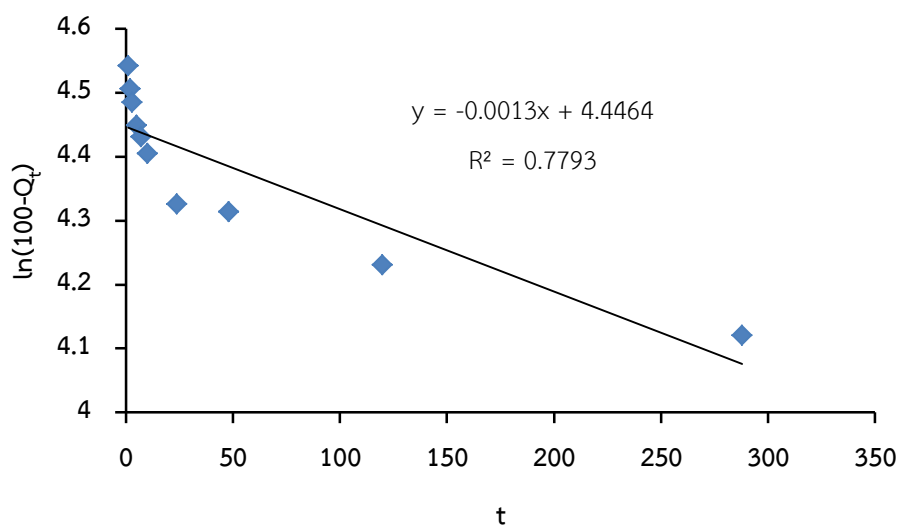


Figure A2 First order plots for release of doxorubicin from SeNPs/CD-FA-CP microflower.

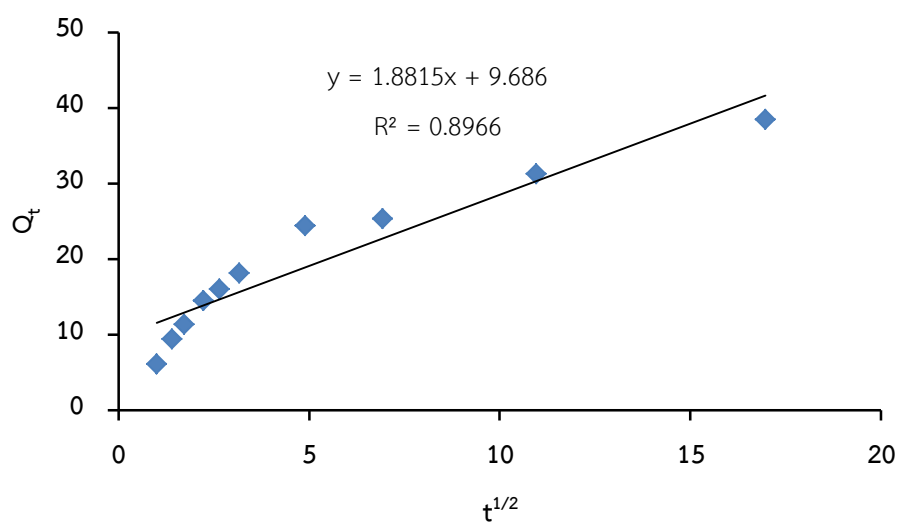


Figure A3 Higuchi plots for release of doxorubicin from SeNPs/CD-FA-CP microflower.

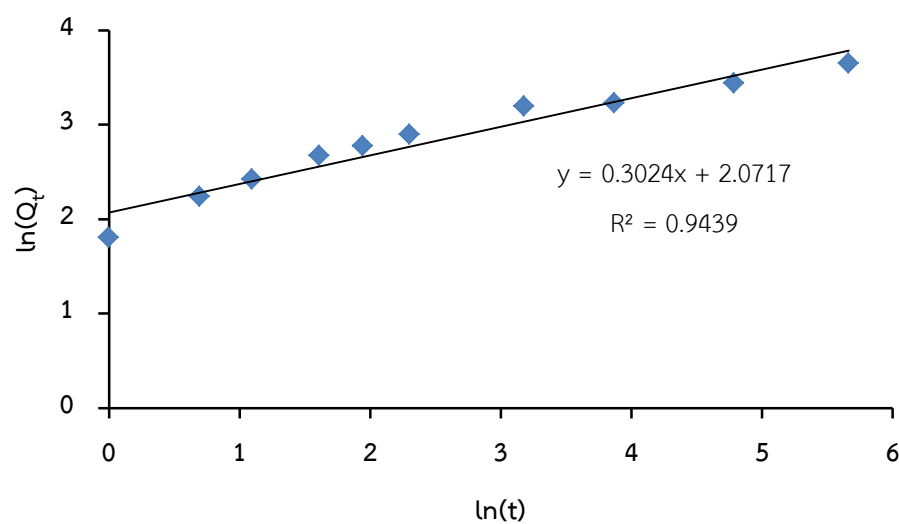


Figure A4 Ritger-Peppas plots for release of doxorubicin from SeNPs/CD-FA-CP microflower.

VITA

NAME	Punnida Nonsuwan
DATE OF BIRTH	27 September 1987
PLACE OF BIRTH	Kalasin
INSTITUTIONS ATTENDED	<p>Bachelor's degree of Science in Chemistry with a second class honor, Silpakorn University, Thailand, February 2009</p> <p>Master's degree (Biotechnology), Chulalongkorn University, Thailand, May 2013</p> <p>Doctor of Philosophy (Materials Science), Japan Advanced Institute of Science and Technology (JAIST), Japan, December 2018</p> <p>Doctor of Philosophy (Chemistry), Chulalongkorn University, Thailand, since 2013 to 2018</p> <p>Received the scholarship from the Development and Promotion of Science and Technology (DPST) since 2003 until present</p>
HOME ADDRESS	664/40-10, Moo 7, Khorplubpla, Muang, Ratchaburi, 70000
PUBLICATION	<p>1. Nonsuwan, P; Matsukami, A; Hayashi, F; Hyon, S; Matsumura, K., Controlling the degradation of an oxidized dextran-based hydrogel independent of the mechanical properties. Carbohydrate Polymers 2019, 204, 131-141.</p> <p>2. Nonsuwan, P.; Puthong, S.; Palaga, T.; Muangsin, N., Novel organic/inorganic hybrid flower-like structure of selenium nanoparticles stabilized by pullulan derivatives. Carbohydrate Polymers 2018, 184, 9-19.</p>
AWARD RECEIVED	Best poster presentation: 9th International Conference on Fiber and Polymer Biotechnology